Turun yliopisto
University of Turku

BLUE AND UV-EMITTING UPCONVERSION NANOPARTICLES:

Synthesis and (Bio) Analytical Applications

Vishal Kale

TURUN YLIOPISTON JULKAISUJA – ANNALES UNIVERSITATIS TURKUENSIS
Sarja - ser. AI osa - tom. 525 | Astronomica - Chemica - Physica - Mathematica | Turku 2015

University of Turku

Faculty of Mathematics and Natural Sciences
Department of Biochemistry / Biotechnology
Molecular Biotechnology and Diagnostics
Doctoral Programme in Molecular Life Sciences

Supervised by

Professor Tero Soukka, PhD
Department of Biochemistry / Biotechnology
University of Turku
Turku, Finland

Adjunct Professor Mika Lastusaari, PhD
Department of Chemistry
University of Turku
Turku, Finland

Reviewed by

Dr. hab. Eng. Dariusz Hreniak, PhD
Polish Academy of Science
Institute of Low Temperature and
Structure Research
Wroclaw, Poland

Professor Sakari Kulmala, PhD
Department of Chemistry
Aalto University
Espoo, Finland

Opponent

Assistant Professor Hans-Heiner Gorris, PhD
Institute of Analytical Chemistry,
Chemo and Biosensors
University of Regensburg
Regensburg, Germany

The originality of this thesis has been checked in accordance with the University of Turku quality assurance system using the Turnitin OriginalityCheck service.

ISBN 978-951-29-6288-4 (PRINT)
ISBN 978-951-29-6289-1 (PDF)
ISSN 0082-7002
Painosalama Oy - Turku, Finland 2015

"Progress is impossible without change,
and those who cannot change their
minds cannot change anything."

- *Georger Bernard Shaw*

CONTENTS

LIST OF ORIGINAL PUBLICATIONS

This thesis is based on the following original publications, referred to in the text by their Roman numerals **(I-IV)**.

I. **Vishal Kale,** Tero Soukka, Jorma Hölsä and Mika Lastusaari (2013). Enhancement of blue upconversion luminescence in hexagonal $NaYF_4$:Yb,Tm by using K and Sc ions. *Journal of Nanoparticle Research* 15:1-12.

II. Timo Valta, **Vishal Kale,** Tero Soukka and Carina Horn (2015). Near-infrared excited ultraviolet emitting upconverting phosphors as an internal light source in dry chemistry test strips for glucose sensing. *Analyst* 140:2638-2643.

III. **Vishal Kale,** Mika Lastusaari, Jorma Hölsä and Tero Soukka (2015). Intense UV upconversion through highly sensitized $NaRF_4$:Tm (R:Y,Yb) crystals. *RSC Advances* 5:35858-35865.

IV. **Vishal Kale,** Henna Päkkilä, Jiri Vainio, Anna Ahomaa, Nina Sirkka, Annika Lyytikäinen, Sheikh M. Talha, Matti Waris, Ilkka Julkunen and Tero Soukka. Spectrally and spatially multiplexed serological array-in-well assay utilizing upconverting nanophosphors. *Manuscript.*

ABBREVIATIONS

CSU	Cooperative sensitization upconversion
CTAB	Cetyltrimethyl ammonium bromide
EBT	Energy back transfer
EDC	1-ethyl-3-(3-dimethylaminopropyl)carbodiimide
EDTA	Ethylenediaminetetraacetic acid
EDX	Energy dispersive X-ray spectroscopy
EMU	Energy migration-mediated upconversion
ESA	Excited state absorption
ETU	Energy transfer upconversion
FAD	Flavin adenine dinucleotide
FWHM	Full width at half maximum
FITC	Fluorescein isothiocyanate
FRET	Fluorescence resonance energy transfer
GSA	Ground state absorption
HSA	Human serum albumin
ICPMS	Inductively coupled plasma mass spectrometer
LF	Lateral flow
LH	Luteinizing harmone
LOD	Limit of detection
LRET	Luminescence resonance energy transfer
MPA	Mercaptopropionic acid
MSA	Mercaptosuccinic acid
NADH	Nicotinamide adenine dinucleotide
NC	Nanocrystal
NIR	Near-infrared
NPs	Nanoparticles
OA	Oleic acid
ODE	1-Octadecene
OM	Oleylamine
PA	Photon avalanche
PAA	Poly(acrylic acid)
PEG	Poly(ethylene glycol)
PEI	Poly(ethylene imine)
PMAO	Poly(maleic anhydride-*alt*-1-octadecene)
PSA	Prostate specific antigen
PVP	Polyvinylpyrrolidone
QDs	Quantum dots
QY	Quantum yield
R	Rare-earth
RET	Resonance energy transfer

SEM	Scanning electron microscope
Sulfo-NHS	N-hydroxysulfosuccinimide sodium salt
TAMRA	Tetramethyl rhodamine
TEM	Transmission electron microscopy
TEOS	Tetraethyl orthosilicate
TMED	N-(3-trimethoxysilyl) propyl) ethylenediamine
TRITC	Tetramethylrhodamine isothiocyanate
TSH	Thyroid stimulating harmone
TTA	Triplet-triplet annihilation
TTET	Triplet-triplet energy transfer
UC	Upconversion
UCNP	Upconverting nanoparticle
UV	Ultraviolet
XPD	X-ray powder diffraction

ABSTRACT

Rare-earth based upconverting nanoparticles (UCNPs) have attracted much attention due to their unique luminescent properties. The ability to convert multiple photons of lower energy to ones with higher energy through an upconversion (UC) process offers a wide range of applications for UCNPs. The emission intensities and wavelengths of UCNPs are important performance characteristics, which determine the appropriate applications. However, insufficient intensities still limit the use of UCNPs; especially the efficient emission of blue and ultraviolet (UV) light *via* upconversion remains challenging, as these events require three or more near-infrared (NIR) photons.

The aim of the study was to enhance the blue and UV upconversion emission intensities of Tm^{3+} doped $NaYF_4$ nanoparticles and to demonstrate their utility in *in vitro* diagnostics. As the distance between the sensitizer and the activator significantly affect the energy transfer efficiency, different strategies were explored to change the local symmetry around the doped lanthanides. One important strategy is the intentional co-doping of active (participate in energy transfer) or passive (do not participate in energy transfer) impurities into the host matrix. The roles of doped passive impurities (K^+ and Sc^{3+}) in enhancing the blue and UV upconversions, as well as in influencing the intense UV upconversion emission through excess sensitization (active impurity) were studied. Additionally, the effects of both active and passive impurity doping on the morphological and optical performance of UCNPs were investigated.

The applicability of UV emitting UCNPs as an internal light source for glucose sensing in a dry chemistry test strip was demonstrated. The measurements were in agreement with the traditional method based on reflectance measurements using an external UV light source. The use of UCNPs in the glucose test strip offers an alternative detection method with advantages such as control signals for minimizing errors and high penetration of the NIR excitation through the blood sample, which gives more freedom for designing the optical setup. In bioimaging, the excitation of the UCNPs in the transparent IR region of the tissue permits measurements, which are free of background fluorescence and have a high signal-to-background ratio. In addition, the narrow emission bandwidth of the UCNPs enables multiplexed detections. An array-in-well immunoassay was developed using two different UC emission colours. The differentiation between different viral infections and the classification of antibody responses were achieved based on both the position and colour of the signal. The study demonstrates the potential of spectral and spatial multiplexing in the imaging based array-in-well assays.

TIIVISTELMÄ

Harvinaisia maametalleja sisältävät käänteisviritteiset nanopartikkelit ovat kasvavan kiinnostuksen kohteena niiden ainutlaatuisten luminesenssiominaisuuksien vuoksi. Käänteisviritteisten nanopartikkelien kyky muuntaa matalaenergisiä fotoneja käänteisvirityksen avulla korkeaenergisiksi mahdollistaa niiden hyödyntämisen monenlaisissa sovelluksissa. Käänteisviritteisten nanopartikkelien tärkeät ominaisuudet, kuten valoteho ja emissioaallonpituudet määrittelevät soveltuvat käyttökohteet. Heikko valoteho rajoittaa toistaiseksi käänteisviritteisten nanopartikkelien käyttöä. Erityisen haastavaa on tuottaa käänteisvirityksellä sinisen ja ultraviolettivalon emissiota, sillä nämä tarvitsevat virittyäkseen vähintään kolme lähi-infrapunafotonia.

Tutkimuksen tavoitteena oli tehostaa tuliumia (Tm^{3+}) sisältävien $NaYF_4$ nanopartikkelien sinisen ja ultraviolettivalon emissiotehokkuutta sekä osoittaa niiden käytettävyys *in vitro* diagnostiikassa. Koska herkistin- ja aktivaattori-ionien välinen etäisyys vaikuttaa merkittävästi energiansiirtotehokkuuteen, tässä väitöstyössä tutkittiin eri tapoja muuttaa näiden optisesti aktiivisten lantanidi-ionien paikallissymmetriaa. Yksi tärkeä strategia oli sisällyttää nanopartikkelin hilarakenteeseen muita optisesti aktiivisia (osallistuvat energiansiirtoon) tai passiivisia (eivät osallistu energiansiirtoon) ioneja. Tässä työssä tutkittiin sekä passiivisten ionien (K^+ ja Sc^{3+}) merkitystä sinisen ja UV-valon emissiotehokkuuteen että aktiivisten ionien merkitystä tehokkaan UV-emission tuotossa lisätyn herkistyksen avulla. Tämän lisäksi tutkittiin lisättyjen aktiivisten ja passiivisten ionien vaikutusta näiden nanopartikkelien morfologiaan ja optiseen suorituskykyyn.

UV-emittoivien käänteisviritteisten nanopartikkelien käyttökelpoisuus osoitettiin hyödyntämällä niitä sisäisenä valonlähteenä verensokeritestilastuissa. Saadut tulokset olivat vertailukelpoisia perinteiseen, ulkoista UV-valonlähdettä hyödyntävään, reflektanssiin perustuvaan mittaukseen. Käänteisviritteisten nanopartikkelien käyttö verensokeritestilastuissa tarjoaa vaihtoehtoisen mittaustekniikan, jonka etuina on sisäisen referenssisignaalin käyttömahdollisuus ja lähi-infrapunavirityksen hyvä läpäisykyky, mikä mahdollistaa mittalaitteiston optisen kokoonpanon vapaamman suunnittelun. Biokuvantamisessa käänteisviritteisten nanopartikkelien viritys kudosta helposti läpäisevällä lähi-infrapunasäteilyn aallonpituudella mahdollistaa taustafluoresenssista vapaat mittaukset ja suuren signaali-taustasuhteen. Tämän lisäksi näiden partikkelien kapeat emissioaallonpituusalueet mahdollistavat käytön monianalyyttimäärityksissä. Kahta käänteisviritysemission aallonpituutta hyödyntämällä kehitettiin mikrotitterilevyn kaivon pohjalla tehtävä array-tyyppinen monianalyytti-immunomääritys. Eri virusinfektiot ja vasta-ainevasteet eroteltiin toisistaan sekä paikka- että värispesifisesti. Tutkimus osoitti käänteisviritteisten nanopartikkelien hyödyntämispotentiaalin spektraaliseen ja paikkaspesifiseen erotteluun perustuvissa array-tyyppisissä määrityksissä.

1 INTRODUCTION

In the past decade a fast amount of research has been carried out on the use of nanomaterials in molecular diagnostics. Nanomaterial-based detection agents overcome many of the limitations associated with conventional diagnostic technologies in terms of assay sensitivity, selectivity and practicality [1]. The ability of lanthanide doped nanoparticles to up-convert NIR radiation into shorter visible and UV wavelengths has stimulated their use in biomedical diagnostics. Especially the use of upconverting nanoparticles as biomarker has revolutionized the field of bioimaging [2]. Although conventional contrast agents, such as organic dyes or semiconductor quantum dots which rely on the Stokes process, demonstrate many useful features, the short wavelength needed to excite them (by a UV or visible light source) limits their use [3]. On the other hand, lanthanide doped UCNPs, due to their unique upconversion property, offers remarkable advantages for bioimaging. For example, the absence of background fluorescence improves the signal-to-noise ratio, a sharp emission bandwidth makes UCNPs suitable for multiplexing and a high resistance to photodamage as well as photobleaching allow repetitive measurements. In addition, the optical transparency window of tissues permits the deep penetration of the NIR excitation [2].

The emission wavelength of the UCNPs can be tuned by doping different combinations of lanthanides into the crystals lattice [4]. The photophysics of the doped lanthanide, as determined by their *4f-4f* transitions and the optical properties of the UCNPs, can be tailored by changing the local environment around the lanthanides [5]. The synthesis of brighter UCNPs is the crucial part, as the sensitivity of their applications depends on the emission intensity.

Bioanalytical assays, especially, multiplexed assays, are able to detect a large number of analytes or analyte concentrations in a single run [6]. This simultaneous detection of multiple analytes reduces the consumption of reagents and sample, and decreases the assay time. Array based multiplexing offers more sensitive and faster measurements due to the short diffusion distances [7]. The analyte binding in the bioanalytical assay is recognised by using fluorescent-labeled detection antibodies which provides number of advantages, such as high sensitivity and a wide dynamic range. Inorganic upconverting particles with high UC efficiencies make promising luminescent labels for ultrasensitive immunoassays [8].

In addition to acting as diagnostic tools, UCNPs can also be utilized as a light source in many UV-visible radiation mediated photochemical reactions in material science and chemical biology in order to circumvent the use of expensive and phototoxic external light sources [9].

2 REVIEW OF THE LITERATURE

2.1 Upconverting nanoparticles (UCNPs)

Upconversion (UC) refers to a nonlinear optical process, which requires two or more low energy photons to generate a higher energy photon with a shorter wavelength. The emission of light at a shorter wavelength than the excitation wavelength is also known as anti-Stokes photoluminescence. This general concept was first introduced by Auzel in the mid-1960s [10]. Since then, the UC process has gained more interest in generating visible emissions from IR radiation and led to remarkable developments in optical devices. Unlike the nonlinear multiphoton absorption process, which is observed in organic dyes and quantum dots (QDs), the efficiency of the UC process means it can be produced by cheap continuous-wave NIR diodes [11, 12].

Currently, a few upconversion techniques are available, including upconversion with triplet-triplet annihilation (TTA), inorganic crystals and rare earth materials. Basically in TTA, a triplet sensitizer and a triplet acceptor (annihilator/emitter) are mixed together [13]. The sensitizer is excited by photo-irradiation and it transfers energy to the acceptor via a triplet-triplet energy transfer (TTET), and the acceptor then emits at a higher energy level than the excitation. The TTA based upconversion has its advantages, such as a low excitation power density and a high quantum yield. The possible excitation of the sensitizer with solar light makes TTA a very promising approach for applications such as, photovoltaics, photocatalysis and many other photochemical processes [13, 14]. UC with inorganic materials, also called upconverting nanoparticles (UCNPs), is another widely used technique, which involves an optically inactive inorganic host doped with optically active lanthanide ions [15]. This technique has gained more attention recently, due to the inherent advantages of the UCNPs. The UC process seen in lanthanide doped inorganic crystals is the main focus of this thesis.

Lanthanide-based upconverting nanoparticles (UCNPs) consist of a guest-host system, where the guest lanthanides are dispersed into the host matrix. Most of the UCNPs known so far are lanthanide based materials. The direct excitation of lanthanide ions is a relatively inefficient process because of the forbidden nature of the *4f* transitions [16]. To overcome this, lanthanide doping in a host material is the appropriate way to achieve desirable luminescence. Doped lanthanides in UCNPs have the superior advantages of intra *4f* electronic transitions such as a sharp emission bandwidth, high resistance to photobleaching and photochemical degradation [17-19]. The primary forbidden nature of the *f-f* transition produces very long lifetimes, thus favouring sequential excitations in the excited states [2].

Due to difficulties in preparing small upconverting nanoparticles (UCNPs) with strong UC emission intensities and dispersibility in an aqueous medium, their applicability has

been limited. It wasn't until after the 1990s that, the UC process became well-known in the biological and medical fields. The lower energy excitation in the UC offers several advantages, which makes it a very useful process for biological applications [20-22]. A brief overview of lanthanide based upconverting nanoparticles, their synthesis, factors affecting the UC emissions and their applications is presented in the Review of The Literature section.

2.1.1 Composition of UCNPs

UCNPs are inorganic crystals composed of a transparent host matrix doped with optically active lanthanide ions (Figure 1). The dopant ion replaces cations in the host matrix. The UC efficiency of the material can be enhanced by tuning the host lattice, dopant ions and dopant concentrations [15].

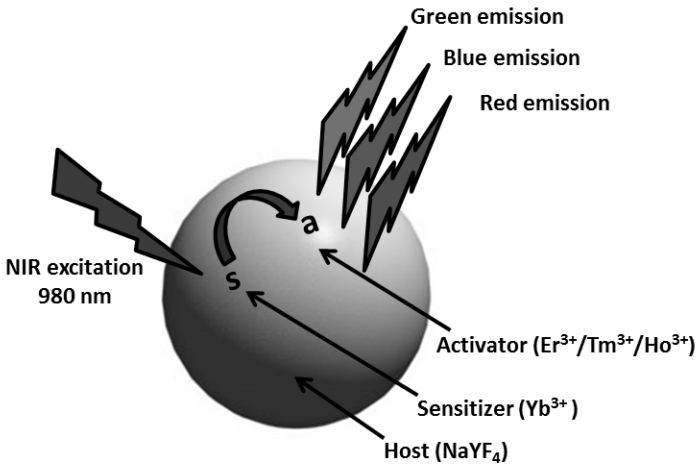

Figure 1. Schematic illustration of the structure and constituents of a UCNP showing the blue, green and red emissions after NIR excitation (modified from Min et al., 2014 [23]).

Host materials

For a high efficiency UC emission, the selection of appropriate host material is essential. Host materials differ in their coordination numbers and energy transfer efficiencies. An ideal host material has low phonon energies to boost the radiative emission [24]. In addition, the host should be chemically and thermally stable to be able to retain its original crystal structure.

Host materials that have been investigated in nanophosphors include rare-earth (R) based oxides (e.g., Y_2O_3, ZrO_2) [25], fluorides ($NaYF_4$) [26], vanadates (YVO_4) [27] and oxysulfides (Y_2O_2S) [28]. Additionally, some other compounds based on alkaline earth ions (Ca^{2+}, Sr^{2+} and Ba^{2+}) and transition metal ions (Zr^{4+} and Ti^{4+}) are also frequently used as host materials [29, 30]. Among the investigated hosts, fluoride based host

materials are frequently used because of their low photon cut-off energy and high chemical stability. The formation of crystal defects and lattice stress can be avoided by introducing cations (Na^+ and Ca^{2+}), whose ionic radii close to the doped lanthanide ions, into the fluoride based host materials.

The $NaRF_4$ series are reported to be the most excellent host till the date [31]. Two structures for $NaRF_4$ are available: α-$NaRF_4$ (cubic) and β-$NaRF_4$ (hexagonal). Crystal structure variation in host materials has a significant influence on the optical properties of the nanocrystals. In case of the $NaRF_4$ hosts, the β-$NaRF_4$ families are more efficient UC emitters than their cubic phase counterparts [32]. The presence of different crystal fields around dopant ions in the host lattice of various symmetries has serious effects on the UC efficiency [24]. A less symmetric crystal is generally favourable since the crystal field contains more uneven components around the dopant ions, which increases the *f-f* transition probabilities of the dopant ions.

Dopant ions

The dopant ions are in the form of localized luminescence centres. The dopants play a crucial role in the UC process by actually absorbing and emitting photons. Usually, relatively low concentrations of dopants (20-40% Yb, 0.2-0.5% Tm and 2% Er) are added to the host lattice.

Sensitizers

Upconversion emissions can be expected in singly doped lanthanide ions where two major parameters affect the UC processes; the distance among the neighbouring activators and their absorption cross-section [33, 34]. Attempts of increase the concentration of the doped activator are restricted by the concentration quenching effect. Hence, singly doped nanocrystals have relatively low upconversion efficiencies.

In order to enhance the UC efficiency, a sensitizer with a reasonable absorption cross-section in the NIR region is co-doped along with the activator. The ion that is first directly excited is called the sensitizer. An absorption cross-section of 9.11×10^{-21} cm^{-2} makes Yb^{3+} a particularly suitable sensitizer for Tm^{3+}, Er^{3+} and Ho^{3+} ions [24]. The energy level diagram of Yb^{3+} is quite simple, with only one excited state of $^2F_{5/2}$. Additionally, the energy separation between the ground state and only excited state of Yb^{3+} matches well with the *f-f* transitions of multiple lanthanide ions, and thus facilitates efficient energy transfer between the two ions [34].

Normally, Yb^{3+} is co-doped into the host material in an optimal range (20-40 mol%). Higher concentrations of Yb^{3+} doping can increase the absorption, but can also promote energy back-transfer (EBT) from the activator ions to Yb^{3+}. The energy back transfer mechanism depopulates the emitting levels of the activator and may be used for tuning the colour of the emission [35].

Activators

The luminescent centre in the UCNPs which emits the output photon is called the activator. Among the up-conversion materials, trivalent rare earth ions with sharp and narrow *f-f* transition bands, such as Er^{3+}, Tm^{3+} and Ho^{3+}, are typically used as activators due to their abundant electronic states, long lived excited state and ladder-like arrangement of energy levels [34].

During the energy transfer upconversion process, electrons at the ground state level in the activator become excited to the intermediate level and absorb energy from nearby excited sensitizers to promote further transitions. If the energy levels of the activators are close to each other the UC results in detrimental non-radiative relaxations. Table 1 shows the UC emissions of activators in their typical hosts.

Table 1. Typical activator-host combinations and corresponding UC emissions (modified from Dong et al., 2015 [24]).

Activators	Hosts	UC emissions (nm)
Pr^{3+}	KPb_2Cl_5, $Gd_3Ga_5O_{12}$	485, 520, 538, 605, 635, 645, 670, 690, 720
Nd^{3+}	YVO_4, Pb:TeO_2	430, 482, 525, 535, 580, 600, 664, 766
Sm^{3+}	$NaYbF_4$, $NaGdF_4$	520, 541, 555, 590, 646, 657, 700, 799–873
Eu^{3+}	$NaGdF_4$, $Gd_3Ga_5O_{12}$, $Y_3Al_5O_{12}$	416, 429, 490, 510, 535, 554, 590, 613
Gd^{3+}	$NaYF_4$	278, 305, 312
Tb^{3+}	$NaGdF_4$, α-$NaYF_4$, $Gd_3Ga_5O_{12}$, $Y_3Al_5O_{12}$	381, 415, 438, 489, 541, 584, 619
Dy^{3+}	Al_2O_3, $NaGdF_4$	378, 408, 487, 543, 569, 570, 610, 655, 663
Ho^{3+}	LaF_3, Y_2O_3	542, 655
Er^{3+}	$NaYF_4$	415, 525, 542, 655
Tm^{3+}	$NaYF_4$	290, 345, 362, 450, 475, 644, 694, 800
Yb^{3+}	$YbPO_4$	450–500

2.1.2 Photon upconversion mechanism

In general, UC mechanisms are grouped into five classes.

a) Excited state absorption (ESA)
b) Energy transfer upconversion (ETU)
c) Photon avalanche (PA)
d) Cooperative sensitization upconversion (CSU)
e) Energy migration-mediated upconversion (EMU)

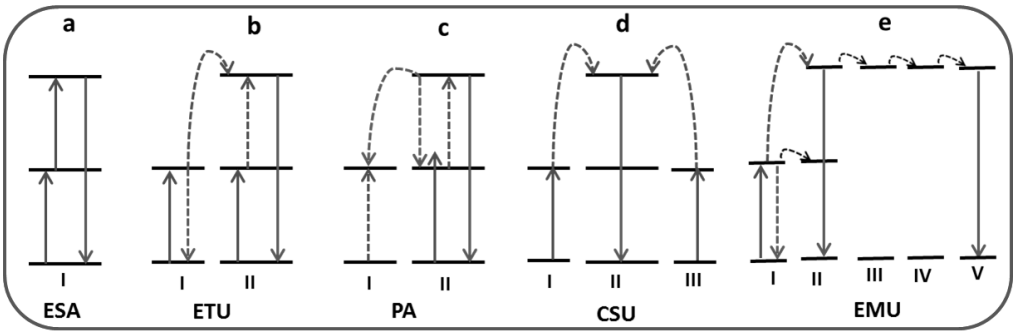

Figure 2. Schematic representation of UC processes seen in lanthanide-doped materials. a) Excited-state absorption, b) energy transfer upconversion, c) photon avalanche, d) cooperative sensitization upconversion, and e) energy migration-mediated upconversion (modified from Sun et al., 2015 [37]).

ESA involves a single ion, with a ladder-like arrangement of the energy states. The general scheme for ESA is shown in the Figure 2a. The ground state ion is excited to a long-lived intermediate state by the first photon absorption (called ground state absorption, GSA). Another pump photon boosts the ion from the intermediate state to a higher excited state, which further results in UC emission [34]. This UC process is only observed in materials with low dopant concentrations, as a high concentration results in non-radiative cross relaxations.

The **ETU** process was first discovered by Auzel in the mid-1960's [10, 38]. Even though both ESA and ETU absorb two photons to populate the metastable level, ESA involves a single lanthanide ion, while ETU needs two neighbouring ions (Figure 2b) [36, 39, 40]. Two different ions, namely the sensitizer (ion I) and the activator (ion II), are embedded in the upconversion unit, excited by low energy photons. The excited sensitizer ion donates energy to the neighbouring activator ion non-radiatively via a dipole-dipole interaction. The UC efficiency of ETU is dependent on the distance between ions I and II. ETU is the most efficient UC process in actual use.

PA is also known as absorption avalanche and was first discovered by Chivian in 1979 [41]. This process requires excitation pump intensity above a certain threshold. The PA process starts with the population of the intermediate level by GSA followed by resonant ESA to populate the upper emitting level. A cross-relaxation occurs between the ion at the upper emitting level and the neighbouring ion in the ground state and produces two ions at an intermediate level (Figure 2c). Subsequently, the feedback looping of ESA and cross-relaxation will exponentially increase the population of the intermediate and luminescent levels, thus producing strong PA UC. Even though efficient UC is possible with PA, it has many limitations including pump power dependence and a slow response to excitation.

CSU is a three ion process, which occurs less frequently; with ion I and ion III being generally of the same type (Figure 2d) [42, 43]. After the absorption of the excitation photon, ions I and III are excited to an excited state and cooperatively transfer energy to ion II simultaneously. The excited ion II can relax back to the ground state with the UC emission. This process usually occurs in singly doped Yb^{3+} or in Yb^{3+}/Tb^{3+} or Yb^{3+}/Eu^{3+} bulk materials [44, 45].

EMU was first discovered by Liu and Wang [46, 47]. EMU involves four different luminescent centres a sensitizer (ion I), an accumulator (ion II), a migrator (ion III and IV) and an activator (ion V) incorporated into separate layers (Figure 2e). In the actual process, the ETU populates the excited state of the accumulator, which then transfers energy to the migrator. Finally, energy is trapped by a neighbouring activator. The activator and the accumulator emit as the electrons return to their ground states.

UC mechanism in Yb, Er/Tm codoped UCNPs

The UC spectra for UCNPs, with the frequently used activator (Er/Tm) and sensitizer (Yb) combinations are shown in the Figure 3a. In Yb^{3+}-Er^{3+} co-doped nanoparticles emission peaks at green (520-550 nm) and red (650-660 nm) colours are most commonly observed along with a weak violet emission at 415 nm [24]. In the actual UC mechanism of the Yb^{3+}-Er^{3+} co-doped system, the $^2F_{7/2} \rightarrow {}^2F_{5/2}$ transition of Yb^{3+} matches closely with the $^4I_{15/2} \rightarrow {}^4I_{11/2}$ transition of Er^{3+} (Figure 3b), which offers efficient energy transfer between the activator and sensitizer. After 980 nm irradiation, Yb^{3+} resonantly transfers energy to Er^{3+}, which is responsible for the $^4I_{15/2} \rightarrow {}^4I_{11/2}$, $^4I_{11/2} \rightarrow {}^4F_{7/2}$ and $^4I_{13/2} \rightarrow {}^4F_{9/2}$ transitions. The excited ions relax non-radiatively to $^2H_{11/2}$ and $^4S_{3/2}$, which correspond to the 525 nm and 542 nm emissions. The non-radiatively transferred energy to $^4F_{9/2}$, or the resonant energy transfer from $^4I_{13/2}$, results in emission at 655 nm *via* the $^4F_{9/2} \rightarrow {}^4I_{15/2}$ transition. Thus, the red and green emissions can be produced by the sequential absorption of two photons. The $^4F_{9/2}$ state absorbs a third photon from Yb^{3+} and is excited to $^4G_{11/2}$ which, after relaxation to the $^2H_{9/2}$, gives a weak violet emission at 415 nm *via* the $^2H_{9/2} \rightarrow {}^4I_{15/2}$ transition.

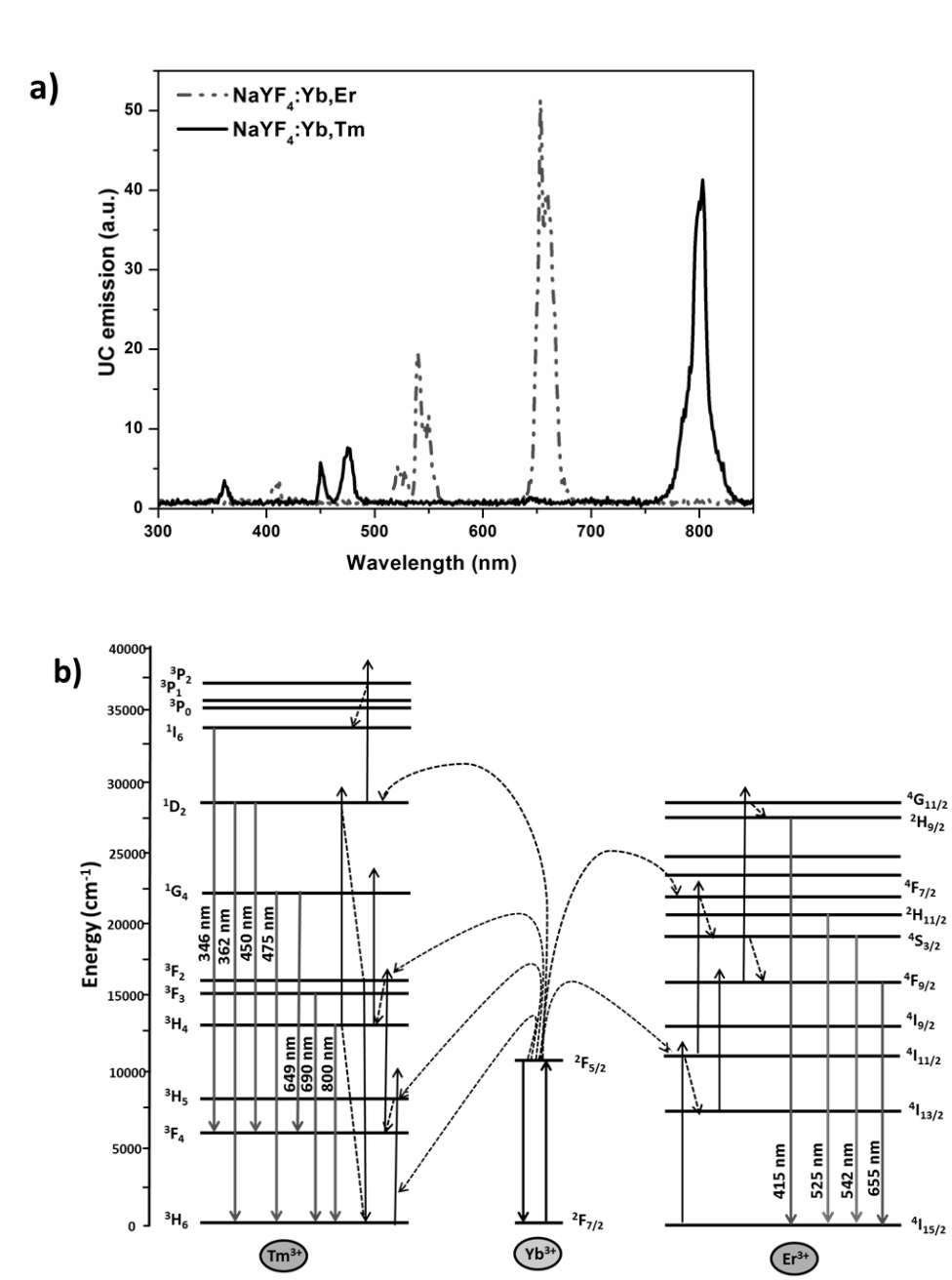

Figure 3. a) Upconversion spectra of $NaYF_4$:Yb,Er (dotted line) and $NaYF_4$:Yb,Tm (solid line) UCNPs with b) proposed energy transfer mechanism of the Yb,Er/Tm co-doped system (modified from Haase et al.,[15]).

The red to green intensity ratio can be enhanced by increasing the concentration of the Yb^{3+} ion. The reason for this might be that the increased Yb^{3+} concentration decreases the Yb-Er interatomic distance and further promotes more to the EBT from Er to Yb which decreases the green emission ($^2H_{11/2}$,$^4S_{3/2} \rightarrow {}^4I_{15/2}$) and enhances the red emission ($^4F_{9/2} \rightarrow {}^4I_{15/2}$) [48-50].

The excitation paths in Yb^{3+}-Tm^{3+} pairs are complex, as the UC process in the Yb^{3+}-Tm^{3+} system involves more than two photons (Figure 3b). This might be due to a discrete and ladder-like arrangement of the Tm^{3+} energy levels, which reduces the possibility of non-radiative relaxations. After a 980 nm excitation, energy is transferred from the $^2F_{5/2}$ state of Yb^{3+} to the $^3H_5$ state of Tm^{3+}. After a few upward transitions, $^3H_6 \rightarrow {}^3H_5$, $^3F_4 \rightarrow {}^3F_2$, $^3H_4 \rightarrow {}^1G_4$, $^1G_4 \rightarrow {}^1D_2$, $^1D_2 \rightarrow {}^3P_2$ and some non-radiative relaxations, $^3F_2 \rightarrow {}^3F_3$, $^3F_2 \rightarrow {}^3H_4$, $^3P_2 \rightarrow {}^1I_6$, the emission bands are resolved at 290 and 345 nm (five photon), 362 and 450 nm (four photon), 475 and 649 (three photon), 690 and 800 nm (two photon) which correspond to the $^1I_6 \rightarrow {}^3H_6$, $^1I_6 \rightarrow {}^3F_4$, $^1D_2 \rightarrow {}^3H_6$, $^1D_2 \rightarrow {}^3F_4$, $^1G_4 \rightarrow {}^3H_6$, $^1G_4 \rightarrow {}^3F_4$ and, $^3F_3 \rightarrow {}^3H_6$, $^3H_4 \rightarrow {}^3H_6$ transitions respectively [51]. The strong emission at 800 nm makes Tm^{3+} doped UCNPs excellent candidates for NIR-NIR bioprobes [52].

The UC emissions in the blue and UV region are extremely important for a wide range of applications; for example, colour displays, medical diagnostics, and many photochemical reactions [53, 54]. Although an UC emission at 415 nm is seen in $NaYF_4$:Yb,Er UCNPs, its practical applications are limited due to the weak emission intensity. Compared to the extensive studies on the Er co-doped UCNPs with the green and red emission, research on the Tm co-doped UCNPs with the blue and UV emission is still scarce. Although this thesis focuses on blue and UV emissions from $NaYF_4$:Yb,Tm UCNPs, the literature section includes a brief review of $NaYF_4$:Yb,Er UCNPs.

2.1.3 Nanocrystal synthesis

For tuning the UC emissions, nanocrystal synthesis is the crucial step, as it tailors the crystal size, chemical composition, morphology and optical properties. Powder phosphors prepared with solid state synthesis often suffer from inhomogeneous composition and morphology [55]. On the other hand, soft chemical routes, which have improved enormously in the past decade, overcome the above mentioned drawbacks and offer many outstanding advantages. For instance, the introduction of a ligand to the surface of the final product is much easier by this route. It also prevents the aggregation of particles by utilizing organic or aqueous dispersions. By changing various parameters like the temperature, solvent, reaction time, concentration, raw materials etc., it is possible to control the size and shape of the final product [56]. A variety of soft chemical methods have been developed to synthesize UCNPs with tunable sizes and shape, such as coprecipitation, thermal decomposition, hydrothermal synthesis; sol-gel processing and combustion synthesis, a few of them are discussed below.

Co-precipitation

Co-precipitation is perhaps one of the earliest and easiest approaches for synthesizing nano-sized lanthanide-doped UCNPs. This method for UCNP synthesis was first reported by Stouwdam et al. for LaF_3:Ln (Ln = Eu, Er, Nd, Ho) nanoparticles (NPs) using ammonium di-n-octadecyldithiophosphate assisted rare earths and fluoride ion coprecipitation [57]. Later, Yi et al synthesized $NaYF_4$:Yb,Er UCNPs by injecting an R-EDTA complex into a NaF solution, which resulted in α-$NaYF_4$:Yb,Er nanocrystals [58]. By varying the molar ratio of EDTA and rare earth ions, the particle size could be controlled. An annealing treatment was used to enhance the UC intensity.

Coprecipitation is less expensive, more simple and less time consuming than many techniques. Even though post heat treatment is typically required, in some rare cases, coprecipitation directly yields UCNPs, leaving out the need for post annealing.

Thermal decomposition

This method was first developed by Zhang et al. for the synthesis of monodispersed LaF_3 nanocrystals (NCs) via the thermal decomposition of lanthanum trifluoroacetate [59]. After its discovery the method has become the common route for preparing monodisperse and highly crystalline rare earth based NCs. The thermal decomposition method is an oxygen free organic synthesis involving the decomposition of precursors along with surfactants in high-boiling organic solvents. A combined solvent system i.e. octadecene with a high boiling point (315 °C) to provide the high-temperature, and oleic acid (OA) or oleylamine (OM), with polar capping groups which act as shape modifiers, were chosen for the synthesis [60]. This method allows the successful synthesis of α and β-$NaYF_4$:Yb,Er/Tm UCNPs, especially for the core-shell nanostructure.

The work of Zhang et al. involves the thermal decomposition of a single-source precursor i.e., $R(CF_3COO)_3$, providing both R^{3+} ions and a fluorine source, which makes the crystallization process easy to control. Although, the process is suitable for high quality UCNP synthesis, it is not environmentally friendly as the use of trifluoroacetate precursors generates the very toxic fluorinated and oxyfluorinated carbon species. Later, the nontoxic thermal decomposition method using a NaF and R-oleate complex was introduced for lanthanide doped $NaYF_4$ and $NaGdF_4$ NCs [61-63]. The morphology of the NCs can be tuned from nanoplates to nanorods to nanosphere by simply changing the NaF/R-oleate ratio or OA/ODE ratio. This method was further modified to synthesize the OA- coated β-$NaYF_4$ nanocrystals, where methanol solutions of NaOH and NH_4F were added to the homogeneous solution of RCl_3, OA and ODE [64, 65]. Haase et al. reported the synthesis of smaller UCNPs (5 to 30 nm), using methanol assisted N-(2-hydroxyethyl)ethylenediamine (HEEDA) solutions of Na^+, R^{3+} and fluorides. The reaction was carried out at a low temperature (180-200 °C) in an oxygen free environment [66, 67].

Hydro(solvo)thermal synthesis

Hydro (solvo) thermal reactions are performed in a sealed environment under high pressure and a temperature above the critical point of the solvent, whereas the traditional solvent method is limited by the boiling point. This important feature makes the solvothermal method more flexible. Special types of reaction vessels called Teflon-lined autoclaves are used for these kinds of sealed reactions. Even though targeted materials with different shapes can be prepared by the organic additive free solvothermal method, the addition of organic additives provides the most efficient way for achieving the precise and gradual evolution of morphology [68-70]. Additives used are either hydrophilic such as citrate, EDTA, PVP, CTAB and PEI or hydrophobic such as OA [3, 71-75].

In addition to the methods described, there are others, e.g. the sol-gel method which usually requires a long heating time of up to a few days, while the combustion method takes a few minutes, but the required temperature for the reaction is relatively high from 500 to 3000 °C.

2.1.4 Upconversion quantum yield and power dependence

Upconversion quantum yield (UCQY)

The quantum yield (QY) is a direct measure of the efficiency of the conversion of absorbed light into emitted light [76]. In the case of an upconversion, the QY is the ratio of the number of upconverted photons and the number of absorbed photons. The upconversion quantum yield (UCQY) gives a measure of the optical performance of UC materials. The product of the UCQY and the absorption coefficient (ε) at the excitation wavelength gives the brightness of the fluorescent material and determines the analytical performance of the material. The UCQY can be calculated using the following equation:[2]

$$UCQY = \frac{photon\ emitted}{photon\ absorbed}$$

$$\propto \frac{emitted\ UC\ \ intensity}{absorbed\ excitation\ light} = \frac{I_{UC}}{\varepsilon P}$$

where, P is the IR excitation power. The UCQY of the UCNPs depends on the power density; hence, it is important to determine the excitation power for the QY measurement. Usually, nanomaterials show lower QYs than their bulk counterparts. This is because of the higher surface related quenching in the nano-sized materials [76]. An integrating-sphere setup is generally used for the UCQY measurement [77].

The UCQY of a few UCNPs with their particle size and excitation power are listed in table 2. The highest QYs recorded for Er and Tm doped UCNPs are 3.6% and 7.6%, respectively, under an excitation power density of 127 W cm^{-2} [78]. It should be noted that for a high QY, a high excitation power is used, which is not suitable for *in vivo* bioapplications.

Table 2. Typical QYs of UCNPs along with particle size and power density. All values have been measured at a 980 nm NIR excitation unless otherwise noted [76].

UCNPs	Size (nm)	Power density (W cm^{-2})	QY (%)
$NaYF_4$:Yb,Er	30	150	0.1 ± 0.05
$NaYF_4$:Yb,Er@$NaYF_4$	100		0.3 ± 0.1
	30		0.3 ± 0.1
$LiYF_4$:Er	85	150 (1490 nm)	1.2
$NaLuF_4$:Yb,Tm	8	17.5	0.47 ± 0.06
$NaYbF_4$:Tm@CaF_2	27	0.3	0.6 ± 0.1
$NaYF_4$:Yb,Er	5.4	1000	0.0022
$NaYF_4$:Yb,Er@$NaYF_4$	9		0.14
	37		0.18
$NaYF_4$:Yb,Tm@$NaYF_4$	42	78	3.5
$NaGdF_4$:Yb,Er@$NaYF_4$	17	100	0.51 ± 0.01
$NaYF_4$:Yb,Tm	33	3.8	0.45
$NaYF_4$:Yb,Tm@$NaYF_4$	43	1.3	1.2
$NaGdF_4$:Er@$NaYF_4$	38	18 (1523 nm)	3.9 ± 0.3
$NaScF_4$:Yb,Er	20	60	0.02
	42		0.09
	115		0.61
$LiLuF_4$:Yb,Er	28	127	0.11
$LiLuF_4$:Yb,Er@$LiLuF_4$	40		3.6
$LiLuF_4$:Yb,Tm	50		5.0
$LiLuF_4$:Yb,Tm@$LiLuF_4$	28		0.61
	40		6.7
	50		7.6

Power dependence of UC luminescence intensity

In the upconversion mechanism, the upconversion intensity (I_{UC}) is related to the IR excitation power (P) by the following equation.

$$I_{UC} \propto P^n$$

where, n is the number of IR photons absorbed per visible photon emitted, and calculated from the slope of the fitted line of the plot log (I_{UC}) *versus* log (P). It was observed that the UC luminescence intensity increases with the excitation power, under lower excitation density. After the maximum, the slope of the upconversion luminescence intensity *versus* pump power decreases, indicating that the intensity of the upconversion luminescence saturates with the higher pump power [79]. A study of the power dependent behaviour of the upconversion intensity in Y_2O_3:Ho/Yb nanoparticles shows an increase in the intensity at power densities lower than 1 W/mm^2. At 1 W/mm^2, the UC intensity reaches its maximum and then continues to decrease with increasing power density [80]. Bai et al. correlate this behaviour to thermal quenching. According to them, at high excitation densities the strong absorption leads to an increase in the sample temperature at the irradiated area, which results in the thermal quenching of the UC luminescence [81].

2.1.5 Tuning of upconversion multicolour emissions

The ability of lanthanide doped UCNPs to emit at different wavelengths is particularly important in multiplexed bioimaging and multiplexed assays for the real-time tracking of multiple targets [82, 83] and parallel detection of multiple analytes [84, 85]. The emission colour tuning of UCNPs has been implemented by different strategies, a few of them are discussed here.

Using different combinations of lanthanide dopants and controlling their concentrations

Lanthanide dopants have their own set of energy levels, which emit at different wavelengths, covering a broad spectrum starting from UV light, extending through the entire region of visible light into the mid-IR region. Depending on the type of lanthanides and their combinations, the emission colour output can be tuned. The commonly used activators i.e. Er^{3+}, Tm^{3+} and Ho^{3+} in combination with a Yb^{3+} sensitizer emit at different wavelengths giving a multicolour output. Er^{3+} doped UCNPs have 3 distinct emission bands, 2 green (525 and 545 nm) and one red (660 nm), while Ho^{3+} ions have one green (541 nm) and one red (647 nm) emission. In case of Tm^{3+} ions, along with the major 800 nm NIR emission, another three UC emission bands are observed at around 475, 450 (blue) and 365 nm (violet). The choice of activators or different lanthanide combinations is a straight forward approach for multicolour emission tuning, e.g. colloidal suspensions of Yb-Er and Yb-Tm codoped $NaYF_4$ nanoparticles give strong yellow and blue emissions, respectively [26]. A series of multicolour upconversion nanocrystals ($NaYbF_4$:Tm (blue), $NaYbF_4$:Ho (green), $NaYbF_4$:Er (green and red) and $NaYF_4$:Yb (magenta)) was also reported by Ehlert et al.[52].

Efficient energy transfer between the sensitizer and the activator is a key factor in producing highly intense multicolour emissions. This energy transfer is more efficient if

the distance between the sensitizer and the activator is short; logically transfer improves when the activator concentration increases [86], but an excess of activators also leads to concentration quenching caused by non-radiative cross relaxation between adjacent activator ions [50, 87]. For example, in Yb-Er co-doped UCNPs, low Yb^{3+} doping favours the green emission, while an increase in the Yb^{3+} concentration enhances the $^4F_{9/2} \rightarrow {}^4I_{15/2}$ transition resulting in stronger red emission, which generates a yellow colour output [88]. Same trend was observed for elevated Er^{3+} concentration doping. The enhanced red emission was attributed to the cross-relaxation of $^4F_{7/2} + {}^4I_{11/2} \rightarrow {}^4F_{9/2} + {}^4F_{9/2}$ [89]. In α-$NaYF_4$:Yb,Tm nanoparticles, the increased Tm/Yb doping favors the $^1G_4 + {}^3F_4 \rightarrow {}^3H_4 + {}^3F_2$ cross-relaxation, which results in to the dominant 800 nm emission [50], while in β-$NaYF_4$:Yb,Tm nanoparticles the decrease in Tm^{3+} concentration shows enhancement in the emissions from the $^1D_2$ energy state over the $^1G_4$ energy state [90]. High Yb^{3+} doping populates the high-lying state, favouring the 4 photon over the 3 photon processes. In addition to the cross-relaxation, energy back transfer from the activator to the sensitizer also plays an important role in highly doped UCNPs. High Yb^{3+} doping decreases interatomic distances, which facilitates EBT and results in an enhanced red emission [50].

The appropriate selection of lanthanides, their combinations and doping concentrations generates a library of emission spectra, which has a wide range of applications including multiplexing.

Tuning the host matrix

The composition of the host material was discussed in section 2.1.1. An important function of the host matrix is to support the luminescent lanthanide ions. Besides the role of adoption, different host matrices may create various spatial distances, coordination numbers and energy transfer efficiencies and thus affect the UC emission. The luminescence intensity is sensitive towards changes in the host lattice. In addition, the different phonon energies of different hosts are also responsible for non-radiative relaxations through lattice vibrations.

The effect of the host matrix on the sensitivity of the UC emission in Yb^{3+}-Er^{3+} doped upconverting particles was investigated by Soukka et al. 2005 [91]. They observed a enhanced red to green emission ratio in oxides and oxychlorides compared to oxysulfides, fluorides and fluoride double salts. The Sc^{3+} ion-based $NaScF_4$:Yb/Er and KSc_2F_7:Yb/Er nanocrystals show the dominated red emission over the other visible emissions [92, 93]. In the orthorhombic crystal structure of Er^{3+} activated KYb_2F_7 nanocrystals, the rare earth ions are uniquely distributed in an array of tetrad clusters. This arrangement preserves the excitation energy in a sublattice domain and enhances the four photon process [94]. Like the visible emissions, also the UV emission of Tm^{3+} ions depends on the host matrix. For example, an intense UV emission can be obtained with Li or Gd doped $NaYF_4$ crystals [95, 96]. In addition, different phase structures of the $NaYF_4$ crystals i.e. cubic and hexagonal forms, also result in different colour outputs [60].

Introducing extraneous energy levels

Multicolour emissions originate from the different energy levels of the doped rare earths. For an intense emission, lanthanides or transition metal ions with abundant energy levels are usually used. They interact with each other and control the population of high-lying energy states. Various energy transfer pathways can be responsible for populating different energy states, such as simple upward energy transitions, cross relaxations and energy transfer from neighbouring dopants. The emission output can be tuned by doping different activators together. For instance, In $NaYbF_4$ based UCNPs, several activator combinations have been proposed e.g. Er-Tm, Er-Ho and Tm-Ho, where the emission output was tuned by simply changing their doping ratios [97]. In $NaYF_4$ based UCNPs, for the Yb-Er-Tm tridoped system, the increase in the Er doping tuned the emission output from blue to white [50], while in the Yb-Ce-Ho tridoping, the increased Ce doping concentration changed the emission colour from green to red [98]. Doping with multiple activators tailors the original emissions by introducing new emission bands.

In addition to multiple lanthanide activators, several transition metals such as Mn^{2+} and Mo^{3+} have been recently incorporated into UCNPs. The unique $^4T_1$ state of Mn^{2+} makes it a popular transition metal for tailoring the UC emission. The energy levels of Mn^{2+} lie at such a position in the $KMnF_3$:Yb,Er and $KMnF_3$:Yb,Ho and $KMnF_3$:Yb,Tm nanoparticles that the spectrally pure red emission from the Er^{3+} ($^4F_{9/2} \rightarrow {}^4I_{15/2}$) and Ho^{3+} ($^5F_5 \rightarrow {}^5I_8$) doped particles and the NIR emission from the Tm^{3+} ($^3H_4 \rightarrow {}^3H_6$) doped particles are possible [99, 100].

Luminescence resonance energy transfer

Energy transfers from the excited donor species to the nearby acceptor species either radiatively or non-radiatively. The energy transfer between two singlet fluorophores is called fluorescence resonance energy transfer (FRET), while luminescence resonance energy transfer (LRET) involves emission from lanthanides, which arises from 4f-4f transitions [101]. In LRET, after NIR irradiation, excited luminescent lanthanide doped nanoparticles transfer energy to nearby absorbing species (energy acceptors), which might be fluorescent or photosensitizing agents e.g fluorescent dyes, quantum dots or noble metals [2]. The UC emission from UCNPs can be absorbed by the spectrally matched energy acceptors.

UCNPs are popular donors in the resonance energy transfer process because of their sharp emissions, long luminescence lifetime and large anti-Stokes shift. Different colour emissions can be generated by selecting different energy acceptors in combination with the UCNP donors e.g. different concentrations of gold NPs can be used in combination with $NaYF_4$:Yb,Er to tune the green emission from Er^{3+}[8]. LRET from UCNPs to organic acceptor dyes, including fluorescein isothiocyanate (FITC) and tetramethylrhodamine isothiocyanate (TRITC) encapsulated into the surface coating outside of the UCNPs was successfully used to generate a multicolour emission [102].

2.1.6 Architecting UCNPs for high emission intensities

The synthesis of UCNPs with enhanced UC luminescence has always been an interesting and challenging topic of research, which is fuelled by the potential applications of UCNPs in many research fields. The advantages of UCNPs over fluorescent dyes and quantum dots, make them superior bioimaging tools. However, the low brightness levels of the UCNPs still limit their applicability. Thus studies on enhancing the UC emission to achieve the exceptionally high sensitivity required in diagnostics are necessary [103]. Several efforts have been made to achieve an intense UC emission, for instance, tuning of the local crystal field, plasmonic enhancement, architecting nanoparticle structure and prevention of surface quenching.

Tailoring the crystal field

4f-4f intra-configurational transitions are parity-forbidden in lanthanides, but they become partially allowed when *4f* states are intermixed with higher electronic configurations by embedding them in an inorganic lattice. Once the host lattice is fixed it is difficult to change the crystal field around the lanthanide ions. One possible way of tailoring the crystal field around lanthanides is the intentional doping of optically inert ions, usually cations with different sizes and valence states are considered [5, 104]. These doped non-luminescent ions occupy both the substitution as well as interstitial positions in the crystal lattice. Substituted ions disturb the local symmetry and change the crystal field, which results in an enhanced UC efficiency. Such a tailoring process changes the spatial distances in the dopant ions and generates different energy transition probabilities.

Several alkali ions and transition metals are used for the regulation of crystal fields e.g. Li^+ ions are most frequently used for this purpose as they have a small ionic radius and are located randomly at the crystal sites. The Li^+ doping successfully enhances the UC efficiency in oxide based UCNPs by two orders of magnitudes [5, 105, 106]. The tailoring of the crystal field has been confirmed by shifts in the diffraction peaks. Along with Li^+, there are reports of UC enhancement by doping K^+ in $NaYF_4$:Yb,Er nanocrystals [107]. The different ionic radii of Li^+ and K^+, compared to Na^+, affect the crystal structure, the spatial distance between luminescent centers and subsequently the UC emission. In Gd_2O_3:Yb,Tm nanocrystals, up to 10-fold enhancement in the blue emission was observed with a 6% Li^+ co-doping [108].

Besides alkali ions, transition metals such as Fe^{3+}, Pb^{2+} and Bi^{3+} have also been used to tune the local crystal field, e.g. doping Fe^{3+} into β-$NaGdF_4$:Yb,Er nanocrystals enhances the green and red emissions [109], while increasing the Bi^{3+} concentration in Zn_2SiO_2, lowers the local symmetry and enhances the UC intensity up to 20 fold [110]. In addition, also a few post-transition metals, such as Sn^{2+} and Pb^{2+}, have been successfully used for crystal field tailoring [111, 112]. Even though the UC luminescence is remarkably enhanced by doping with nonluminescent ions, evidence for crystal field

tailoring is lacking. Extended x-ray absorption fine structure (EXAFS) spectroscopic investigation of the lanthanide environment can be useful for that purpose.

Nanoparticle size and structure

The optical properties of UCNPs can be modified by manipulating their particle size and structure [113, 114]. A small nanoparticle size can lead to a number of desirable properties: small particles can have good colloidal stability and be easy to process, which makes them very useful in the fields of biology and energy [2, 115]. The reduced particle size of the UCNPs can alter the lifetime of the intermediate states of the doped ions [57, 116]. Compared with bulk materials, the doped rare earths in the nanoscopic region can lead to the generation of new types of photoemission [94]. Even though the upconversion mechanism is same in bulk and nanoscale materials, the ion-ion and ion-lattice interactions can be tuned in various degrees in the nanomaterials. Capobianco et al. studied the size dependent UC emission properties in Y_2O_3:Yb,Er nanoparticles and observed the enhanced red emission with a decrease in particle size [88]. The luminescence intensity ratio of the different emissions can also be tuned by varying the particle size. For example, the red–to-green emission intensity ratio can be increased by decreasing particle size from 45 nm to 6 nm [116]. However, smaller nanoparticles possess a higher surface to volume ratio and are more susceptible to surface quenching compared to larger ones [117]. The surface quenching can be minimized by core shell formation.

Apart from size, the structure of the nanoparticle also has profound effect on the UC properties. For example, in $NaYF_4$ particles, the hexagonal phase nanocrystals (β-$NaYF_4$) show a higher UC efficiency than their cubic counter parts [32, 118]. The morphological influence on the UC emission was reported by Ding et al.[119]. In their experiments, the β-$NaYF_4$:Yb,Er NPs with six different morphologies (microprisms, microtubes, microsphere, microrods, micro-pyramids and microplates) were synthesized by a hydrothermal process. Among all of the morphologies, the microprisms showed the highest UC emission intensity. This significant UC enhancement in the microprisms was due to the smallest surface area and high crystallinity without visible defects and dislocations.

Constructing core/shell structure

The UC efficiency decreases with particles size which is due to the high surface to volume ratio at the nanometer dimensions. The lanthanides in the UCNPs are subjected to many surface deactivations like surface defects, lattice strain or surface ligands with high-energy vibrational modes [116]. The most often used high sensitizer concentration (Yb^{3+}) leads to long distance energy migration from the center to the surface of the particle through adjacent dopant ions and decreases the UC efficiency. A typical way of reducing these energy losses is by coating the surface of the UCNPs [120]. There are two types of core/shell structures commonly used for UC luminescence enhancement.

Shell without dopants: This is a simple and very effective way to minimise surface related quenching. In this kind of a core shell, the shell and the host material of the core particles are identical (Figure 4b). The enhancement in the UC intensity by the formation of an un-doped core on the $NaYF_4$ core particle was demonstrated by Yi and co-workers [121]. Their conclusions were later verified by different reports; e.g. it was observed that $NaYF_4$:Yb,Er@$NaYF_4$ UCNPs show a three times higher quantum yield than that of core $NaYF_4$:Yb,Er particles [122]. A notable UC enhancement has also been observed in $NaGdF_4$:Yb,Er@$NaGdF_4$ [123], SrF_2:Yb,Er@SrF_2 [124], $KGdF_4$:Yb,Tm@$KGdF_4$ [125] etc. It has been demonstrated that the un-doped core shell structure reduces surface quenching and improves the UC emission efficiency. As the shell is made up of same composition as core, it is difficult to show direct evidence of their existence. The core/shell formation is often confirmed by enhanced emissions, increased particle size or decay of the UC luminescence. There are also reports of UC enhancement by having different shell composition than those of the core host e.g. core/shell $NaYF_4$:Yb,Tm/Er@$NaGdF_4$, where the doped Gd in the shell allows MRI properties [126, 127]. The efficient generation of NIR to UV enhancement from α-$NaYF_4$:Yb,Tm@CaF_2 is also one of the recent examples [54].

Shell with dopants: Like the shell without a dopant, the sole role of a shell with dopant UCNPs is to enhance the UC luminescence. The only difference is that the shell contains optically active centres (mostly sensitizer, Figure 4c). This strategy has three important roles; i) lanthanides in the shell interact with the luminescence centres in the core, resulting in the enhancement of the luminescence, ii) surface related quenching is reduced and iii) multicolour emissions can be generated with a different activator doped shell. Significant enhancement in the visible UC and the suppression of surface related deactivation was obtained by synthesizing $NaGdF_4$:Yb,Er@$NaGdF_4$:Yb active core/active shell nanoparticles [120]. Along with an increased UC intensity, the multicolour emission was also tuned by Zhang et al. who created the core-shell-shell structure by doping two different activators i.e. β-$NaYF_4$:Yb,Tm@β-$NaYF_4$:Yb,Er@β-$NaYF_4$:Yb,Tm [128].

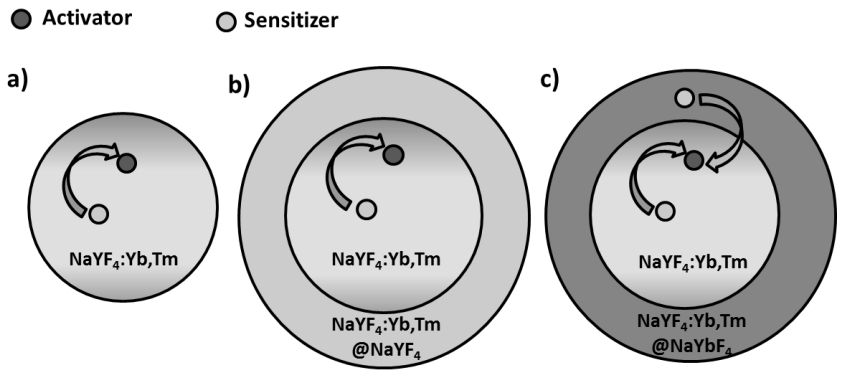

Figure 4. Schematic illustration of the a) core UCNPs ($NaYF_4$:Yb,Tm) b) shell without dopant ($NaYF_4$:Yb,Tm@$NaYF_4$), c) shell with dopant ($NaYF_4$:Yb,Tm@$NaYbF_4$), strategies for enhancing luminescence.

Plasmonic enhancement

Surface plasmon resonance (SPR) is the resonant oscillation of electrons at the interface of metallic structure stimulated by the incident light of a specific wavelength [129, 130]. The fluorescence enhancement of the adjacent fluorophore (dyes or QDs) by the SPR of a metallic structure is already known, and it can be used, in the same way, for UCNPs, when the distance between the fluorophore and the metallic surface is appropriate. Mostly, noble metals (Ag and Au) are used for this purpose. The interaction between the UCNP and the metallic surface can be investigated in three ways: i) Deposition of the UCNPs on the metallic surface, such as a gold island [131], metal nanoparticles [132] or a 3D plasmonic antenna [133]. This method can enhance the luminescence of the UCNPs upto ~300 fold. The most challenging part of this method is to maintain the distance between the UCNP and the metallic surface. ii) Attachment of metallic nanoparticles to the UCNP surface. After the surface modification of the UCNPs, the water dispersible UCNPs carrying the positive charge attract the negatively charged metallic nanoparticles towards their surfaces [134]. The $NaYF_4$:Yb,Er NPs attached with gold nanospheres shows a 3.8 fold enhancement in the UC [135]. iii) Core/shell formation of UCNP/silica/metal or metal/ silica/UCNP [136]. The distance between the UCNP and the metallic surface can be controlled by changing the thickness of the spacer silica layer. The core/shell approach enhances the upconversion luminescence by 4-10 folds.

2.2 Surface engineering

Nowadays, UCNPs have garnered more attention as biomarkers in biolabeling experiments due to their numerous potential advantages over the biolabels currently used. In order to use UCNPs in biological applications, their surfaces need to be modified post synthesis. UCNPs as such are hydrophobic and are only dispersible in nonpolar organic solvents. Thus, the post-synthesis surface engineering of UCNPs is important for a) their protection from surface related quenching, b) functionalization for allowing different chemical functionalities to bind on the surface as well as transfer the hydrophobic UCNPs to the hydrophilic phase, c) conjugation with biomolecules and d) for biocompatibility [137].

2.2.1 Surface functionalization

For the suppression of surface related deactivation and to make the UCNPs water dispersible and chemically functional, several strategies have been used such as a ligand oxidation reaction, ligand exchange, encapsulation of UCNPs with a polymer shell (ligand interaction) and surface silanization.

In the ligand oxidation reactions, the oleic acid (OA) ligands, which contain unsaturated bonds (-C=C-), on the UCNP surface can be directly oxidised into hydrophilic azelaic acids ($HOOC(CH_2)_7COOH$) by using the Lemieux-von Rudloff reagent containing periodate and permanganate (Figure 5a) [138]. The OA ligand can also be oxidised into azelaic acid or azelaic aldehyde using a strong oxidant and readily available ozone [139]. The advantage of this method is that the oxidised azelaic acid on the UCNP surface has one free carboxylic acid group, which allows further conjugations. Drawbacks of the ligand oxidation method are a long reaction time and low yield [140, 141].

Ligand exchange is another effective approach for replacing the hydrophobic surfactants by a hydrophilic phase (Figure 5b). UCNPs are commonly capped by OA or oleylamine (OM) ligands, which bind to the lanthanides by carboxylic (-COOH) or amino ($-NH_2$) groups, respectively. The efficient exchange of the OA ligand is made possible by using hydrophilic ligands, which have a strong coordination ability towards the lanthanides, for example, poly(acrylic acid) [126, 142], poly(ethylene glycol) (PEG) [143], mercapto succinic acid (MSA) [144] and mercaptopropionic acid (MPA) [145]. In case of a weakly bound OM, ligands like poly(ethylene imine) PEI [146] and PEG-diacid [147] can be used. Even though the process is simple, the weak interaction of the surface ligands with nanoparticles makes it suffer from poor colloidal stability in physiological conditions [148]. Recently, an exceptionally simple strategy for the preparation of DNA-modified UCNPs was reported by Li et al, based on the ligand exchange at the liquid-liquid interface [149]. In their report, hydrophobic UCNPs were converted in to hydrophilic DNA-UCNPs, with just mixing UCNPs and oligonucleotides together, without any surface modification.

An amphiphilic polymer layer is used for UCNPs to provide water solubility. The hydrophobic part of the amphiphilic polymers reacts with the hydrophobic surface ligands of the particles due to van der Waals interactions leaving the hydrophilic group of the polymer outside making the nanoparticles water-dispersible (Figure 5c). The amphiphilic polymers used for this purpose include (OA-PAA-PEG) [150] and poly(maleic anhydride-*alt*-1-octadecene) (PMAO) [151]. Even though the amphiphilic capping keeps the UCNPs dispersed in water for several days, these polymers become detached from the particle surface in a few hours when dispersed in physiological buffers. The irreversible detachment might come from the presence of salt in the buffer. Zhang et al. recently reported a click chemistry route for forming functionalizable hydrophilic nanocrystals [152].

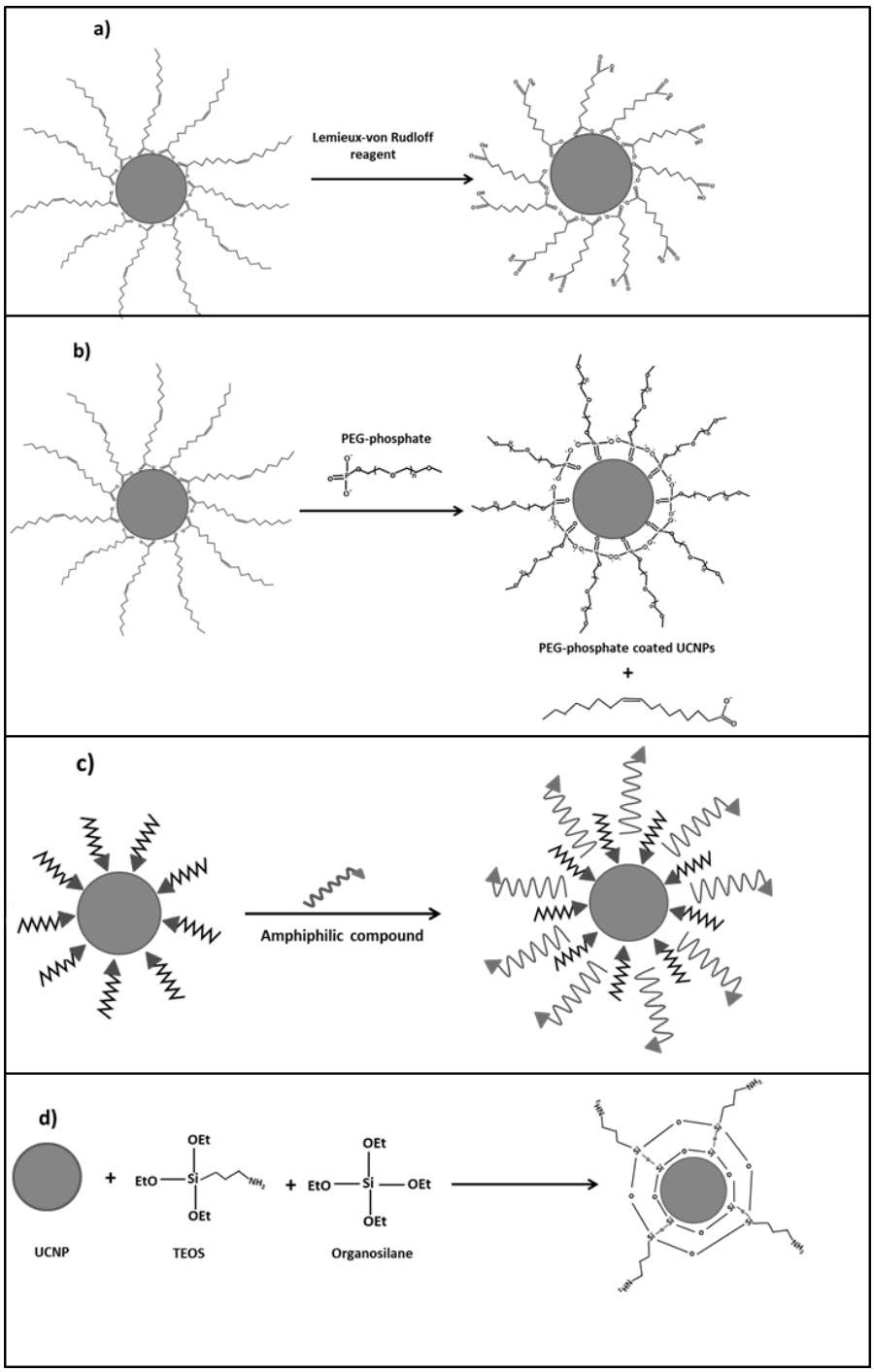

Figure 5. Schematic illustration of the strategies for solubilization and functionalization of UCNPs: a) Oxidation of an oleic acid ligand with the Lemieux-von Rudloff reagent, b) ligand exchange reaction of oleate coated UCNPs with PEG-phosphate, c) ligand interaction and d) silica-encapsulation (modified from Sedlmeier et al., [137]).

Recently, Beyazit et al. developed a new strategy for coating UCNPs with a polymer shell (polyhydroxyethyl methacrylate) using the UCNPs themselves as an internal light source [9]. In their experiments, the ultraviolet or visible light emitting UCNPs were mixed together with the initiators (whose absorption wavelength overlapped with the emission wavelength of the UCNPs) and functional monomers. After 980 nm excitation, the UV or visible emissions of the particles initiate the photopolymerization and form a thin polymer shell around the particles. By incorporating different functional monomers in to the shell, the method provides possibilities for large surface chemistries for functionalization.

The most frequently used method for inorganic surface treatment is surface silanization (Figure 5d) [153-155]. Silica is regarded as highly stable, biocompatible and optically transparent. The silanization method offers abundant functional groups (e.g. -SH, -NH_2, -COOH, etc.) for the further conjugation of biomolecules. The Stöber method is the most commonly used method for silica coating [156]. In this method, UCNPs with hydrophilic surfaces are mixed with an excess of water containing ethanol, ammonia and tetraethyl silicate (TEOS). A thin, uniform silica shell can be obtained by this method [157]. In case of hydrophobic UCNPs the reverse microemulsion strategy is preferred [158]. The method is based on a mixture of UCNPs, an acid or base catalyst (mostly NH_4OH), surfactants (e.g. Igepal CO520) and TEOS [159, 160].

2.2.2 Bioconjugation

The surface modification of the UCNPs makes the particles compatible with water. However, bioconjugation of the UCNPs means that a variety of functional biomolecules can be attached to the UCNP surface, which is required for their use in bioanalytical applications. Basically, the interaction of biomolecules and the UCNP surface involve two methods a) the physisorption of biomolecules by noncovalent interactions and b) covalent coupling.

Physisorption is a very simple method where biomolecules are attached to the nanoparticle surface by noncovalent forces [144]. The main advantage of this method is that the quantum yield of the UCNPs and the reactivity of the protein do not change after bioconjugation. Disadvantages include non-specific binding and limited stability of the conjugates in the assay and under storage conditions. The physisorption can be further modified by using cross-linkers, which bind to the UCNP surface by noncovalent forces and form conjugates with the biomolecules through chemical coupling. Streptavidin or toxic proteins can be bound using cross-linkers [161, 162].

Covalent conjugation is the more favoured method and involves the chemical reaction between the functional groups on the UCNP surface and the biomolecules. In surface modification, many functional groups (e.g. –NH_2, -COOH or maleimide) are introduced to the nanoparticle surface. This creates covalent binding sites for biomolecules, e.g. the carboxylic acid groups on the UCNP surfaces are activated by EDC and N-

hydroxysulfosccinimide sodium salt (sulfo-NHS), which can react with the $-NH_2$ group of the biomolecules and form a stable amide bond [163]. Similarly, the reaction between the thiol and maleimide groups produces a stable thio-ether bond while aldehyde (derived from the oxidation of a carbohydrate) and a hydrazide group form a hydrazide bond.

Click chemistry is another useful strategy for conjugation, which involves the Cu^+-catalysed 1,3-dipolar cycloaddition of an azido group to the terminal alkyne group [164-166].

2.3 (Bio)Analytical applications

Due to high sensitivity and fast detection, fluorescence based bioanalytical measurements are widely used in many fields such as bioimaging, physiological process monitoring and chemical analyses [167, 168]. Due to the unique NIR excitation, lanthanide based UCNPs are emerging as a new class of optical probes for bioimaging, and hold great potential for overcoming the drawbacks associated with organic dyes, fluorescent proteins and QDs [169]. Besides bioimaging, UCNPs find promising applications in diverse applications; for example, solid-state lasers [33], optical data storage [170], solar energy conversion [171-173] and photodynamic therapy [2, 174]. Since the application of UCNPs is a wide topic, only a small part of it is discussed here.

2.3.1 Luminescent sensors

Temperature sensor: Accurate temperature measurements are important in many cellular processes. For examples, the gleaning of temperature changes in a single living cell leads to novel insights about cellular pathology and physiology [175, 176]. Aside from the conventional thermometry, where an electric wiring is required, an alternative methods for temperature sensing using fluorescent nanoparticles, especially lanthanide based fluorescent materials have attracted much attention [177, 178]. The ability of UCNPs to emit at higher energies after NIR excitation and their minimal interactions with the cellular material makes them biocompatible temperature probes. The intensity ratio of the emissions at 520 nm ($^4S_{3/2} \rightarrow {}^4I_{15/2}$ transition) and 550 nm ($^2H_{11/2} \rightarrow {}^4I_{15/2}$ transition) of Er doped UCNPs is sensitive to temperature changes, for example, at low temperature, the intensity of 520 nm is higher than the 550 nm emission, but this inverts when the temperature is higher [179, 180]. In addition to this, the temperature sensing using UCNP size, dopant concentration and core/shell structure is also reported where core/shell $NaYF_4$:20%Yb,2%Er UCNPs are found to be more suitable [181]. Recently, a low temperature sensor based on the $^4D_{7/2}/{}^4G_{9/2} \rightarrow {}^4I_{15/2}$ transitions (UV emission) in Yb-Er codoped $NaLuF_4$ nanocrystals was also reported [182].

Gas sensor: Oxygen and other gases are essential for almost all living systems. The determination of the oxygen, carbon dioxide and ammonia concentrations in gaseous and aqueous samples is of a great significance in many research areas [183, 184]. UCNP based gas sensors are extensively used because of their outstanding properties. Achatz et al. were the first to present an UCNP based oxygen sensor, where $NaYF_4$:Yb,Tm NPs were used as the light source, and iridium (III) complexes as the oxygen indicator [185]. Although, UCNP emissions are inert to the oxygen, the fluorescence produced by the iridium (III) complex due to LRET/FRET from UCNPs is dynamically quenched by oxygen. A bi-functional nanocomposite sensor, based on $NaYF_4$:Yb,Tm NPs and a Ru(III) complex doped SiO_2 shell was also developed for precise detection of oxygen concentration [186]. In addition to this, concentrations of other gases like carbon dioxide and ammonia can also be estimated using UCNPs. $NaYF_4$:Yb,Er NPs in combination with bromothymol blue and phenol red were successfully used for sensing CO_2 and ammonia, respectively [187, 188].

pH sensor: pH monitoring is an important task in many research fields, such as biotechnology, environmental sciences and medicine, the development of sensitive pH sensors is of great importance [189]. Optical sensors are based on changes in optical properties with a changing pH. A pH sensor using $NaYF_4$:Yb,Er NPs and bromothymol blue (BTB) was constructed by Sun et al for studying deeper regions in tissues, where the absorption spectra of BTB changes with pH and also partially overlap with the visible emissions of the UCNPs [190]. UCNP based pH sensors allow the use of NIR light for photoexcitation. The changes in the visible emission intensities were monitored. Very recently, background free pH sensing with a simple readout technique was reported which includes a pH sensing film made up of UCNPs and a pH indicator and a colour camera read-out [191]. The simple, hand-held and cheaper sensor setup allows its use in point-of-care measurements. The advantages of using fluorescent pH sensors include highly sensitive, remote measurements without a reference element enabling contactless sensing. Such methods can be applicable even in strong magnetic fields.

Ion sensor: The most toxic ions such as cyanide ions (CN^-) or mercuric ions (Hg^{2+}) cause serious environmental and health problems. Therefore, the selective detection and quantification of these ions has received much interest. As was discussed above, UCNPs have several advantages, which make them popular tools for biosensing. As, the UCNPs shows inert response to the metal ions, they are usually used in combination with the suitable organic indicators. Emissions from the UCNPs are used as the excitation source for the dye molecules *via* the FRET/LRET process; the fluorescence intensity from the dye molecules is then sensitive to the metal ion concentration. In separate reports, Li et al. presented the chromophoric iridium(III) complex- and ruthenium complex- coated $NaYF_4$:Yb,Er,Tm UCNPs for CN^- and Hg^{2+} ion sensing respectively [192, 193].

In addition to the sensing applications listed above, UCNP emissions can also be used for monitoring enzymatic reactions. For instance, Wilhelm et al. demonstrated the visible (475 nm) and UV (360 nm) emissions from Tm doped UCNPs for the detection of FAD

(Flavin adenine dinucleotide) and NADH (Nicotinamide adenine dinucleotide), which are involved in many enzymatic reactions [194].

2.3.2 Bioaffinity assays

A bioaffinity assay is an analytical tool for measuring the presence or concentration of biomolecules. It plays an important role in point-of-care tests. Luminescence based bioassays are more convenient compared to traditional enzyme based assays because of their high sensitivity and fast measurements [195-197]. UCNPs with desired properties, such as no background signals and inertness for the assay environment make them popular among all of the luminescent bioprobes. Bioassays are divided into two categories depending on the measurement format a) heterogeneous assay and b) homogeneous assay.

Heterogeneous assay: Heterogeneous assays utilize a capture molecule, which is immobilized on the substrate with a high binding affinity for the analyte and the labels for the detection signals [76]. The heterogeneous assay requires multiple washing steps to separate the unbound species before the final measurement step. They are further classified into sandwich or noncompetitive assay and competitive assay. In the sandwich assay, first the capture molecule is immobilized on the substrate, and then the analytes are allowed to conjugate to the captures, followed by a washing step to remove the unreacted species and to avoid a negative effect on the measurement. After washing, the UCNP-labelled capture molecule is added which binds to the analyte. After washing off the excess UCNP-labeled captures, the luminescence measurement gives the concentration of the bound labeled UCNPs which is proportional to the analyte (Figure 6a). In the competitive assay, the competition between the analyte and the UCNP-labeled analyte to anchor on the immobilized capture molecule is used to determine the concentration of the analyte which is inversely proportional to the UCNP signal (Figure 6b). Heterogeneous assays are usually more sensitive compared to separation free homogeneous assays.

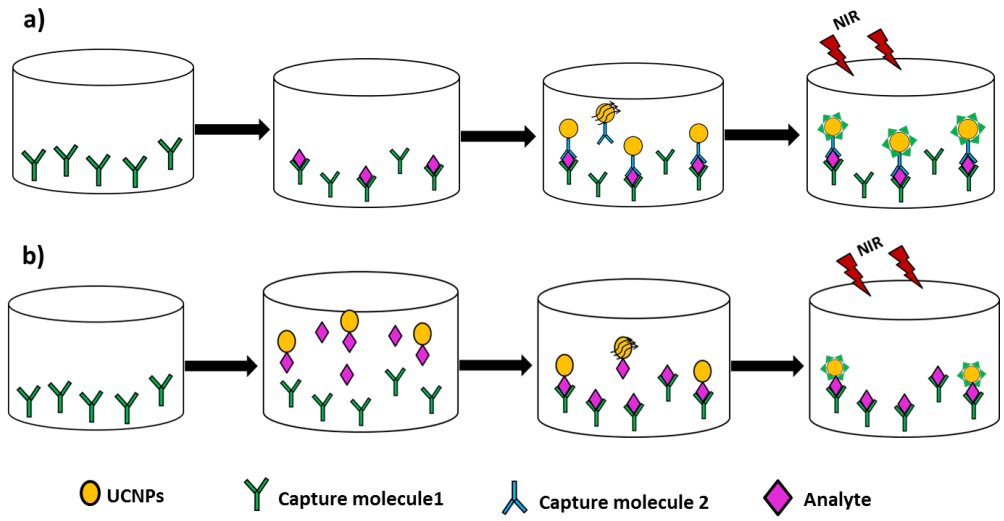

Figure 6. Schematic illustration of typical heterogeneous assays based on upconverting nanoparticles a) sandwich assay and b) competitive assay (modified from Zheng et al.,[76]).

The upconversion luminescence based bioassay was first reported by Zijlmans et al. for the detection of prostate-specific antigens [198]. Since then, many efforts have been made to use UCNPs in different heterogeneous assay techniques such as DNA microarrays, lateral flow assays, microplate assays etc. DNA microarrays using biotinylated Y_2O_2S:Yb,Er for the detection of nucleic acid hybrids gave a better LOD score than the conventionally used probe cyanin 5 [28]. UC microbarcodes based on $NaYF_4$:Yb,Ho,Tm UCNPs in combination with organic dyes can be used for rapid and sensitive analysis of the nucleic acids [199]. A lateral flow (LF) immunoassay is another form of a heterogeneous assay which is more popular due to its suitability for the field use or in point-of-care testing [200]. The simple pregnancy test is a well-known example of this assay. The LF test strip consists of several zones made of different materials (Figure 7). The sample is added on the sample pad which moves through the rest of the strip by capillary action. The applied sample first passes through the conjugate pad to bind with the coloured labels for visual readout. The sample then moves over the nitrocellulose membrane with one or more test lines which contain antibodies specific to the target analytes. One additional control line in order to confirm the correct assay performance is also marked at the end of test lines. LF assays of either the competitive or sandwich type have been used for the detection of nucleic acids, pathogenic microorganisms, cytokines etc.[201-210]. LF assays based on UC were used for the simultaneous detection of amphetamine, methamphetamine, phencyclidine and opiates in saliva [211].

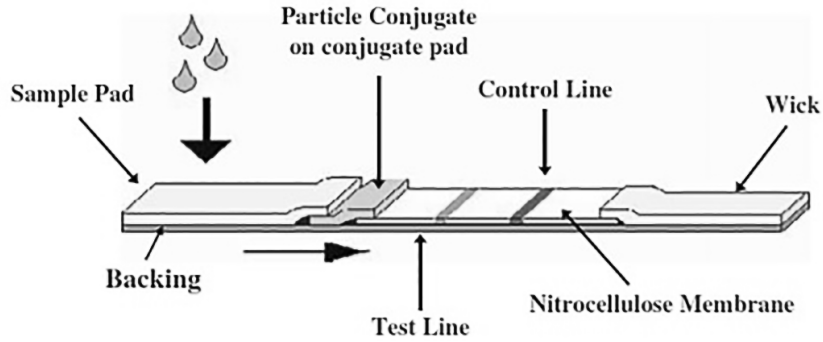

Figure 7. Standard layout of a lateral flow device [212].

Homogeneous assay: The basic principle of the homogeneous assay relies on energy transfer from an energy donor (UCNPs) to a nearby acceptor through dipole-dipole interactions as an indication of a binding event [213, 214]. The acceptor mostly has a high absorption coefficient at a wavelength which can be matched with the emission wavelength of the donor. Example of acceptors include, organic dyes, fluorescent proteins, QDs, carbon nanotubes, graphene and graphene oxides [140, 215-219]. The important conditions for this type of assays are i) the overlapping of the absorption spectra of the acceptor and the emission spectra of the the donor as well as ii) the close proximity of the acceptor and the donor [220]. The emission from the donor excites the acceptor molecules via fluorescence resonance energy transfer (FRET) or lanthanide resonance energy transfer (LRET). Förster (1948) first discovered the resonance energy transfer (RET) in fluorophores, which was then applied for lanthanides, termed as LRET. The efficiency of the LRET process is distance dependent and becomes inefficient for the donor and acceptor with more than a 10 nm distance. The homogeneous assays are separation free, simple, one step, “mix-and-read” assays, for fast detection and automation.

After the introduction of UCNPs into homogeneous assays in 2005 [8], many methods for UC based FRET bioassays have been reported. Kuningas et al. developed a LRET based homogeneous assay using streptavidin coated UCNPs as donors and biotinylated phycobiliprotein as the acceptor [218]. Subsequently, Rantanen et al. reported the design of homogeneous assays for the detection of multiple analytes using multiple emission peaks of the UCNPs [142]. In both of these studies large UCNPs were used. Later, nanosized UCNPs, bound covalently to an oligonucleotide were used as donors in a sandwich assay for the detection of target DNAs with single-base mismatches [221-223].

In UC-FRET based sandwich assays, the donors (UCNPs) and acceptors are attached as labels to the capture molecules, which detect the analytes (Figure 8a). UC-FRETs with a large number of donor-acceptor pairs are known, for instance, human IgG labeled with

UCNPs as the donor and a rabbit anti-goat antibody labelled with Au NPs as the acceptor for the detection of goat anti human IgG, or streptavidin labelled with UCNPs as the donor and DNA-TAMRA as the acceptor in the DNA sensors [140, 224]. UC-FRET can also be performed by the inhibition of the energy transfer process, where the luminescence of the donor UCNPs is quenched by the acceptor dye; the analyte cleaves the linkage and recoveres the UCNP emission (Figure 8b). For this purpose, UC quenchers such as manganese dioxide (MnO_2), carbon NPs and graphene oxides are frequently used [217] [225].

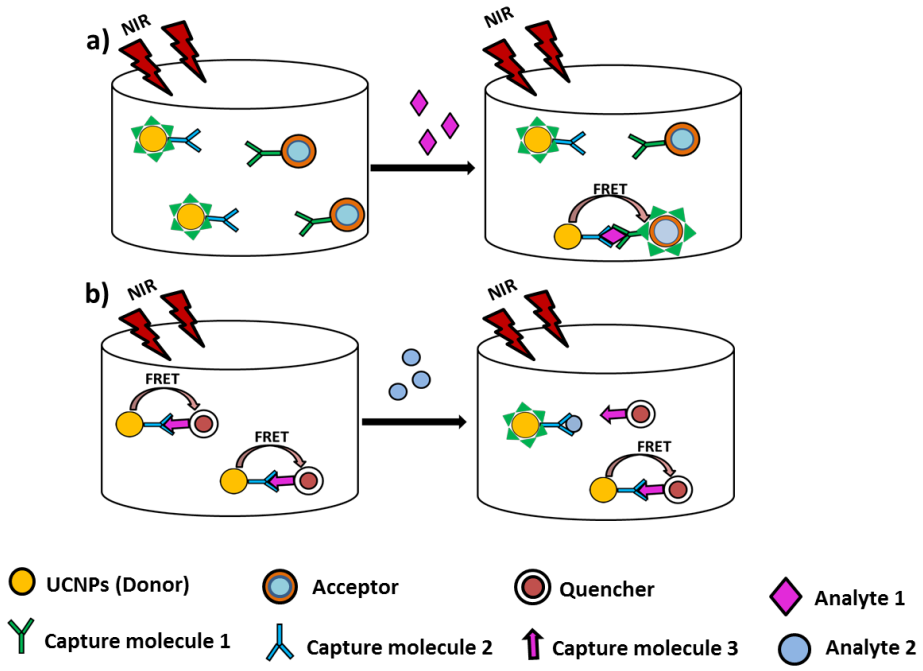

Figure 8. Schematic illustration of typical homogeneous UC-FRET assays based on upconverting nanoparticles: a) sandwich assay and b) inhibition assay (modified from Zheng et al.,[76]).

2.3.3 Multiplexing

Multiplex technology has allowed the simultaneous visualisation of more than one target. It captures several events in a single snapshot, which reduces the amount of reagents, consumables and samples required, also reducing the reaction time and minimizing sample errors [226]. Multiplexed sandwich assays are the most advanced assays among all protein array based assays [227]. Recently, the highly significant optical properties of the upconverting nanoparticles to overcome the limitations of conventional labels, comes in to trend [167]. UCNPs offer higher sensitivity for tracing minute amount of samples due to an improved signal-to-noise ratio. In UCNP based multiplexed assays, crosstalk between the excitation and emission light can also be significantly reduced. Multicolour emission of the UCNPs at a single wavelength

excitation (NIR) allows the simultaneous detection of a large number of analytes or analyte concentrations.

The multiplexed assays are divided into planar and suspension microsphere arrays based on the choice of support (Figure 9). In the suspension multiplexed assays, internally dyed microspheres of about 5.3µm diameter are used as a solid support for the covalent coupling of different capture ligands [228]. The analytes bound to the capture ligands are detected by the use of a spectrally compatible reporter fluorophore. For protein identification, microspheres use classifiers such as size or an internal fluorophore. Flow cytometric principles are used to generate the results. In the serological applications, commercially available SeroMAP™ microspheres with 100 different colour sets are used which are formulated to reduce the nonspecific bindings [229]. Magnetic bead-based suspension arrays are also used for multiplexed assays because of its easy separation steps [230]. The advantages of multiplexed suspension assays include improved precision due to multiple independent measurements, shorter incubation time, easy automation and less sample requirement [7]. There are many reports of using bead suspension arrays for the multiplexed detection of the infectious diseases, for example, in the detection of different respiratory viruses [231], identification of gastroenteritis causing viruses [232] and also for the detection of the influenza virus antibody [233].

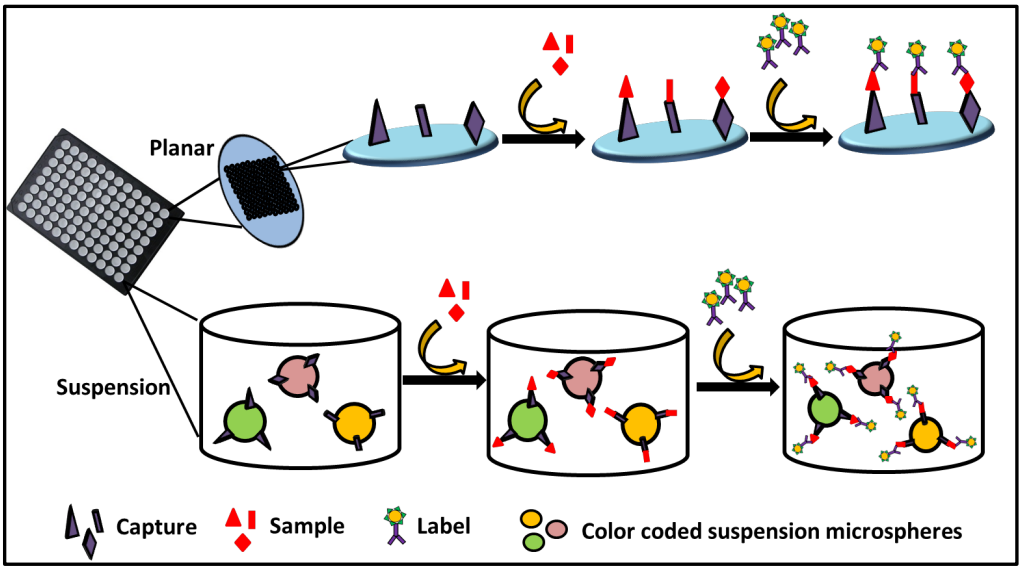

Figure 9. Planar and suspension array formats.

In the planar arrays, capture ligands are immobilized on a rigid support (either a slide or a microtiter well), and each recognising a different analyte. The analyte can be detected with fluorescent labels, enzyme labels or by electrochemical detection [234-236]. The arrays are printed in rows and columns using an array printer. The

advantages of planar arrays, such as the requirement of a single label only and simple instrumentation due to a single excitation source, make them the more frequently used technique compared to suspension arrays. Recently, Ylihärsilä et al. developed the UCNP-based oligonucleotide array-in-well assay for the detection of human adenoviruses [158]. Also, a quantitative multianalyte immunoassay utilizing UCNPs on an antibody array-in-well platform was demonstrated by Päkkilä et al. for the PSA, TSH and LH analytes [237]. In both experiments, biotinylated antibodies for multiple analytes were printed in an array format onto the bottom of the well, the analyte dilutions were added to the well and then the performance of the assay was measured by mixing in UCNPs coated with secondary antibodies.

3 AIMS OF THE STUDY

The overall aim of the study was to synthesize blue and UV emitting UCNPs with improved brightness and to investigate their applications in clinical diagnostics. As the emission intensity of the UCNPs is highly sensitive to the local environment of the doped lanthanides, different strategies were used to change the symmetry around the lanthanides, such as non-luminescent ion co-doping in the host matrix or excessive sensitizer doping. The optical and morphological properties of the modified, highly luminescent UCNPs were studied with different characterization techniques. The feasibility of the blue and UV emitting UCNPs in point-of-care testing was investigated

More specifically the aims were:

1. To enhance the blue upconversion luminescence in the hexagonal $NaYF_4$:Yb,Tm by the stepwise doping of non-luminescent ions (K^+ or Sc^{3+}) in the host lattice and to investigate the effect of this on the size, shape and structure of the crystal and on the luminescence intensity of the UC.

2. To synthesize $NaRF_4$:Tm UCNPs with intense UV emission. For this purpose a high sensitization (Yb^{3+}) route was developed. In addition, the concentration of the activator (Tm^{3+}) was optimized for obtaining brighter UV emitting UCNPs. The effect of the sensitizer and activator concentrations on the morphological and optical properties of the nanocrystals was also investigated.

3. To demonstrate the feasibility of IR-excited UV-emitting UCNPs as an internal light source in glucose sensing dry chemistry test strips.

4. To develop an array-in-well assay for spectral and spatial multiplexing utilizing upconverting nanophosphor label technology.

4 SUMMARY OF MATERIALS AND METHODS

A detailed description of the materials and methods employed in this study can be found in the original publications **(I-IV)**. A brief summary with some additional information is presented here.

4.1 Upconverting nanoparticles (UCNPs)

The UCNPs and their emissions used in the original publications **(I-IV)** are listed in the table.

Publication	UCNPs	UC emissions utilized (nm)
I	$Na_{(1-x)}K_xYF_4$:Yb,Tm and	450, 475 (Tm)
	$NaY_{(1-x)}Sc_xF_4$:Yb,Tm	
II	$Na_{(1-x)}K_xYF_4$:Yb,Tm	362 (Tm)
III	$NaYbF_4$: Tm	346, 365 (Tm)
IV	$NaYF_4$:Yb,Tm and	475 (Tm) and
	$NaYF_4$:Yb,Er	542 (Er)

4.1.1 Synthesis of UCNPs

All of the UCNPs used in the original publications were synthesized by the modified thermal coprecipitation method [238]. In a typical synthesis of optimized $NaYF_4$: (20%)Yb, (0.5%)Tm NPs, the methanol solutions of rare earth chlorides were added to a flask containing 9 mL oleic acid and 21 mL octadecene. The solution was heated to 160 °C for 40 min to form the rare earth oleate complex and then cooled down to room temperature. Thereafter, 15 mL of a methanol solution of NH_4F (4.8 mmol) and NaOH (3 mmol) was added and the solution was stirred for 30 min without argon to evaporate the methanol and to ensure that all of the fluorides were consumed completely. The solution was subsequently heated to 310 ^{0}C under argon for 90 min and cooled down to room temperature. The formed nanoparticles were precipitated by the addition of absolute ethanol to the reaction solution. The solution was then transferred to a centrifuge tube and centrifuged at 3766 g for 8 min, so that the nanoparticles separated out completely. This washing procedure was repeated 6 times to ensure removal of the reaction surfactant and any NaF impurities that may have formed. Finally, the nanoparticles were re-dispersed in toluene for further experiments.

The $Na_{(1-x)}K_xYF_4$ (or $NaY_{(1-x)}Sc_xF_4$) nanocrystals used in publications **I** and **II** were synthesized by replacing Na^+ (or Y^{3+}) with 0, 20, 40, 60, 80 and 100 mol % of K^+ (or Sc^{3+}). Whereas in publication **III**, $NaY_{(1-x)}Yb_xF_4$ NPs were synthesized by substituting Y^{3+} stepwise with 20, 40, 60, 80 and 100 mol% of Yb^{3+}. In addition, syntheses of $NaYbF_4$ NPs with 0.05, 0.2, 0.4, 0.6, 0.8, 1 and 5 mol% Tm were also included in publication **III**. The

$NaYF_4$: Yb, Er NPs used in publication **IV** were synthesized using 17 mol% of Yb^{3+} and 3 mol% of Er^{3+}.

4.1.2 Characterization of UCNPs

X ray powder diffraction (XPD)

The structural phase identification of the synthesized materials was carried out by X-ray powder diffraction (XPD) measurements. The patterns were collected with a Huber G670 image plate Guinier camera (2θ range: 4-100°) with copper $K_{\alpha 1}$ radiation (λ: 1.5406 Å). The reference patterns were calculated with PowderCell [239] based on the structural data reported.[240] The crystallite size, shape and aspect ratio were estimated from the diffraction data using the Scherrer equation [241] with an instrumental correction from the full width at half maximum (FWHM) determined for a Si reference material (NIST standard 640b):

$$d = \frac{0.9\lambda}{\beta\, cos\theta} \qquad \text{with} \qquad \beta^2 = \beta_s^2 - \beta_r^2$$

In this equation, d (m) is the mean crystallite size, λ (m) the X-ray wavelength, β (rad) the FWHM of the chosen reflection and θ (°) half of the Bragg´s angle (2θ). β_r, β_s and β are the reference, sample and corrected FWHM, respectively. The (002) and (200) reflections were used for calculating the length of the hexagonal plates and the width of the hexagonal faces, respectively, thus giving the size and morphology of the crystallites.

Particle size and morphology

The size and morphology of the nanocrystals were examined by transmission electron microscopy (Tecnai12 BioTwin TEM) with an acceleration voltage of 120 kV. The TEM samples were prepared by depositing a drop of the synthesized material dissolved in toluene onto the surface of a carbon coated copper grid and by evaporating the solvent immediately.

Upconversion luminescence and luminescence decay

The UC luminescence spectra of the synthesized materials were recorded at room temperature with a Varian Cary Eclipse fluorescence spectrophotometer (Varian Scientific Instruments, Mulgrave, Australia) with a standard R928 red-sensitive photomultiplier (Hamamatsu Photonics, Shizuoka, Japan) under the excitation of a 980 nm laser diode module C2021-F1 (Roithner Lasertechnik, Vienna, Austria), with an output power of about 200 mW and a focusing area of approximately 2.4 mm^2. The laser module was aligned to the excitation light path and the emitted light was collected to an emission monochromator at a 90° angle to the laser beam. The laser module was connected to an external power source and the spectra were collected using the bio/chemiluminescence mode of the fluorescence spectrophotometer from 300 to 850 nm (without any emission filter, i.e. filter setting open) with a 0.75 nm resolution and a 1.5 nm emission slit [91].

The emission decays were measured with a Plate Chameleon fluorometer equipped with a 980 nm laser diode excitation (Hidex Oy, Finland) in the time domain mode at 800, 475 and 365 nm with a 20 μs resolution. The width of the excitation pulse was 5 milliseconds.

Elemental analysis

The elemental composition of the nanomaterials, included in the publication **I,** was measured by an inductively coupled plasma mass spectrometer (ICP-MS) Perkin-Elmer Elan 6100 DRC Plus (MDS Sciex, Concord, ON) at Åbo Academy University, Turku, Finland. The samples for the ICP-MS analyses were prepared by digesting the UCNPs in a microwave digestion unit with a mixture of acids. The digested samples were then diluted with deionized water and the elemental compositions of the diluted samples were measured.

The EDX analysis maps with the SEM images were obtained with a LEO 1530 Gemini Scanning electron microscope and a Thermo Scintific UltraDry SDD X-ray detector (SEM-EDX) **(III)**.

4.2 Glucose test strip

4.2.1 Materials

The $Na_{(1-x)}K_xYF_4$:Yb,Tm NPs with x = 40 mol% was found to be an excellent UV emitting (362 nm) material and was used as a UV emission source in the glucose test strip **(II)**. The components used for the dry chemistry test strips are: Sipernat FK 320DS (Evonik Industries AG, Hanau, Germany), poly(acrylic acid, sodium salt) (average molecular weight ~15000 g mol^{-1}, Sigma-Aldrich, Steinheim, Germany), Gantrez S-97 BF (Ashland, Marl, Germany), Propiofan 70D (BASF, Ludwigshafen, Germany), Geropon T77 (Rhodia, Milan, Italy) and ZrO_2 TZ-3YS (Tosoh Corporation, Kaisei-cho, Japan). Carba-nicotinamide adenine dinucleotide (cNAD) and the modified glucose dehydrogenase were both produced commercially (Roche Diagnostics GmbH, Penzberg, Germany). The supporting plastic film was Bayfol CR210 (125 μm thick, Bayer MaterialScience AG, Leverkusen, Germany).
The samples used in the glucose assay were either glucose in water (anhydrous β-D-glucose, Merck KGaA, Darmstadt, Germany) at concentrations ranging from 0 to 44.4 mM or a pooled sample of heparinized whole blood from multiple voluntary donors spiked with glucose.

Preparation of a dry chemistry layer

The structure of the test strip was reported elsewhere [242]. The dry chemistry layer on the test strip is made up of a bottom layer of sensing elements and a top layer of UCNPs. The coating masses were prepared in mQ-water. The mixture was homogenized by

mechanical stirring, sonication and by pressing the mixture through a fine mesh cloth. The composition of the bottom layer was 101.1 g L^{-1} Sipernat FK 320DS, 8.1 g L^{-1} polyacrylic acid, 15.3 g L^{-1} Gantrez, 40.4 g L^{-1} Propiofan 70D, 1.6 g L^{-1} Geropon T77, 64.7 g L^{-1} cNAD and 32.3 g L^{-1} glucose dehydrogenase with the pH adjusted to 7.5. For the upper layer the UCNP-particles were bound with the Gantrez polymer by first preparing a solution with 20 mg mL^{-1} Gantrez and 92 mg mL^{-1} UCNP in methanol. Water was added after dissolving the polymer and pH was adjusted with NaOH while mixing until a homogeneous suspension was formed. Methanol was then removed with rotary evaporation and water was added to obtain the final concentrations of 65 g L^{-1} Gantrez and 300 g L^{-1} of UCNP. This mixture was then combined with the rest of the dry layer components at final concentrations of 411.6 g L^{-1} ZrO_2, 8.7 g L^{-1} polyacrylic acid, 54.1 g L^{-1} Propiofan 70D and 1 g L^{-1} Geropon T77. The coating masses were then spread onto the plastic film using a manual blade coating method. The first layer, containing the enzyme and the indicator, was coated at a blade height of 75 µm and dried in a drying oven at +35 °C for 15 minutes. After this, the second layer containing the UCNP was applied on top of this at a blade height of 100 µm from the film and dried in the same way.

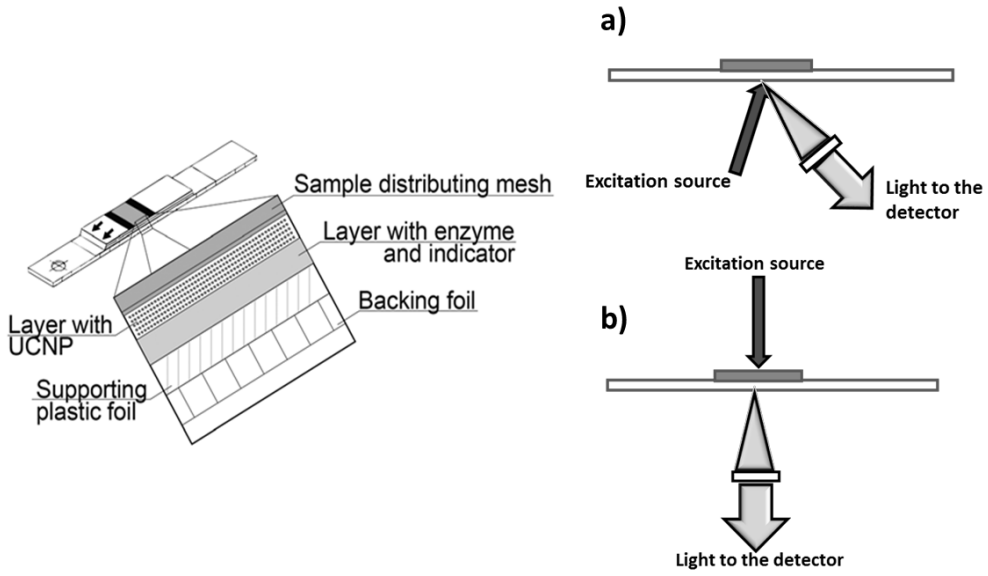

Figure 10. The structure of the glucose test strip showing different constituents of the dry chemistry layer (left (**II**)) and the optical setup for the glucose measurement using a light source a) below or b) above the test strip (right).

4.2.2 Optical setup for the test strip measurement

The detection setup used for the measurement of the UCNP emission or the reflectance is shown in the Figure 10 (right side). There are two ways of taking measurements a) a light source excitation (NIR laser with power 2.4 W cm^{-2} or a broadband light source) from the below of the test strip (the supporting film side) and detecting the decrease in the UV-radiation (originating from the UCNPs or the reflection from the sensing layer) in a 45° angle (Figure 10a, right side), b) in an alternative method, the laser was pointed from the sample side of the test strip with power of 9.1 W cm^{-2}. The excitation light travel through the spiked whole blood sample and the UCNP emission was detected from film side, blow the test strip (Figure 10b, right side). To protect the detector from the laser, a second identical KG5 filter was used.

4.2.3 Glucose measurement

As a result of glucose reacting with glucose dehydrogenase enzyme, the reduction of cNAD to cNADH takes place on the strip. This results in the UV absorption of the indicator in the region matching with the UV emission of UCNPs. The unaffected blue emission of the UCNP can be used as control signal.

The amount of cNADH formed was measured by two setups (by laser diode from two different positions or reflection measurement) described in the previous section. The spectral measurement from 300 to 1000 nm was carried out with an integration time of 550 ms with 5x spectrum accumulation. The exposure time used was 45 s. The measurements were first carried out with a dry strip for reference signals then with 5 µL of glucose solution or whole blood spiked with glucose samples. The ratiometric signals I_{UV}/I_{ctrl} were measured by integrating the background subtracted 330-380 nm (I_{UV}) and 440-490 nm (I_{ctrl}) peaks. In case of reflectance measurement the intensity at 362 nm was used. The reaction endpoint was determined as a point where the slope of the kinetic curve was <2% s^{-1}. In order to compare the two methods, the value in the endpoint was represented as a relative signal determined as a percentage of the respective signal obtained from the dry strip, before the addition of a sample. The limit of detection was calculated as the point on the calibration curve that deviates from the zero (blank) sample by three standard deviations.

4.3 Multiplexed immunoassay

4.3.1 Preparation of label conjugates

The oleic acid used in the UCNP synthesis (discussed in section 4.1.1), coordinate with the particle surface and form the hydrophobic layer. Those hydrophobic UCNPs are chemically inactive with no functional groups on the surface. To make the particles hydrophilic and chemically active for bioconjugation, the UCNPs were coated with polyacrylic acid (PAA) polymer layer (**IV**). At first, the OA was detached from the

particle surface by suspending 5 mg of UCNPs in 0.1 M HCl for 5 h, and acid was removed by centrifuging the solution at 16873 g for 30 min [243]. The precipitate was then washed with 1 mL Milli-Q water. Thereafter, the precipitate was suspended into 1 mL, 2.5% PAA solution (pH adjusted to 9 with 5 M NaOH) by bath sonication for 3 min and incubated on vertex at room temperature for 24 h. The precipitate was collected by centrifugation at 12000 g for 30 min and washed twice with 1 mL Milli-Q water and once with 0.5 mL, 20 mM MES buffer (pH 6.1). Finally the PAA-coated UCNPs were suspended in 250 µL, 20 mM MES buffer (pH 6.1). The PAA- coated UCNPs has carboxylic acid group on the surface [244].

The PAA coated Er and Tm-doped UCNPs were conjugated with anti-hIgG and anti-hIgM antibodies by the procedure described previously [218]. Briefly, the carboxyl groups on the UCNP surface were activated by 20 mM EDC and 30 mM Sulfo-NHS in 260 µL volume. The reaction mixture was incubated for 45 min and washed and suspended in 20 mM MES buffer (pH 6.1). Mabs stock was added to the activated UCNP solution (0.2 mg/mL Mab for 2 mg/ml UCNP) and incubated for 2.5 h. Thereafter, the reaction was stopped by adding 2 M glycine (pH 11) and incubated again for 30 min. Finally, the antibody coated UCNPs were washed and suspended in storage buffer (5 mM Tris pH 8.5, 8.5% Tween-85, 0.5% BSA, 0.05% sodium azide).

Spectral cross-talk

The cross talk between both Er and Tm doped UCNP-conjugate (Er-UCNP-anti-hIgG and Tm-UCNP-anti-hIgM) was studied in 96 well microtiter plates by measuring the anti-Stokes emission of both the particles separately and from their mixture. Briefly, 100 µL assay buffer (50 mM Tris–HCl, pH 7.75, 150 mM NaCl, 0.5% BSA, 0.05% bovine γ-globulin, 0.01% Tween-40, 0.05% NaN_3, 20 µM diethylenetriaminepentaacetic acid) with 1% BSA was added into the whole wells to avoid the adsorption of UCNP-conjugates. The wells were incubated 45 min, at room temperature with shaking. After incubation, wells were washed and 50 µL of UCNP-conjugates with 0.0075, 0.015, 0.03 and 0.06 mg/mL concentrations were added in each well. Similarly, in another series of wells, the concentration of either Er-UCNP-anti-hIgG (Er-conjugate) or Tm-UCNP-anti-hIgM (Tm-conjugate) was fixed at high concentration (0.06 mg/mL) while the other UCNP-conjugate with different concentrations was added. The plate was imaged with anti-Stokes photoluminescence imager [158].

Cross-reactivity

The cross reactivity between detection antibodies and immobilized captured antigens was studied by incubating Er-conjugate in bio-hIgM wells and Tm-conjugate in bio-hIgG wells. Also, mixtures of Er- and Tm-conjugates were incubated in bio-hIgG or bio-hIgM wells. In brief, 50 µL of capture antibodies (bio-hIgG or bio-hIgM) were added in to the streptavidin-coated 96-well microtiter plate in different concentrations (0, 0.01, 0.1, 1, 10 and 100 ng/well). The plate was incubated for 45 min, at room temperature with shaking. After the incubation, plate was washed and UCNP-conjugates (50 µL, 0.015

mg/ml) were added. The plate was incubated for 40 min at room temperature with shaking. The wells were washed and the plate was dried. The bound UCNP signals were measured with modified plate chameleon microplate reader (Hidex, Finland) with 535 and 460 nm emission bandpass filters [91]. Each well was scanned with 3 x 3 raster using 1.5 mm distance between the measurement points and a 2 s reading.

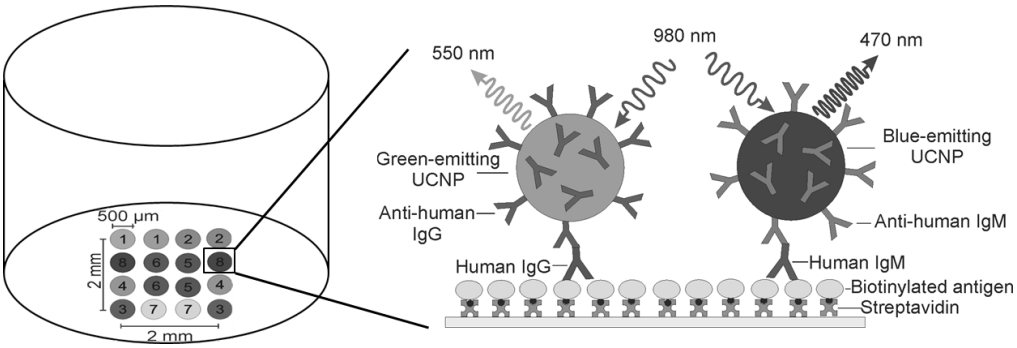

Figure 11. Principle of the spectrally and spatially multiplexed assay. The Er- and Tm-conjugates bind to the serum hIgG and hIgM antibodies respectively. Upon 980 nm excitation, blue or green light observed depending on which antibody class present in the sample. The antibody responses against adenovirus and influenza were differentiated based on the position of the signals while color indicates the antibody class.

4.3.2 Array-in-well immunoassay

The biotinylated antigens (influenza H1N1 and H5N1, adenovirus type 2 and 5(AdHX2, AdHX5)) and antibodies (anti-human IgG (anti-hIgG), human IgG (hIgG), human IgM (hIgM) and human serum albumin (HSA)) were printed on the bottom of streptavidin-coated 96-well plate (Figure 11). The samples were diluted 1:100 in assay buffer. In the prewashed antibody printed microtiter plate, 50 µL of diluted samples were added in duplicates. The assay was incubated for 45 min at room temperature with shaking. After incubation, wells were washed. The anti-hIgG and anti-hIgM coated UCNPs were added (50 µL, 0.015 mg/mL) in each well and incubated for 40 min at room temperature with shaking. After the incubation, wells were washed four times to remove the unbounded UCNPs. The dried plate was imaged with an anti-Stokes photoluminescence imager constructed for multi analyte detection.

Data analysis

The upconverting nanoparticle emission was detected through band pass filters 535/50 nm and 460/20 nm for Er and Tm-doped UCNPs respectively (Chroma Technology, Rockingham, VT) with cooled CCD-camera (Andor Clara with Sony ICX285 CCD; Andor Technology, South Windsor, CT) using 2 × binning, 1 s exposure per well and laser excitation at 976 ± 2 nm with 7W optical power. Image analysis was performed with ImageJ software version 1.43n.

5 SUMMARY OF RESULTS AND DISCUSSION

5.1 Blue emitting UCNPs

The aim of publication **I** was to enhance the blue UC emission (475 nm) of hexagonal $NaYF_4$:Yb,Tm nanoparticles with different ratios of K^+ and Na^+ as well as Y^{3+} and Sc^{3+} doping. The host ion substitution disturbs the local symmetry around luminescent lanthanides and changes the crystal field, which results in to emission intensity enhancement.

X-ray powder diffraction (XPD) and ICPMS analysis

The synthesized products were first examined with XPD to ensure the crystal structure and phase purity of the particles. It is well known that the hexagonal $NaRF_4$ phase is far better host for high UC emission than its cubic counterpart. The XPD graphs with reference patterns are shown in the original publication **I**. In case of the $Na_{(1-x)}K_xYF_4$:Yb,Tm nanocrystals, the reflection positions and intensities of NPs with K doping upto 60 mol% match very well with those of hexagonal $NaYF_4$ [240]. Additional weak reflections of KCl are observed in 40 and 60 mol% K doped materials. A further increase in K content starts dominating poorly crystalline KYF_4 over the $NaYF_4$ reflections [245]. No cubic $Na_{(1-x)}K_xYF_4$ phase was observed in any obtained sample. With increased K content, the unit cell volume of the hexagonal $Na_{(1-x)}K_xYF_4$ remains practically constant, which means that K^+ does not enter into the $NaYF_4$ cell, but it has formed an amorphous phase instead. The decreased R-R distance with increased K^+ concentration indicates the deficit of the larger Na^+ and excess of smaller Y^{3+} [246]. This hypothesis was supported by the ICPMS analysis of the elements Na/K/Y/Yb/Tm in the hexagonal $Na_{(1-x)}K_xYF_4$:Yb,Tm crystals which confirm the presence of a very much lower amount of K in the crystal lattice than the original amount added.

The XPD of the $NaY_{(1-x)}Sc_xF_4$:Yb,Tm nanoparticles with 20 mol% Sc doping shows pure hexagonal $NaYF_4$ phase. With further increase in Sc^{3+} concentration, the minority phase β-Na_3ScF_6 starts to appear. For 80 mol% Sc content, a mixture of cubic α-$NaYF_4$ and β-Na_3ScF_6 is obtained. The pure β-Na_3ScF_6 phase is observed in case of 100 mol% Sc doping [247]. The compaction of the unit cell and decrease in R-R distance indicates the substitution of Y^{3+} by Sc^{3+}. The ICPMS analysis results of the Na/Y/Yb/Tm/Sc elements are coherent with the added Sc quantity.

Table 3 shows the crystallite size and aspect ratio estimated from the diffraction data by using the Scherrer equation.

Size and morphological study

The doping of K^+ and Sc^{3+} in $NaYF_4$ lattice, affects the morphology and size of the synthesized particles. The TEM images of the synthesized particles are shown in the Figure 12. The $NaYF_4$:Yb,Tm NPs without K or Sc show a hexagonal prismatic structure with about 25-30 nm size while UCNPs with 20 mol% K gives spherical particles with

35 nm size. The increased K content from 20 to 60 changes the particle morphology from larger nanoprisms (70-100 nm) to nanorods (150-200 nm). The 80-100 mol% K doped products give 5-10 nm spherical particles. As discussed in the previous section, added K^+ does not enter into the crystal lattice, instead it acts as a diluting agent in the synthesis. The increased K^+ creates the Na^+ deficiency, which results in to fewer nucleation sites and thus larger $NaYF_4$ crystals.

The TEM image of $NaY_{(1-x)}Sc_xF_4$ with 20 mol% Sc content shows uniform, 30-40 nm hexagonal nanoprisms. This uniformity is disturbed with the increase in the Sc concentration up to 60 mol%. In case of the 80 mol% Sc content, the stoichiometry between cubic α-$NaYF_4$ and β-Na_3ScF_6 may be disturbed which in turn breaks the particles in to ≤10 nm crystals which act as seeds for the growth of pure β-Na_3ScF_6 with 30-40 nm size. The increased Sc content does not change the morphology of the crystals, but rather disturbs the uniformity and shows size variations (Table 3).

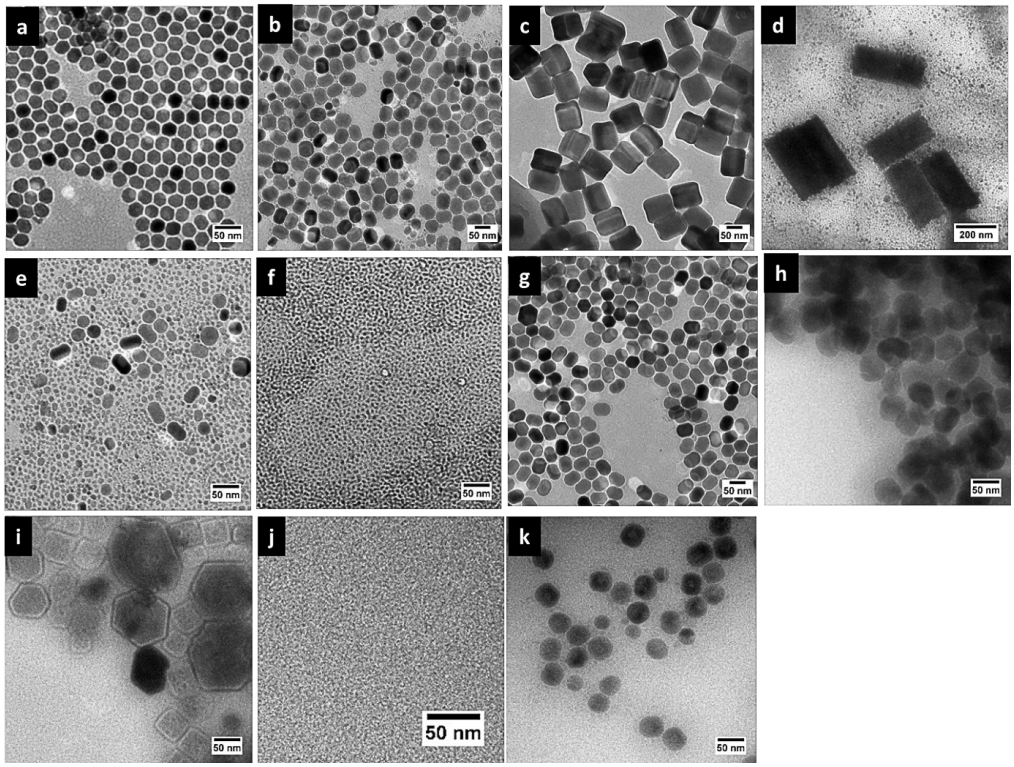

Figure 12. TEM images of hexagonal $Na_{(1-x)}K_xYF_4$:Yb,Tm with different concentrations of K^+: a) 0, b) 20, c) 40, d) 60, e) 80, f) 100% and $NaY_{(1-x)}Sc_xF_4$:Yb,Tm crystals with different concentrations of Sc^{3+}: g) 20, h) 40, i) 60, j) 80, k) 100%.

Table 3. Molar ratio, phase, size and morphology of the as-obtained $Na_{(1-x)}K_xYF_4$:Yb,Tm and $NaY_{(1-x)}Sc_xF_4$:Yb,Tm nanocrystals.

	TEM	XRD[a]				Morphology
x(K) / %	Particle size / nm	Hexagon width / nm	Rod length / nm	Sphericity[b]	Phases	
0	25-35	22	27	0.81	β-$NaYF_4$	Hexagonal nanoprism
20	35-40	32	49	0.65	β-$NaYF_4$	Hexagonal nanoprism
40	80-100	42	67	0.62	β-$NaYF_4$ + KCl	Hexagonal nanoprism
60	150-200	84	295	0.28	β-$NaYF_4$ + KCl + KYF_4	Hexagonal rod
80	10-15	-	-	-	KYF_4 + KCl	Nanosphere
100	≤ 5	-	-	-	KYF_4	Nanosphere
x(Sc)[c]/%						
0	25-35	22	27	0.81	β-$NaYF_4$	Hexagonal nanoprism
20	30-40	23	32	0.72	β-$NaYF_4$	Hexagonal nanoprism
40	40-50	24	37	0.65	β-$NaYF_4$ + Na_3ScF_6	Hexagonal nanoprism
60	50-100	31	41	0.75	β-$NaYF_4$ + Na_3ScF_6	Hexagonal nanoprism
80	≤ 10	-	-	-	α-$NaYF_4$ + Na_3ScF_6	Nanosphere
100	25-30	-	-	-	Na_3ScF_6	Nanosphere

[a]For the hexagonal $NaYF_4$ type phase only [241].

[b]Width/length ratio.

[c]Sum of Y and Sc % is equal to 100.

Note: Sum of Y and Sc % in $NaY_{1-x}Sc_xF_4$:Yb,Tm is 79.5 of total rare earth content; remaining 20.5% are Yb and Tm.

Upconversion luminescence properties

All the synthesized $Na_{(1-x)}K_xYF_4$:Yb,Tm and $NaY_{(1-x)}Sc_xF_4$:Yb, Tm nanocrystal dispersions in toluene (0.1 mg/mL) show 4 distinct bands in the range of 400-700 nm under 980 nm excitation. Figure 13a shows the UC spectra of $Na_{(1-x)}K_xYF_4$:Yb,Tm nanoparticles. When compared to the normal hexagonal $NaYF_4$:Yb,Tm NPs, 20 mol% K content showed 3-4 fold enhancement in the UC intensity (475 nm emission). This is the maximum of the intensity obtained, since it decreases with further increase in K^+ percentage. The nature of the UC curve significantly changes after 60 mol% K doping indicating the dominance of the K^+ containing phase over the $NaYF_4$ phase. The $NaY_{(1-x)}Sc_xF_4$:Yb,Tm NPs show the same behaviour as 20 mol% Sc shows the highest UC emission, but this is still lower than with 20 mol% K (Figure 13b).

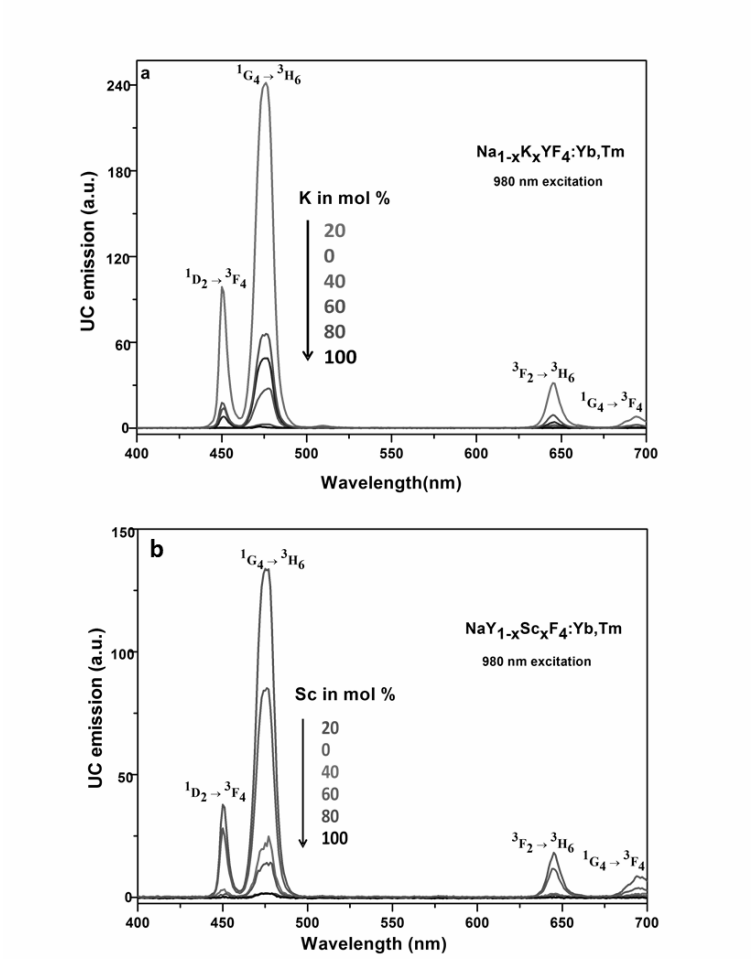

Figure 13. Upconversion luminescence spectra of a) $Na_{(1-x)}K_xYF_4$:Yb,Tm with different concentrations of K^+ and b) $NaY_{(1-x)}Sc_xF_4$:Yb,Tm crystals with different concentrations of Sc^{3+}.

The doping of K^+ and Sc^{3+} ions affect the distance between Yb^{3+} and Tm^{3+} ions which in turn changes the Yb-Tm energy transfer. These changes in the distance explain the different emission intensities for the different percentages of doping. The UC enhancement can be explained by two theories. The first is a change in Na/R ratio inside the crystals. In $Na_{(1-x)}K_xYF_4$ samples, even though the added K^+ does not enter into the crystal, it does affect the Na/R ratio inside the crystal. The Na/R ratio decreases with an increase in K^+ content (confirmed by ICPMS) which results into the decrease in unit cell volume as well as average R-R distances. But this alone cannot explain the enhancement since the R-R distance decrease even further with 20 mol% Sc content. Another explanation might be that the hexagonal $NaYF_4$ has two cationic sites, one ideally occupied with a statistical 25:75 ratio by Na and R, and the other with 50% Na only

[240]. The Na site may start to accommodate also R^{3+} when the K or Sc content increases. This R^{3+} cation clustering results into efficient Yb-Tm energy transfer at low K or Sc amounts while it quenches with increased K or Sc concentrations. Also, with higher K or Sc content the less luminescent KYF_4 or Na_3ScF_6 phases dominate, which decreases the overall luminescence intensity.

5.2 UCNPs for glucose sensing

The UV emission of the $Na_{(1-x)}K_xYF_4$:Yb,Tm nanocrystals, synthesized for publication **I** was measured and it was found that the UCNPs with 40 mol% K content shows the highest UV emission centered at 365 nm (Figure 14). Those UCNPs were used as the internal light source in the dry chemistry test strip for the glucose sensing **(II)**. The behaviour of the UCNPs on the test strip was studied by using two optical setups (Figure 10 a and b) and it was found that the UC emission decreases after the addition of H_2O, caused by the quenching effect of water, UCNP migration with the sample to the lower layer and the change in optical properties of the strip. The quenching effect can be minimized by core shell formation [116], while the particle migration could be avoided by immobilization of the particles and the indicator in separate layers or could be brought close to each other for energy transfer between them.

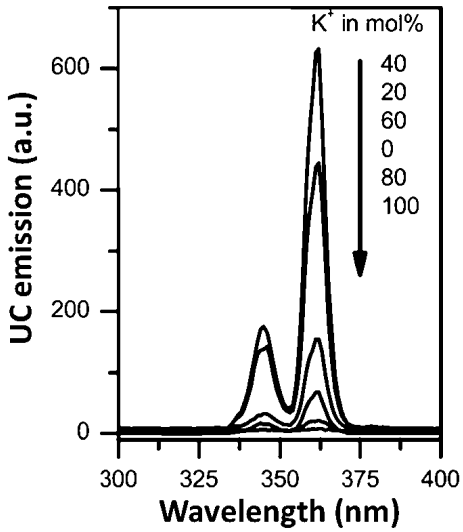

Figure 14. Upconversion spectra of $NaYF_4$:Yb,Tm UCNPs doped with different K^+ concentrations.

5.2.1 Glucose assay

The glucose-water solution was first used for the glucose assay. The two different setups i.e. reflection of light or UCNP emission were used for the measurements. The

results from both setups agreed with the actual concentration of glucose in the sample with practically the same sensitivity and dynamic range. The limit of detection improved from 0.93 mM to 0.49 mM by using UCNPs with internal control signal. The coefficient of variation for both measurements was, 0.64 and 6.7 % for the UCNPs with internal control and 0.92 and 9.1 % for the reflectance measurement. In another experiment, the assays were performed by using heparinized whole blood spiked with glucose as a sample. The diode laser was moved to the top of the strip where the excitation light passed through the blood sample. When compared with the traditional reflectance measurements, the results showed a good correlation between them.

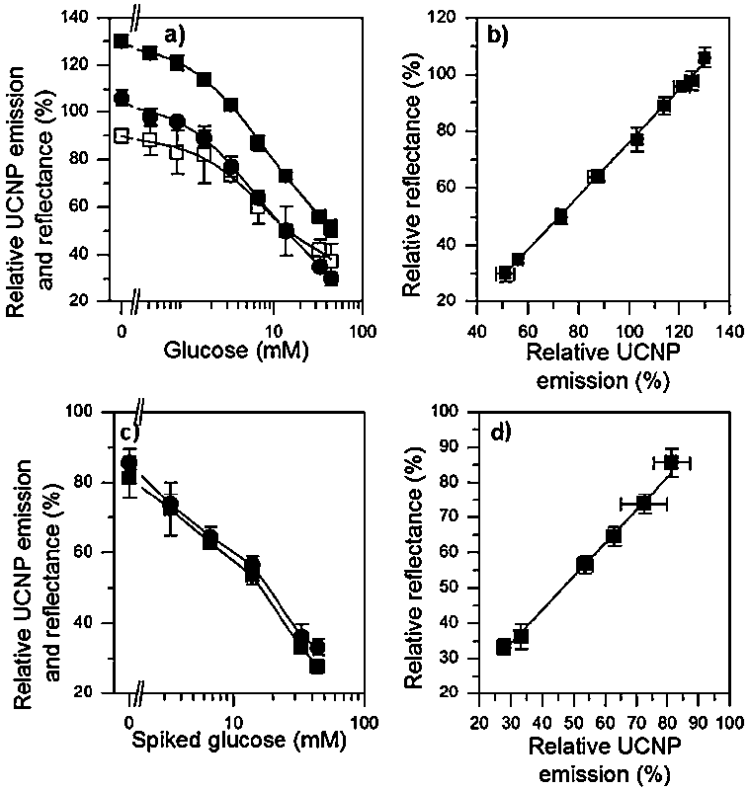

Figure 15. Glucose assay results from 1) glucose dissolved in water sample with light source from below the test strips. a) The glucose calibration curves by using emission of UCNPs (squares) or reflectance (spheres). The dark squares represent the ratio metric signals and open squares the data from UV emission of UCPs alone. b) The co-relation of the relative reflectance and ratiometric UCNP emission. 2) Whole blood as a sample and UCNPs excited from above the strip and broadband source from below the strip. c) The relative signals obtained from the UCNPs (squares) or reflectance (spheres) measurements. d) The correlation of the relative reflectance and ratiometric UCNP emission. R^2 of the linear fitting was >0.99. Error bars represent standard deviation.

5.3 UV emitting UCNPs

Publication **III** comprises the synthesis of intense UV emitting UCNPs by stepwise increasing the sensitizer concentration ($NaY_{(1-x)}Yb_xF_4$:0.5%Tm). In addition, the activator concentration was also optimized for high UV emitting UCNPs ($NaYbF_4$:Tm (x%)).

X-ray powder diffraction (XPD)

All XPD patterns agreed well with the hexagonal $NaYF_4$ reference pattern indicating no phase change with increased Yb^{3+} and Tm^{3+} concentrations in the $NaY_{(1-x)}Yb_xF_4$:0.5%Tm and $NaYbF_4$ (x%) NPs, respectively [240]. Additional reflections of small amounts of NaCl and cubic $NaRF_4$ impurities are also observed in few samples (refer publication **III**). The width to length ratio (W/L) was calculated by using the Scherrer equation (Table 4).

Size and morphological study

The TEM images of the as prepared $NaY_{(1-x)}Yb_xF_4$:0.5%Tm with different concentrations of Yb^{3+}: 10, 40, 60, 80 and 100 mol% and $NaYbF_4$ (x%) with different concentrations of the Tm^{3+}: 0.05, 0.2, 0.4, 0.6, 0.8, 1 and 5 mol% are shown in the figure 16. The rare earth concentration change does not affect the phase of the particle. While in case of crystal size and shape, the Y/Yb ratio plays an important role: the increased Yb^{3+} concentration results into particle growth. On the other hand, different Tm^{3+} concentrations show very small changes in the particle size distribution. The effect of different Yb^{3+} and Tm^{3+} concentrations doping on the particle size are summarised in table 4.

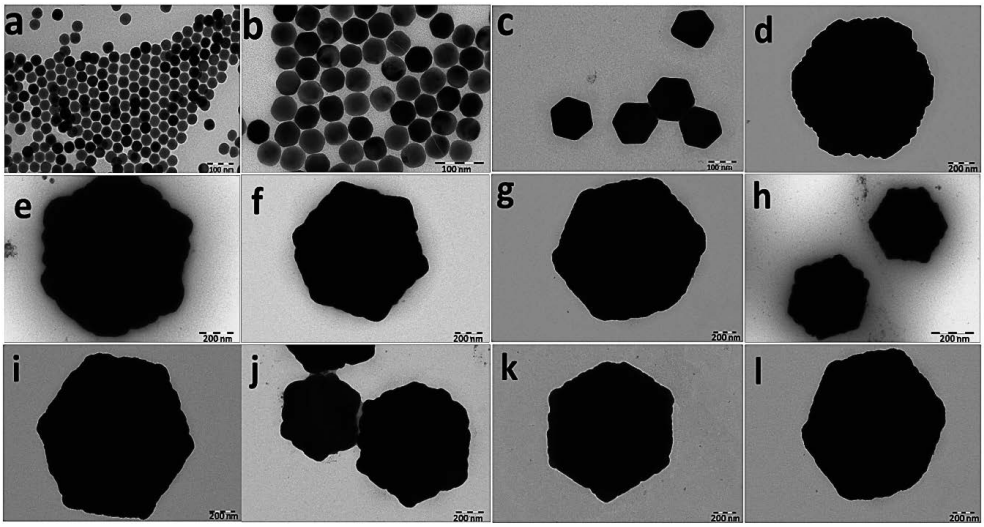

Figure 16. TEM images of hexagonal $NaY_{1-x}Yb_xF_4$:Tm (0.5%) with different concentrations of Yb^{3+}: a) 20, b) 40, c) 60, d) 80, e) 100% and $NaYbF_4$:Tm (x%) crystals with different concentrations of Tm^{3+}: f) 0.05, g) 0.2, h) 0.4, i) 0.6, j) 0.8, k) 1 and l) 5%.

Crystal growth

After dissolution and renucleation the unstable α-$NaYF_4$ phase transformed in to stable β-$NaYF_4$. As the increased Yb^{3+} concentration lowers the phase transition temperature[248], the formation of β-$NaYF_4$ will be faster and there is more time for further growth. Once the hexagonal β-$NaYF_4$ is formed, the oleic acid strongly reacts with top/bottom (001) surfaces of the crystallite and results into the growth along the sides of the crystal (Figure 17). In case of the highest Yb^{3+} concentration samples, the second heating may assist the formed hexagonal plates to self-assemble and anneal into larger hexagonal polycrystalline structures.

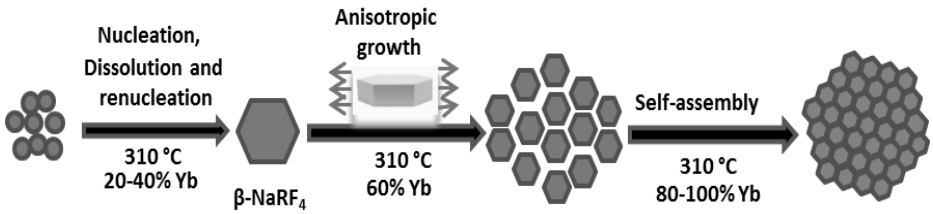

Figure 17. Schematic illustration of the Yb concentration dependent growth mechanism of $NaYF_4$:Yb,Tm NPs.

Upconversion luminescence properties

The UC photoluminescence of the $NaY_{(1-x)}Yb_xF_4$:Tm (0.5%) and $NaYbF_4$:Tm (x%) particles (0.1 mg/mL oleic acid) produced six emission bands centered at 346, 365, 450, 475, 649 and 800 nm corresponding to the $^1I_6 \rightarrow {}^3F_4$, $^1D_2 \rightarrow {}^3H_6$, $^1D_2 \rightarrow {}^3F_4$, $^1G_4 \rightarrow {}^3H_6$, $^1G_4 \rightarrow {}^3F_4$, and $^3H_4 \rightarrow {}^3H_6$ transitions of Tm^{3+}, respectively (Figure 18). Three energy transfer processes from Yb^{3+} to Tm^{3+} along with some non-radiative relaxations are responsible for the 475, 650, 690 and 800 nm emissions. The cross relaxation $^3F_2 + {}^3H_4 \rightarrow {}^3H_6 + {}^1D_2$ between the two Tm^{3+} ions plays an important role in populating the $^1D_2$ level which after radiative relaxation gives the 365 and 450 nm emissions. The Tm^{3+} ions in the $^1D_2$ level can be further excited to the $^3P_2$ level by the fourth energy transfer from Yb^{3+} which relaxes to the $^1I_6$ level and emits the UV band at 346 nm.

With an increase in sensitizer concentration upto 100 mol%, The UV UC intensities at 346 and 365 nm emissions were measured to be about 20 and 18 times higher than that of the 20 mol% Yb^{3+} sample (Figure 18a). The enhancement in the UV emission through high sensitization partly comes from increased particle size with increased Yb^{3+} content, which decreases the surface quenching sites of the particles by decreasing the surface to volume ratio and facilitates the high UC emission [90]. The other possible explanation is, the excess sensitization increases the absorption of NIR photons and enhances the energy transfer probabilities between Yb-to-Yb and also Yb-to-Tm, which results in increased population in the $^1I_6$ and $^1D_2$ levels.

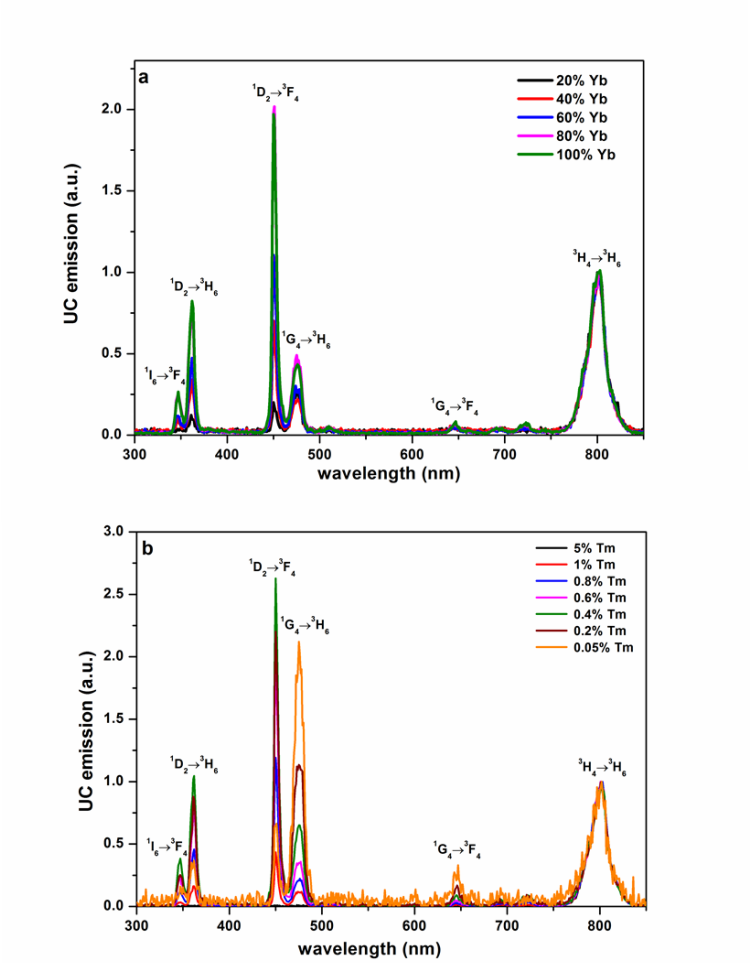

Figure 18. Upconversion luminescence spectra of colloidal a) $NaY_{1-x}Yb_xF_4$:Tm (0.5%) (x_{Yb} = 20, 40, 60, 80 and 100%) and b) $NaYbF_4$:Tm (x%) (x_{Tm} = 0.05, 0.2, 0.4, 0.6, 0.8, 1 and 5%) crystals under 980 nm excitation in oleic acid suspension, normalized at the emission peak of 800 nm.

The UV emission intensity of the different Tm^{3+} concentration doped $NaYbF_4$ crystals increases up to 0.4 mol% doping, remains steady in the range of 0.4 to 0.8 mol% and decreases with a further increase in the Tm^{3+} content (Figure 18b). The dramatic decrease in the UV and visible emission intensities with higher Tm^{3+} concentration is due to the self-quenching of the Tm^{3+} $^1D_2$ and $^1G_4$ levels. The $^1D_2$ energy level is depopulated by three different cross relaxations $^1D_2 + {}^3H_6 \rightarrow {}^3F_3 + {}^3H_4$, $^1D_2 + {}^3F_3 \rightarrow {}^1G_4 + {}^1G_4$ and $^1D_2 + {}^3H_6 \rightarrow {}^3H_4 + {}^3F_2$ and two of them feed the $^3H_4$ energy level which may explain the enhancement in the 800 nm emission with increase in the Tm^{3+} concentration up to 0.8%.

The emission decays were studied for the $^1D_2 \rightarrow {}^3H_6$ (365 nm), $^1G_4 \rightarrow {}^3H_6$ (475 nm) and $^3H_4 \rightarrow {}^3H_6$ (800 nm) transitions with 980 nm excitation (Table 4). The decay data were fitted with single, second and third order exponential decay functions (refer publication **III**). It was observed that the rise and decay time decreases with increasing Yb^{3+} concentration. This might be because of an efficient energy transfer between Yb^{3+} and Tm^{3+} due to higher sensitization. Another possible reason for the short decay time is the efficient non-radiative vibrational processes which are caused by the decreased distance between the luminescent centers and the surface related high frequency vibrational modes. As the Yb^{3+} and Tm^{3+} concentration increases, the Tm → Yb energy back transfer and self-quenching can partially explain the noticeable decrease in the $^3H_4$ level emission [249]. In addition, the particles shape can also play an important role on the fluorescence decay behaviour. It is observed that the hexagonal plates with higher W/L ratios show lower decays i.e. the W/L ratio and decay time are inversely proportional to each other.

Table 4. Summary of decay times from the emitting $^3H_4$, $^1G_4$ and $^1D_2$ level of $NaY_{1-x}Yb_xF_4$:Tm (0.5%) and $NaYbF_4$:Tm (x%) with particle size measured from TEM and width to length (W/L) ratio calculated with the Scherrer method.

$NaY_{1-x}Yb_xF_4$:Tm (0.5%) Yb^{3+} (mol %)#	**TEM Particle Size (nm)**	**XRD**			**Decay times (µs)§**		
		W (nm)	**L (nm)**	**W/L**	**$^3H_4 \rightarrow {}^3H_6$**	**$^1G_4 \rightarrow {}^3H_6$**	**$^1D_2 \rightarrow {}^3H_6$**
20	25	27	24	1.12	630 ± 8	576 ± 2	168 ± 0.3
40	≈ 90	30	28	1.04	422 ± 5	547 ± 2	142 ± 0.3
60	≈ 150	53	34	1.55	378 ± 7	224 ± 2	138 ± 0.3
80	900-950	56	35	1.59	440 ± 5	362 ± 2	157 ± 0.4
100	950-1000 and ≈ 20	149	79	1.89	375 ± 1	293 ± 4	137 ± 0.3
$NaYbF_4$:Tm (x%) Tm^{3+} (mol %)#	**TEM Particle Size (nm)**	**XRD**			**Decay times (µs)§**		
		W (nm)	**L (nm)**	**W/L**	**$^3H_4 \rightarrow {}^3H_6$**	**$^1G_4 \rightarrow {}^3H_6$**	**$^1D_2 \rightarrow {}^3H_6$**
0.05	≈ 950	212*	104	2.04	481 ± 4	510 ± 5	272 ± 1
0.2	≈ 1000-1200	117	68	1.72	470 ± 5	427 ± 0.5	235 ± 2
0.4	900-950	92	70	1.31	430 ± 7	358 ± 1	169 ± 0.5
0.6	900-950	125	89	1.40	321 ± 5	256 ± 3	125 ± 76
0.8	800 and ≤ 10	146	115	1.27	337 ± 2	169 ± 2	98 ± 0.2
1	900 and ≈ 25	1011*	95	---	275 ± 2	148 ± 0.5	82 ± 0.3
5	900 and ≈ 25	325*	162	---	70 ± 0.5	82 ± 3	80 ± 10

Note: * indicates the crystals are too large for Scherrer method, which commonly can treat sizes up to 150 nm, § indicates the decay time with high amplitude selected from the multiple lifetimes, # indicates the percentages are with respect to the added quantity in the synthesis.

5.4 Multiplexed immunoassay

In publication **IV**, spectrally and spatially multiplexed serological assay utilizing UCNPs was demonstrated to detect the influenza and adenovirus specific IgM and IgG antibodies present in the patients' serum during infection.

Cross-talk and cross-reactivity

Two types of UCNPs with different emission spectra were used together for simultaneous detection of different serum antibodies. Therefore the spectral cross-talk between UCNPs, and the cross reactivity between UCNP and capture antibodies was tested. In order to study the spectral cross-talk, four different concentrations of Er- and Tm-conjugates were tested (Figure 19). The 550 nm and 470 nm emission of different concentrations of Er- and Tm-conjugates were measured separately with anti-Stokes photoluminescence imager. Both UCNPs gave emissions at their corresponding wavelengths (Figure 19a and b). To investigate the spectral behavior of UCNPs in each other's presence, both Er-UCNP-anti-hIgG and Tm-UCNP-anti-hIgM were mixed together in such a way that one UCNP was fixed at high concentration and other varied. The presence of Tm-UCNP-anti-hIgM did not interfere the measurement of Er-UCNP-anti-hIgG in the 550 nm emission and vice versa (Figure 19c and d). The spectral cross-talk between UCNPs in the assay was found to be <0.06%.
The cross-reactivity of the captured antibodies and detection antibodies were tested. In the experiment, the Er- and Tm-conjugates specific for hIgG and hIgM antibodies respectively were mixed together in either hIgG or hIgM coated wells and measured with anti-Stokes photoluminescence imager. It was found that the hIgG coated wells gives only Er emission (Figure 20). Similarly, Tm signal was obtained from wells containing hIgM, confirming the bound Tm-UCNP-anti-hIgM. The signal from UCNP-conjugates in their opposite capture antibody well stays lower and constant even with increase in capture antibody concentration, which confirms minimal cross reactivity among the UCNP-conjugates and proteins in the assay.

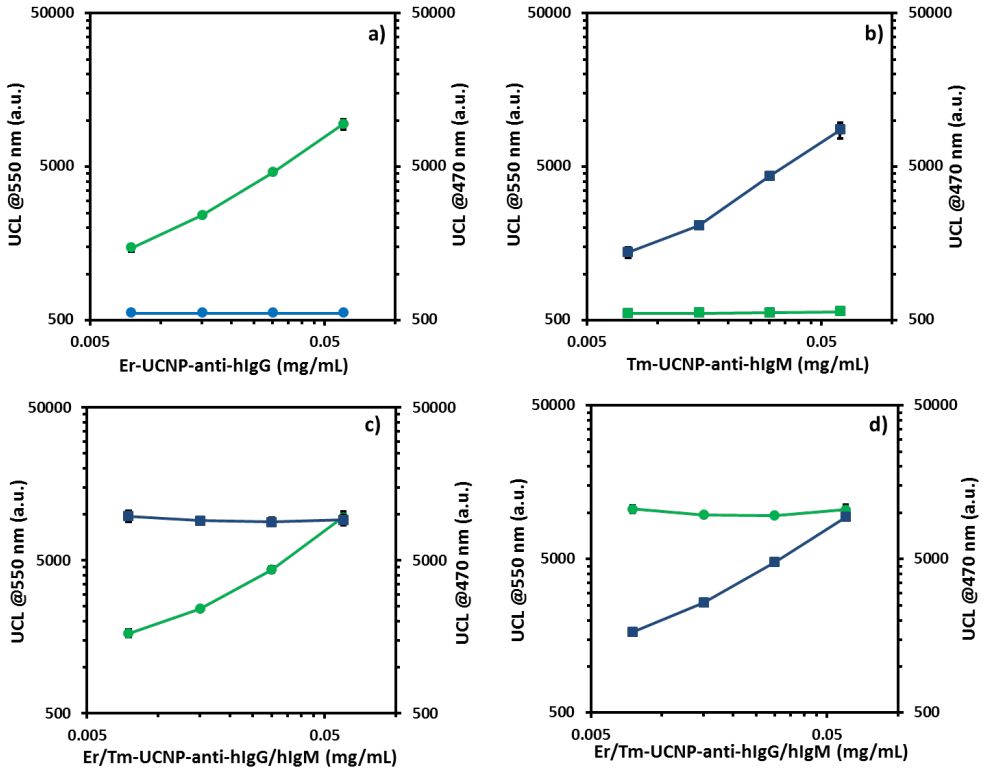

Figure 19. The upconversion luminescence (UCL) of a) Er-UCNP-anti-hIgG (circles) and b) Tm-UCNP-anti-hIgM (squares) measured at 550 nm (green line) and 470 nm (blue line) emission wavelengths. Luminescence cross-talk between Er-UCNP-anti-hIgG (circles) and Tm-UCNP-anti-hIgM (squares) in a well with c) fixed high Tm-UCNP-anti-hIgM concentration and variable Er-UCNP-anti-hIgG and d) fixed high Er-UCNP-anti-hIgG concentration and variable Tm-UCNP-anti-hIgM, measured at 550 nm (green line) and 470 nm (blue line) emission wavelengths.

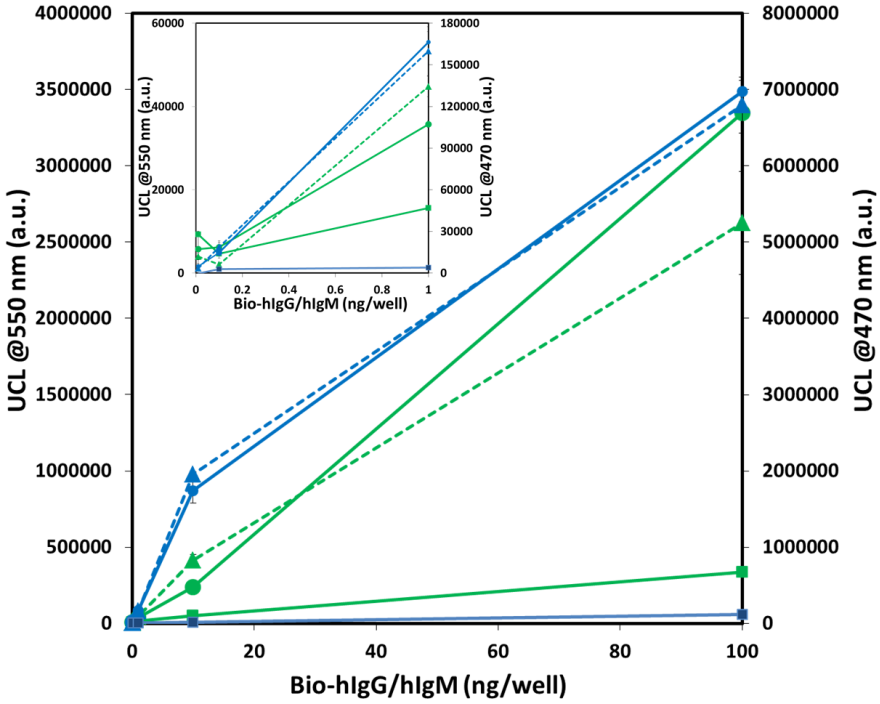

Figure 20. Study of the cross-reactivity of detection antibodies (Er-UCNP-anti-hIgG and Tm-UCNP-anti-hIgM) with captured proteins (bio-hIgG and bio-hIgM). The Er (550 nm) and Tm (470 nm) emissions are indicated by green and blue lines respectively. The dotted lines indicate the measurements of Er-UCNP-anti-hIgG and Tm-UCNP-anti-hIgM in their corresponding antibody containing wells, while the solid lines represent the mixture of both Er-UCNP-anti-hIgG and Tm-UCNP-anti-hIgM in either bio-hIgG or bio-hIgM containing well. The emission of Er measured from hIgG containing well (green circles) and hIgM containing well (green squares) as well as Tm emission from hIgM containing well (blue circles) and hIgG containing well (blue squares) are shown. The inset shows three smallest concentrations of the antibodies (0.01, 0.1 and 1 ng/well).

Assay performance

To demonstrate spectral and spatial multiplexing, multicolour UCNPs with major emission peaks at 470 and 550 nm were conjugated directly to the secondary antibodies specific for primary antibodies against influenza and adenovirus infections. Biotinylated H5N1, H1N1, AdHX2 and AdHX5 antigens were printed on the array along with control spots for hIgG, hIgM, anti-hIgG and HSA. The array format is shown in figure 21A. Luminescence imaging of the array with 1 s exposure without any sample gave green and blue emissions from hIgG and hIgM positive control spots as a result of bound Er-UCNP-anti-hIgG and Tm-UCNP-anti-hIgM, respectively (Figure 21B, i). With negative sample the anti-hIgG spot gave signal along with hIgG and hIgM spots (Figure 21B, ii). When the anti-adenovirus IgG positive sample was added in the array, the AdHX2 and AdHX5 spots emitted green light as a result of Er-UCNP-anti-hIgG antibody

and captured adenovirus antigen reaction (Figure 21B, iii). Similarly, the presence of anti-influenza A/H1N1 IgM positive sample was detected by the blue emission of Tm-UCNP-anti-hIgM from H1N1 antigen printed spots (Figure 21B, iv). With the anti-influenza A/H1N1 sample the H5N1 antigen printed spots were also luminescent. The detected cross reaction between H1N1 and H5N1 antigen was expected as both the antigens belongs to group A and the structures of the H1N1 and H5N1 hemagglutinins were known to resemble each other very much. Similarly, the AdHX2 and AdHX5 antigens belongs to group C and show high homology in their amino acid sequence [250]. The added IgG positive sample for both adenovirus and influenza shows green luminescence from all the antigen printed spots (Figure 21B, v). Also the presence of anti-influenza IgG positive sample was detected by the green emission from H1N1 and H5N1 printed spots (Figure 21B, vi).

The specific signal intensities were calculated from each spot for all the samples (Figure 21C). The 550 nm photoluminescence was observed from the hIgG, anti-hIgG, AdHX2 and AdHX5 spot as a result of a bound Er-conjugate (Figure 21C i). The strong green emission from the AdHX2 and AdHX5 spots confirms the presence of IgG antibodies against human adenovirus in the sample. Also, some green emission was detected in the H1N1 and H5N1 spot, indicating the presence of anti-influenza A IgG, which could be due to an earlier immunity to H1N1. Similarly, the blue emission (470 nm) was observed from the control spots hIgM and anti-hIgG. From a sample derived three weeks after influenza vaccination, H1N1 and H5N1 spots emitted intense blue emission confirming the presence of anti-influenza IgM antibodies in the sample (Figure 21C ii).

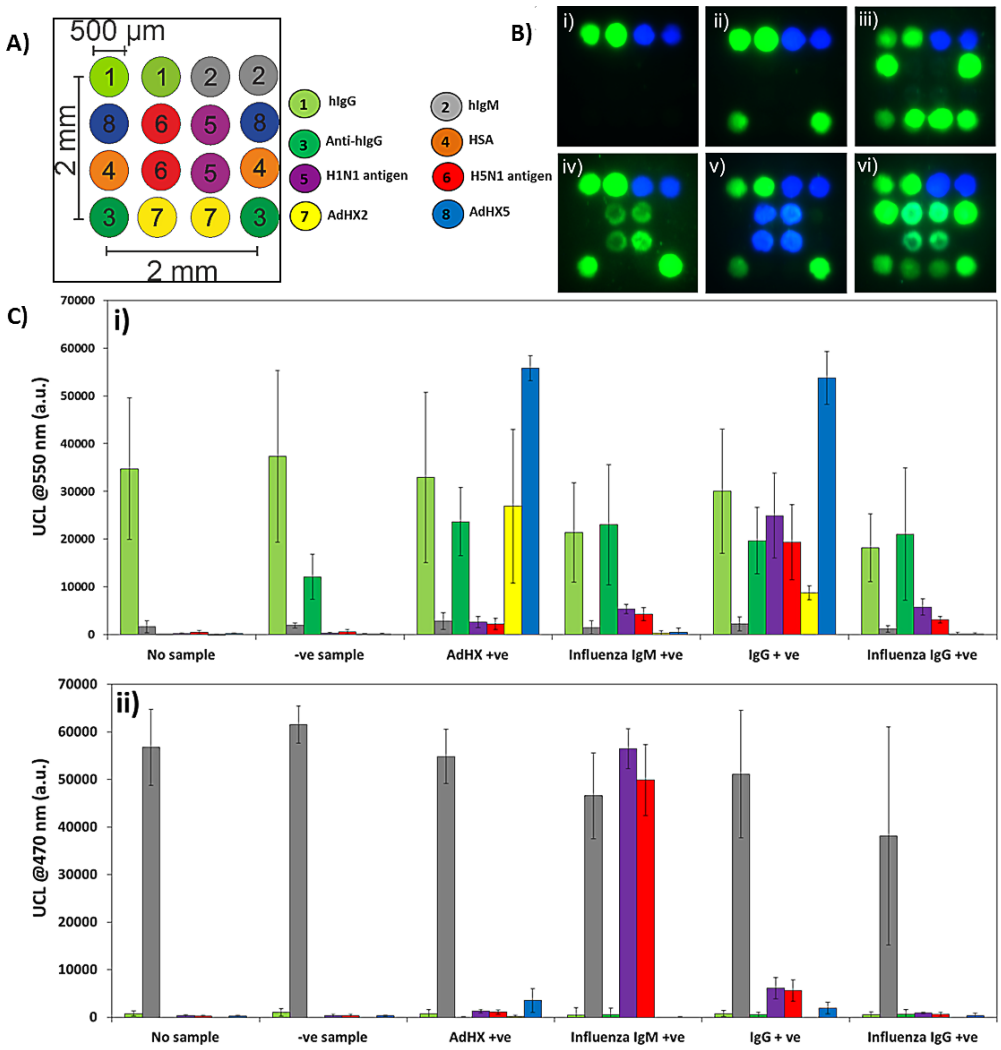

Figure 21. A) Spectrally and spatially multiplexed array-in-well immunoassay principle showing the array layout with antigen (H1N1, H5N1, AdHX2 and AdHX5), positive controls (hIgG, hIgM and anti-hIgG) and negative control (HSA) spots. B) Fluorescence images of the array area with i) no sample, ii) negative sample, iii) anti-adenovirus positive sample (AdHX +ve) and iv) anti-influenza IgM positive sample (Influenza IgM +ve) v) IgG positive sample for both adenovirus and influenza (IgG +ve) and vi) anti-influenza IgG positive sample (Influenza IgG +ve). The images are composite overlays from two separate pseudocolored images. C) Specific upconversion luminescence (UCL) signals from each spot in the array measured at i) 550 nm (for Er-UCNP-anti-hIgG) and ii) 470 nm (for Tm-UCNP-anti-hIgM). The bar colors corresponds to the colors of the spotted proteins from figure A. Er-UCNP-anti-hIgG and Tm-UCNP-anti-hIgM bind to the serum hIgG and hIgM antibodies respectively. Upon 980 nm excitation, blue or green light was observed depending on which antibody class was present in the sample. The antibody responses against adenovirus and influenza were differentiated based on the position of the signal while color indicates the antibody class.

6 CONCLUSIONS

Due to their unique luminescence properties, lanthanide doped upconverting crystals are a promising alternative to the traditional contrast agents used in many bio-medical applications. The anti-Stokes emission from upconverting nanoparticles offers background free measurements of the biological samples with high penetration depth and practically no photobleaching; this enables the more sensitive and accurate medical diagnostics. Despite the many useful properties of UCNPs, the low emission intensity remains one of the obstacles hindering their applications. This property can be improved by changing the crystal field around the doped lanthanides in the crystal lattice.

In this thesis, the enhancement of the blue and UV upconversion intensities of Tm doped, fluoride based upconverting particles was studied. Different doping concentrations of non-luminescent and luminescent ions in the host matrix and their effects on the structural and optical properties of the resultant UCNPs were investigated in detail. Also different UC emissions were successfully used in a glucose assay as well as in a multiplexed bioaffinity assay.

The main conclusions based on the publications are

1. The blue emission from a $NaYF_4$:20%Yb,0.5%Tm nanocrystal was enhanced by substituting the host ions (Na^+ or Y^{3+}) with optimal concentrations of non-luminescent ions (K^+ or Sc^{3+}) with different ionic radius, during synthesis. The substituted ion changes the crystal field around the doped lanthanides, which affects the energy transfer efficiency and tunes the UC luminescence intensity. The host substitution not only alters the UC emission intensities, but also has a significant influence on the structure and size of the nanoparticles.

2. The UV emitting UCNPs act as an internal light source in the glucose sensing test strip. This was demonstrated by a simple glucose assay, using glucose in water or whole blood spiked with glucose as a sample. The results of the glucose measurement using UCNPs were compatible with the traditional method based on a reflectance measurement using an external UV source. The high penetration of the excitation light for UCNPs through blood sample offers a high degree of freedom for the detection setup. An additional benefit of the UCNPs is the internal control signal, which can be used to minimize the error arise in the assay.

3. The effect of increasing the sensitizer (Yb^{3+}) concentration in the $NaYF_4$ host lattice on the UV UC emission intensity was studied. The results shows a 20-fold increase in the UV emission intensity when all of the Y^{3+} ions in the host were replaced by Yb^{3+} ions. The optimal activator (Tm^{3+}) concentration was also fixed for an intense UV emitting nanoparticle.

4. Dual-mode multiplexing based on the spectral and spatial differentiation of signals using UCNPs as labels was demonstrated. The differentiation between antibody responses against influenza and adenovirus antigens and the detection of antibody classes was achieved based on both the position and the color of the signal. The same excitation source was used for both particles thus enabling a relatively simple instrumentation. This method could allow the diagnosis of infectious diseases and differentiation between primary and secondary infections.

ACKNOWLEDGMENTS

This research was carried out at the Department of Biotechnology, University of Turku during the years 2011-2015. The work was supported by the European Union under the Initial Training Network for Chemical Bioanalysis (ITN CHEBANA) and by the doctoral programme in Molecular Life Sciences of the University of Turku.

At this moment of accomplishment, the warmest possible thanks go first to my supervisor and mentor, Professor Tero Soukka. There are really no words to express my gratitude to you. Your guidance, support, encouragement and patience have been endless. I truly admire your integrity and dedication to your work and feel extremely privileged to have had you as my supervisor. I owe my sincere gratitude to my co-supervisor Adjunct Professor Mika Lastusaari for his valuable guidance and extensive discussions around my work.

I am grateful to Dr. Dariusz Hreniak and Professor Sakari Kulmala for reviewing this thesis. Their valuable advice and detailed comments helped to improve the thesis. I also want to thank Helen Cooper for reviewing the language of the thesis.

I wish to thank my co-authors Professor Jorma Hölsä, Dr. Timo Valta, Dr. Henna Päkkilä, Jiri Vainio, Anna Ahomaa and Dr. Shaikh M. Talha. The manuscripts would not have been possible without your help. I especially want to acknowledge Timo for collaborative manuscript with Roche Diagnostics and his friendship.

I am indebted to my present and previous colleagues at Department of Biotechnology for providing a stimulating and fun filled environment. My thanks go in particular to Susanne Lahdenperä, Dr. Terhi Riuttamäki, Maija Karp, Satu Lahtinen, Dr. Riikka Arppe, and Leena Mattsson. It was bit difficult for me when I switched from Chemistry to Biotechnology laboratory, but you people made it so easy for me. I would also like to acknowledge Minnea Tuomisto and Emilia Palo from Department of Chemistry for sharing their expertise on UCNP synthesis. I am very grateful to Susanne Lahdenperä for being such a wonderful colleague and best travel companion during all our CHEBANA trips. Your endless enthusiasm and energy is inspiring. I also owe thanks to Susanne and Timo for writing Finnish abstract of the thesis.

I was very fortunate to be a part of ITN CHEBANA programme. This network provided great opportunities to connect internationally. I wish to thank the coordinator of the programme Dr. Heike Mader for answering many of my silly questions. Huge thanks to all my CHEBANA colleagues for making our meetings memorable; I am hoping to see you all again in future. I also thank CHEBANA for giving me the opportunity to work with research groups from Regensburg and Compiegne where I spend some of the best time with the most amazing friends.

I expand my thanks to the Indian community in Turku, especially, Priyanka Negi for the great company in the lab and homemade food. My deepest gratitude goes to “Turku Marathi Mandal” (Maharashtrian community) for their love, hospitality, celebrations and amazing food; because of you guys Turku always felt home for me.

I would like to take this opportunity to thank my best friend Bhushan Gadgil for helping me get through the difficult times, and for all support, combraderie, entertainment and caring you provided. Your suggestions and criticisms always helped me to improve myself everyday both personally and professionally. We dreamed our PhD together long time before and now here we are; I wish you all the best for your doctoral dissertation. I am sure our friendship will last for the rest of our lives.

Finally, a special thanks to my family. Words cannot express how grateful I am to my parents and all the sacrifices you’ve made on my behalf. Your prayer for me was what sustained me thus far. I would like to express my gratitude to my sister Smita and brother Shivaji for always trusting in my capabilities and supporting me in all these years. I want to thank my brother-in-law Kiran for filling a family void created by my absence. A special thanks to my lovely little niece Kashvi and a new family member, my nephew Anay who brings a lot of happiness in the family.

Turku, November 2015

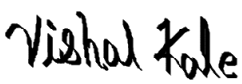

Vishal Kale

REFERENCES

[1] Rosi NL, Mirkin CA. Nanostructures in biodiagnostics. *Chem. Rev.* 2005;105:1547-62.

[2] Chen G, Qiu H, Prasad PN, Chen X. Upconversion nanoparticles: design, nanochemistry, and applications in theranostics. *Chem. Rev.* 2014;114:5161-214.

[3] Wang F, Chatterjee DK, Li Z, Zhang Y, Fan X, Wang M. Synthesis of polyethylenimine/$NaYF_4$ nanoparticles with upconversion fluorescence. *Nanotechnology*. 2006;17:5786.

[4] Chan EM. Combinatorial approaches for developing upconverting nanomaterials: High-throughput screening, modeling, and applications. *Chem. Soc. Rev.* 2015;44:1653-1679

[5] Chen G, Liu H, Liang H, Somesfalean G, Zhang Z. Upconversion emission enhancement in Yb^{3+}/Er^{3+}-codoped Y_2O_3 nanocrystals by tridoping with Li^+ ions. *J. Phys. Chem. C.* 2008;112:12030-36.

[6] Yu X, Schneiderhan-Marra N, Joos T. Protein microarrays for personalized medicine. *Clin. Chem.* 2010;56:376-87.

[7] Ellington AA, Kullo IJ, Bailey KR, Klee GG. Antibody-based protein multiplex platforms: technical and operational challenges. *Clin. Chem.* 2010;56:186-93.

[8] Wang L, Yan R, Huo Z, Wang L, Zeng J, Bao J, Wang X,Peng Q, Li Y. Fluorescence resonant energy transfer biosensor based on upconversion-luminescent nanoparticles. *Angew. Chem. Int. Ed.* 2005;44:6054-7.

[9] Beyazit S, Ambrosini S, Marchyk N, Palo E, Kale V, Soukka T, Bui B, Haupt K. Versatile synthetic strategy for coating upconverting nanoparticles with polymer shells through localized photopolymerization by using the particles as internal light sources. *Angew. Chem. Int. Ed.* 2014;53:8919-23.

[10] Auzel F. Compteur quantique par transfert denergie de Yb^{3+} a Tm^{3+} dans un tungstate mixte et dans un verre germanate. Comptes Rendus Hebdomadaires *Des Seances De L Academie Des Sciences Serie B.* 1966;263:819-&.

[11] He GS, Markowicz PP, Lin T-C, Prasad PN. Observation of stimulated emission by direct three-photon excitation. *Nature.* 2002;415:767-70.

[12] Zhou J, Liu Q, Feng W, Sun Y, Li F. Upconversion Luminescent Materials: Advances and Applications. Chem Rev. 2015;115:395-465.

[13] Singh-Rachford TN, Castellano FN. Photon upconversion based on sensitized triplet–triplet annihilation. Coordination *Chem. Rev.* 2010;254:2560-73.

[14] Zhao J, Ji S, Guo H. Triplet–triplet annihilation based upconversion: from triplet sensitizers and triplet acceptors to upconversion quantum yields. *Rsc Adv*. 2011;1:937-50.

[15] Haase M, Schäfer H. Upconverting nanoparticles. *Angew. Chem. Int. Ed.* 2011;50:5808-29.

[16] Stouwdam JW, Raudsepp M, van Veggel FCJM. Colloidal nanoparticles of Ln^{3+}-doped $LaVO_4$: energy transfer to visible- and near-infrared-emitting lanthanide ions. *Langmuir.* 2005;21:7003-8.

[17] Nichkova M, Dosev D, Gee SJ, Hammock BD, Kennedy IM. Microarray immunoassay for phenoxybenzoic acid using polymer encapsulated $Eu:Gd_2O_3$ nanoparticles as fluorescent labels. *Anal. Chem.* 2005;77:6864-73.

[18] Goldys EM, Drozdowicz-Tomsia K, Jinjun S, Dosev D, Kennedy IM, Yatsunenko S, Godlewski M. Optical characterization of Eu-doped and undoped Gd_2O_3 nanoparticles synthesized by the hydrogen flame pyrolysis method. *J. Am. Chem. Soc.* 2006;128:14498-505.

[19] Gordon WO, Carter JA, Tissue BM. Long-lifetime luminescence of lanthanide-doped gadolinium oxide nanoparticles for immunoassays. *J. Lumin.* 2004;108:339-42.

[20] Abdul Jalil R, Zhang Y. Biocompatibility of silica coated $NaYF_4$ upconversion fluorescent nanocrystals. *Biomaterials.* 2008;29:4122-8.

[21] Yu M, Li F, Chen Z, Hu H, Zhan C, Yang H, Chunhui H. Laser scanning up-conversion luminescence microscopy for imaging cells labeled with rare-earth nanophosphors. *Anal. Chem.* 2009;81:930-5.

[22] Xu CT, Svensson N, Axelsson J, Svenmarker P, Somesfalean G, Chen G, Liang H, Liu H, Zhang Z, Andersson-Engels S. Autofluorescence insensitive imaging using upconverting nanocrystals in scattering media. *Appl. Phys. Lett.* 2008;93:171103.

[23] Min Y, Li J, Liu F, Padmanabhan P, Yeow EK, Xing B. Recent advance of biological molecular imaging based on lanthanide-doped

upconversion-luminescent nanomaterials. *Nanomaterials.* 2014;4:129-54.

[24] Dong H, Sun L-D, Yan C-H. Energy transfer in lanthanide upconversion studies for extended optical applications. *Chem. Soc. Rev.* 2015;44:1608-34

[25] Capobianco JA, Vetrone F, Boyer JC, Speghini A, Bettinelli M. Enhancement of red emission ($^4F_{9/2}\rightarrow{}^4I_{15/2}$) via upconversion in bulk and nanocrystalline cubic Y_2O_3:Er^{3+}. *J. Phys. Chem. B.* 2002;106:1181-7.

[26] Heer S, Kömpe K, Güdel HU, Haase M. Highly efficient multicolour upconversion emission in transparent colloids of lanthanide-doped $NaYF_4$ nanocrystals. *Adv. Mater.* 2004;16:2102-5.

[27] Sun Y, Liu H, Wang X, Kong X, Zhang H. Optical spectroscopy and visible upconversion studies of YVO_4:Er^{3+} nanocrystals synthesized by a hydrothermal process. *Chem. mater.* 2006;18:2726-32.

[28] van de Rijke F, Zijlmans H, Li S, Vail T, Raap AK, Niedbala RS, Tanke HJ. Up-converting phosphor reporters for nucleic acid microarrays. *Nat. Biotech.* 2001;19:273-6.

[29] Chen D, Lei L, Zhang R, Yang A, Xu J, Wang Y. Intrinsic single-band upconversion emission in colloidal Yb/Er (Tm): Na_3Zr (Hf) F_7 nanocrystals. *Chem. Commun*. 2012;48:10630-2.

[30] Wang G, Peng Q, Li Y. Upconversion luminescence of monodisperse CaF_2: Yb^{3+}/Er^{3+} nanocrystals. *J. Am. Chem. Soc.* 2009;131:14200-1.

[31] Menyuk N, Dwight K, Pierce J. $NaYF_4$: Yb, Er—an efficient upconversion phosphor. *Appl. Phys. Lett.* 1972;21:159-61.

[32] Krämer KW, Biner D, Frei G, Güdel HU, Hehlen MP, Lüthi SR. Hexagonal sodium yttrium fluoride based green and blue emitting upconversion phosphors. *Chem. Mater.* 2004;16:1244-51.

[33] Auzel F. Upconversion and anti-stokes processes with f and d ions in solids. *Chem. Rev.* 2004;104:139-74.

[34] Wang F, Liu X. Recent advances in the chemistry of lanthanide-doped upconversion nanocrystals. *Chem. Soc. Rev.* 2009;38:976-89.

[35] Liang L, Wu H, Hu H, Wu M, Su Q. Enhanced blue and green upconversion in hydrothermally synthesized hexagonal $NaY_{1-x}YbxF_4$:Ln^{3+}(Ln^{3+}= Er^{3+} or Tm^{3+}). *J. alloys compd.* 2004;368:94-100.

[36] Sun L-D, Dong H, Zhang P-Z, Yan C-H. Upconversion of rare earth nanomaterials. *Annu Rev Phys Chem.* 2015;66.

[37] Auzel F. Compteur quantique par transfert denergie entre deux ions de terres rares dans un tungstate mixte ET dans un verre. Comptes Rendus Hebdomadaires. *Des Seances De L Academie Des Sciences Serie B.* 1966;262:1016-&.

[38] Zou X, Izumitani T. Spectroscopic properties and mechanisms of excited state absorption and energy transfer upconversion for Er^{3+}-doped glasses. *J. Non-Cryst. Solids*. 1993;162:68-80.

[39] Liu Y, Luo W, Zhu H, Chen X. Optical spectroscopy of lanthanides doped in wide band-gap semiconductor nanocrystals. *J. Lumin*. 2011;131:415-22.

[40] Luo W, Fu C, Li R, Liu Y, Zhu H, Chen X. Er^{3+}-doped anatase TiO_2 nanocrystals: crystal-field levels, excited-state dynamics, upconversion, and defect luminescence. *Small*. 2011;7:3046-56.

[41] Chivian JS, Case WE, Eden DD. The photon avalanche: A new phenomenon in Pr^{3+}-based infrared quantum counters. *Appl. Phys. Lett.* 1979;35:124.

[42] Dexter DL. Possibility of luminescent quantum yields greater than unity. *Phys. Rev.* 1957;108:630.

[43] Auzel F. Auzel, F. Upconversion processes in coupled ion systems. *J Lumin*. 1990;45:341.

[44] Maciel GS, Biswas A, Kapoor R, Prasad PN. Blue cooperative upconversion in Yb^{3+}-doped multicomponent sol-gel-processed silica glass for three-dimensional display. *Appl. Phys. Lett.* 2000;76:1978-80.

[45] Wang H, Duan C-k, Tanner PA. Visible upconversion luminescence from Y_2O_3:Eu^{3+},Yb^{3+}. *J. Phys. Chem. C.* 2008;112:16651-4.

[46] Su Q, Han S, Xie X, Zhu H, Chen H, Chen C-K, Liu RS, Chen X, Wang F. Liu X. The effect of surface coating on energy migration-mediated upconversion. *J. Am. Chem. Soc.* 2012;134:20849-57.

[47] Wang F, Deng R, Wang J, Wang Q, Han Y, Zhu H, Chen X, Liu X. Tuning upconversion through energy migration in core–shell nanoparticles. *Nat Mater.* 2011;10:968-73.

[48] Chen G, Qiu H, Fan R, Hao S, Tan S, Yang C, Han G. Lanthanide-doped ultrasmall yttrium fluoride nanoparticles with enhanced multicolor upconversion photoluminescence. *J. Mater. Chem.* 2012;22:20190-6.

[49] Niu N, Yang P, He F, Zhang X, Gai S, Li C, Lin J. Tunable multicolor and bright white emission of one-dimensional $NaLuF_4:Yb^{3+},Ln^{3+}$ (Ln = Er, Tm, Ho, Er/Tm, Tm/Ho) microstructures. *J. Mater. Chem.* 2012;22:10889-99.

[50] Wang F, Liu X. Upconversion multicolor fine-tuning: visible to near-infrared emission from lanthanide-doped $NaYF_4$ nanoparticles. *J. Am. Chem. Soc.* 2008;130:5642-3.

[51] Qiu H, Yang C, Shao W, Damasco J, Wang X, Ågren H, Prasad P, Chen G. Enhanced upconversion luminescence in Yb^{3+}/Tm^{3+}-codoped fluoride active core/active shell/inert shell nanoparticles through directed energy migration. *Nanomaterials.* 2014;4:55-68.

[52] Ehlert O, Thomann R, Darbandi M, Nann T. A four-color colloidal multiplexing nanoparticle system. *ACS Nano.* 2008;2:120-4.

[53] Sivakumar S, van Veggel FCM, Raudsepp M. Bright white light through up-conversion of a single NIR source from sol-gel-derived thin film made with Ln^{3+}-doped LaF_3 nanoparticles. *J. Am. Chem. Soc.* 2005;127:12464-5.

[54] Shen J, Chen G, Ohulchanskyy TY, Kesseli SJ, Buchholz S, Li Z, Prasad P, Han G. Tunable near infrared to ultraviolet upconversion luminescence enhancement in $(\alpha\text{-}NaYF_4:Yb,Tm)/CaF_2$ Core/Shell nanoparticles for in situ real-time recorded biocompatible photoactivation. *Small.* 2013:9:3213-3217.

[55] Lin J, Yu M, Lin C, Liu X. Multiform oxide optical materials via the versatile pechini-type sol–gel process: Synthesis and characteristics. *J. Phys. Chem. C*. 2007;111:5835-45.

[56] Gai S, Li C, Yang P, Lin J. Recent progress in rare earth micro/nanocrystals: soft chemical synthesis, luminescent properties, and biomedical applications. *Chem. Rev.* 2013;114:2343-89.

[57] Stouwdam JW, van Veggel FC. Near-infrared emission of redispersible Er^{3+}, Nd^{3+}, and Ho^{3+} doped LaF_3 nanoparticles. *Nano lett.* 2002;2:733-7.

[58] Yi G, Lu H, Zhao S, Ge Y, Yang W, Chen D, Guo L. Synthesis, characterization, and biological application of size-controlled nanocrystalline $NaYF_4$:Yb,Er infrared-to-visible up-Conversion phosphors. *Nano Lett.* 2004;4:2191-6.

[59] Zhang Y-W, Sun X, Si R, You L-P, Yan C-H. Single-crystalline and monodisperse LaF_3 triangular nanoplates from a single-source precursor. *J. Am. Chem. Soc*. 2005;127:3260-1.

[60] Mai H-X, Zhang Y-W, Si R, Yan Z-G, Sun L-d, You L-P, Yan C-H. High-quality sodium rare-earth fluoride nanocrystals: controlled synthesis and optical properties. *J. Am. Chem. Soc*. 2006;128:6426-36.

[61] Liu C, Wang H, Zhang X, Chen D. Morphology- and phase-controlled synthesis of monodisperse lanthanide-doped $NaGdF_4$nanocrystals with multicolor photoluminescence. *J. Mater. Chem.* 2009;19:489-96.

[62] Liu C, Wang H, Li X, Chen D. Monodisperse, size-tunable and highly efficient [small beta]-$NaYF_4$:Yb,Er(Tm) up-conversion luminescent nanospheres: controllable synthesis and their surface modifications. *J. Mater. Chem.* 2009;19:3546-53.

[63] Wei Y, Lu F, Zhang X, Chen D. Synthesis of oil-dispersible hexagonal-phase and hexagonal-shaped $NaYF_4$:Yb,Er nanoplates. *Chem. Mater.* 2006;18:5733-7.

[64] Li Z, Zhang Y. An efficient and user-friendly method for the synthesis of hexagonal-phase $NaYF_4$:Yb,Er/Tm nanocrystals with controllable shape and upconversion fluorescence. *Nanotechnology.* 2008;19:345606.

[65] Qian H, Li Z, Zhang Y. Multicolor polystyrene nanospheres tagged with up-conversion fluorescent nanocrystals. *Nanotechnology.* 2008;19:255601.

[66] Heer S, Kömpe K, Güdel HU, Haase M. Highly Efficient Multicolour Upconversion Emission in Transparent Colloids of Lanthanide-Doped $NaYF_4$ Nanocrystals. *Adv. Mater*. 2004;16:2102-5.

[67] Schäfer H, Ptacek P, Kömpe K, Haase M. Lanthanide-doped $NaYF_4$ nanocrystals in aqueous solution displaying strong up-conversion emission. *Chem. Mater.* 2007;19:1396-400.

[68] Yang J, Li C, Cheng Z, Zhang X, Quan Z, Zhang C, Lin J. Size-tailored synthesis and luminescent properties of one-dimensional Gd_2O_3: Eu^{3+} nanorods and microrods. *J. Phys. Chem. C*. 2007;111:18148-54.

[69] Wang X, Li Y. Synthesis and characterization of lanthanide hydroxide single-crystal nanowires. *Angew. Chem. Int. Ed.* 2002;41:4790-3.

[70] Ju Q, Liu Y, Tu D, Zhu H, Li R, Chen X. Lanthanide-doped multicolor GdF_3 nanocrystals for time-resolved photoluminescent biodetection. *Chem. Eur. J.* 2011;17:8549-54.

[71] Li Z, Zhang Y. Monodisperse Silica-Coated Polyvinylpyrrolidone/$NaYF_4$ nanocrystals with

multicolor upconversion fluorescence emission. *Angew. Chem. Int. Ed.*2006;118:7896-9.

[72] Zhao J, Sun Y, Kong X, Tian L, Wang Y, Tu L, Zhao J, Zhang H. Controlled synthesis, formation mechanism, and great enhancement of red upconversion luminescence of $NaYF_4$:Yb^{3+},Er^{3+} nanocrystals/submicroplates at low doping level. *J. Phys. Chem. B*. 2008;112:15666-72.

[73] Sun Y, Chen Y, Tian L, Yu Y, Kong X, Zhao J, Zhang H. Controlled synthesis and morphology dependent upconversion luminescence of $NaYF_4$:Yb,Er nanocrystals. *Nanotechnology.* 2007;18:275609.

[74] Wang M, Liu J-L, Zhang Y-X, Hou W, Wu X-L, Xu S-K. Two-phase solvothermal synthesis of rare-earth doped $NaYF_4$ upconversion fluorescent nanocrystals. *Mater. Lett.* 2009;63:325-7.

[75] Zhang F, Wan Y, Yu T, Zhang F, Shi Y, Xie S, Li Y, Xu L, Tu B, Zhao D. Uniform Nanostructured Arrays of Sodium Rare-Earth Fluorides for Highly Efficient Multicolor Upconversion Luminescence. *Angew. Chem. Int. Ed.*2007;46:7976-9.

[76] Zheng W, Huang P, Tu D, Ma E, Zhu H, Chen X. Lanthanide-doped upconversion nano-bioprobes: electronic structures, optical properties, and biodetection. *Chem. Soc. Rev.* 2015.

[77] Boyer J-C, Van Veggel FC. Absolute quantum yield measurements of colloidal $NaYF_4$:Er^{3+},Yb^{3+} upconverting nanoparticles. *Nanoscale.* 2010;2:1417-9.

[78] Huang P, Zheng W, Zhou S, Tu D, Chen Z, Zhu H, Li R, Ma E, Huang M, Chen X. Lanthanide-doped $LiLuF_4$ upconversion nanoprobes for the detection of disease biomarkers. *Angew. Chem. Int. Ed.*2014;53:1252-7.

[79] Singh S, Geusic J. Observation and Saturation of a Multiphoton Process in Nd Cl 3. *Phys Rev Lett.* 1966;17:865.

[80] Yang L, Song H, Yu L, Liu Z, Lu S. Unusual power-dependent and time-dependent upconversion luminescence in nanocrystals Y2O3:Ho^{3+}/Yb^{3+}. *J. lumin.* 2006;116:101-6.

[81] Bai X, Song H, Pan G, Lei Y, Wang T, Ren X, Lu S, Dong B, Dai Q, Fan L. Size-dependent upconversion luminescence in Er^{3+}/Yb^{3+}-codoped nanocrystalline yttria: Saturation and thermal effects. *J. Phys. Chem. C*. 2007;111:13611-7.

[82] Wilson R, Cossins AR, Spiller DG. Encoded microcarriers for high-throughput multiplexed detection. *Angew. Chem. Int. Ed.*2006;45:6104-17.

[83] Finkel NH, Lou X, Wang C, He L. Peer Reviewed: Barcoding the Microworld. *Anal. Chem.* 2004;76:352 A-9 A.

[84] Gorris HH, Wolfbeis OS. Photon-upconverting nanoparticles for optical encoding and multiplexing of cells, biomolecules, and microspheres. *Angew. Chem. Inte. Ed.*2013;52:3584-600.

[85] Meldal M, Christensen SF. Microparticle matrix encoding of beads. *Angew. Chem. Int. Ed.*2010;49:3473-6.

[86] Zhao J, Jin D, Schartner EP, Lu Y, Liu Y, Zvyagin AV, Zhang L, Dawes J, Xi P, Piper J, Goldys E, Monro T. Single-nanocrystal sensitivity achieved by enhanced upconversion luminescence. *Nat. Nano.* 2013;8:729-34.

[87] Zhang H, Li Y, Lin Y, Huang Y, Duan X. Composition tuning the upconversion emission in $NaYF_4$:Yb/Tm hexaplate nanocrystals. *Nanoscale.* 2011;3:963-6.

[88] Vetrone F, Boyer J-C, Capobianco JA, Speghini A, Bettinelli M. Significance of Yb^{3+} concentration on the upconversion mechanisms in codoped Y_2O_3:Er^{3+},Yb^{3+} nanocrystals. *J. Appl. Phys.* 2004;96:661-7.

[89] Mai H-X, Zhang Y-W, Sun L-D, Yan C-H. Highly efficient multicolor up-conversion emissions and their mechanisms of monodisperse $NaYF_4$:Yb,Er core and core/shell-structured nanocrystals. *J. Phys. Chem. C*. 2007;111:13721-9.

[90] Yin A, Zhang Y, Sun L, Yan C. Colloidal synthesis and blue based multicolor upconversion emissions of size and composition controlled monodisperse hexagonal $NaYF_4$:Yb,Tm nanocrystals. *Nanoscale*. 2010;2:953-9.

[91] Soukka T, Kuningas K, Rantanen T, Haaslahti V, Lövgren T. Photochemical characterization of up-converting inorganic lanthanide phosphors as potential labels. *J Fluoresc.* 2005;15:513-28.

[92] Teng X, Zhu Y, Wei W, Wang S, Huang J, Naccache R, Hu W, Tok A, Han Y, Zhang Q, Fan Q, Huang W, Capobianco J, Huang. Lanthanide-doped Na_xScF_{3+x} nanocrystals: crystal structure evolution and multicolor tuning. *J. Am. Chem. Soc.* 2012;134:8340-3.

[93] Ding Y, Teng X, Zhu H, Wang L, Pei W, Zhu J-J, Huang L, Huang W. Orthorhombic KSc_2F_7:Yb/Er nanorods: controlled synthesis and strong red upconversion emission. *Nanoscale*. 2013;5:11928-32.

[94] Wang J, Deng R, MacDonald MA, Chen B, Yuan J, Wang F, Chi D, Hor A, Zhang P, Liu G, Han Y, Liu

X. Enhancing multiphoton upconversion through energy clustering at sublattice level. *Nat. mater*. 2014;13:157-62.

[95] Mahalingam V, Vetrone F, Naccache R, Speghini A, Capobianco JA. Colloidal Tm^{3+}/Yb^{3+}-Doped $LiYF_4$ Nanocrystals: Multiple Luminescence Spanning the UV to NIR Regions via Low-Energy Excitation. *Adv. Mater.* 2009;21:4025-8.

[96] Shi F, Zhao Y. Sub-10 nm and monodisperse β-$NaYF_4$:Yb,Tm,Gd nanocrystals with intense ultraviolet upconversion luminescence. *J. Mater. Chem. C.* 2014;2:2198-203.

[97] Wang M, Mi C, Zhang Y, Liu J, Li F, Mao C, Xu S. NIR-responsive silica-coated $NaYbF_4$:Er/Tm/Ho upconversion fluorescent nanoparticles with tunable emission colors and their applications in immunolabeling and fluorescent imaging of cancer cells. *J. Phys. Chem. C*. 2009;113:19021-7.

[98] Wang G, Peng Q, Li Y. Luminescence tuning of upconversion nanocrystals. Chemistry. *Chem. Euro. J.* 2010;16:4923-31.

[99] Zeng JH, Xie T, Li ZH, Li Y. Monodispersed Nanocrystalline Fluoroperovskite Up-Conversion Phosphors. *Cryst. Growth.* 2007;7:2774-7.

[100] Wang J, Wang F, Wang C, Liu Z, Liu X. Single-Band Upconversion Emission in Lanthanide-Doped $KMnF_3$ Nanocrystals. *Angew. Chem. Int. Ed.*2011;50:10369-72.

[101] Selvin PR. Lanthanide-based resonance energy transfer. *Selected Topics in Quantum Electronics, IEEE Journal of.* 1996;2:1077-87.

[102] Li Z, Zhang Y, Jiang S. Multicolor Core/Shell-Structured Upconversion Fluorescent Nanoparticles. *Adv. Mater.* 2008;20:4765-9.

[103] Zhu S, Fischer T, Wan W, Descalzo AB, Rurack K. Luminescence amplification strategies integrated with microparticle and nanoparticle platforms. Luminescence applied in sensor science: *Springer*; 2011. p. 51-91.

[104] Cheng Q, Sui J, Cai W. Enhanced upconversion emission in Yb^{3+} and Er^{3+} codoped $NaGdF_4$ nanocrystals by introducing Li^+ ions. *Nanoscale*. 2012;4:779-84.

[105] Chen G, Liu H, Somesfalean G, Sheng Y, Liang H, Zhang Z, et al. Enhancement of the upconversion radiation in $Y_2O_3:Er^{3+}$ nanocrystals by codoping with Li^+ ions. *Appl.Phys. Lett.* 2008;92:113114--3.

[106] Bai Y, Wang Y, Yang K, Zhang X, Song Y, Wang C. Enhanced upconverted photoluminescence in Er^{3+} and Yb^{3+} codoped ZnO nanocrystals with and without Li^+ ions. *Opt. Commun*. 2008;281:5448-52.

[107] Dou Q, Zhang Y. Tuning of the structure and emission spectra of upconversion nanocrystals by alkali ion doping. *Langmuir*. 2011;27:13236-41.

[108] Sun Q, Zhao H, Chen X, Wang F, Cai W, Jiang Z. Upconversion emission enhancement in silica-coated $Gd_2O_3:Tm^{3+},Yb^{3+}$ nanocrystals by incorporation of Li^+ ion. *Mater. Chem. Phys*. 2010;123:806-10.

[109] Ramasamy P, Chandra P, Rhee SW, Kim J. Enhanced upconversion luminescence in $NaGdF_4$: Yb, Er nanocrystals by Fe^{3+} doping and their application in bioimaging. *Nanoscale.* 2013;5:8711-7.

[110] Jiang L, Xiao S, Yang X, Ding J, Dong K. Enhancement of up-conversion luminescence in Zn_2SiO_4: Yb^{3+}, Er^{3+} by co-doping with Li^+ or Bi^{3+}. *Appl Phys B.* 2012;107:477-81.

[111] Li Y, Wang G, Pan K, Fan N, Liu S, Feng L. Controlled synthesis and tunable upconversion luminescence of $NaYF_4$: Yb^{3+}/Er^{3+} nanocrystals by Pb^{2+} tridoping. *RSC Adv*. 2013;3:1683-6.

[112] Yu H, Cao W, Huang Q, Ma E, Zhang X, Yu J. Upcoversion performance improvement of $NaYF_4$: Yb, Er by Sn codoping: Enhanced emission intensity and reduced decay time. *J. Solid State Chem.* 2013;207:170-7.

[113] Qu X, Yang HK, Pan G, Chung JW, Moon BK, Choi BC, Jeong JH. Controlled fabrication and shape-dependent luminescence properties of hexagonal $NaCeF_4$, $NaCeF_4$: Tb^{3+} nanorods via polyol-mediated solvothermal route. *Inorg. chem.* 2011;50:3387-93.

[114] Hao S, Shao W, Qiu H, Shang Y, Fan R, Guo X, Zhao L, Chen G, Yang C. Tuning the size and upconversion emission of $NaYF_4$: Yb^{3+}/Pr^{3+} nanoparticles through Yb^{3+} doping. *RSC Adv.* 2014;4:56302-6.

[115] Huang X, Han S, Huang W, Liu X. Enhancing solar cell efficiency: the search for luminescent materials as spectral converters. *Chem. Soc. Rev.* 2013;42:173-201.

[116] Zhao J, Lu Z, Yin Y, McRae C, Piper JA, Dawes JM, Jin D, Goldys E. Upconversion luminescence with tunable lifetime in $NaYF_4$:Yb,Er nanocrystals: role of nanocrystal size. *Nanoscale*. 2013;5:944-52.

[117] Wang F, Wang J, Liu X. Direct Evidence of a Surface Quenching Effect on Size-Dependent

Luminescence of Upconversion Nanoparticles. *Angew. Chem.* 2010;122:7618-22.

[118] Li Z, Zhang Y. An efficient and user-friendly method for the synthesis of hexagonal-phase $NaYF_4$:Yb,Er/Tm nanocrystals with controllable shape and upconversion fluorescence. *Nanotechnology.* 2008;19:345606.

[119] Ding M, Lu C, Cao L, Ni Y, Xu Z. Controllable synthesis, formation mechanism and upconversion luminescence of β-$NaYF_4$:Yb^{3+}/Er^{3+} microcrystals by hydrothermal process. *CrystEngComm.* 2013;15:8366-73.

[120] Vetrone F, Naccache R, Mahalingam V, Morgan CG, Capobianco JA. The Active-Core/Active-Shell Approach: A Strategy to Enhance the Upconversion Luminescence in Lanthanide-Doped Nanoparticles. *Adv. Funct. Mater.* 2009;19:2924-9.

[121] Yi G-S, Chow G-M. Water-Soluble $NaYF_4$:Yb,Er(Tm)/$NaYF_4$/Polymer Core/Shell/Shell Nanoparticles with Significant Enhancement of Upconversion Fluorescence. *Chem. Mater.* 2007;19:341-3.

[122] Boyer J-C, van Veggel FCJM. Absolute quantum yield measurements of colloidal $NaYF_4$: Er^{3+}, Yb^{3+} upconverting nanoparticles. *Nanoscale.* 2010;2:1417-9.

[123] Liu Y, Tu D, Zhu H, Li R, Luo W, Chen X. A Strategy to Achieve Efficient Dual-Mode Luminescence of Eu^{3+} in Lanthanides Doped Multifunctional $NaGdF_4$ Nanocrystals. *Adv.mater.* 2010;22:3266-71.

[124] Du Y-P, Sun X, Zhang Y-W, Yan Z-G, Sun L-D, Yan C-H. Uniform alkaline earth fluoride nanocrystals with diverse shapes grown from thermolysis of metal trifluoroacetates in hot surfactant solutions. *Cryst. Growth.* 2009;9:2013-9.

[125] Wong H-T, Vetrone F, Naccache R, Chan HLW, Hao J, Capobianco JA. Water dispersible ultra-small multifunctional $KGdF_4$:Tm^{3+}, Yb^{3+} nanoparticles with near-infrared to near-infrared upconversion. *J. Mater. Chem.* 2011;21:16589-96.

[126] Chen G, Ohulchanskyy TY, Law WC, Agren H, Prasad PN. Monodisperse $NaYbF_4$: Tm^{3+}/$NaGdF_4$ core/shell nanocrystals with near-infrared to near-infrared upconversion photoluminescence and magnetic resonance properties. *Nanoscale.* 2011;3:2003-8.

[127] Dong C, Korinek A, Blasiak B, Tomanek B, van Veggel FCJM. Cation Exchange: A Facile Method To Make $NaYF_4$:Yb,Tm-$NaGdF_4$ Core–Shell Nanoparticles with a Thin, Tunable, and Uniform Shell. *Chem. Mater.* 2012;24:1297-305.

[128] Qian H-S, Zhang Y. Synthesis of Hexagonal-Phase Core–Shell NaYF4 Nanocrystals with Tunable Upconversion Fluorescence. *Langmuir.* 2008;24:12123-5.

[129] Jain PK, Huang X, El-Sayed IH, El-Sayed MA. Noble metals on the nanoscale: optical and photothermal properties and some applications in imaging, sensing, biology, and medicine. *Acc. Chem. Res.* 2008;41:1578-86.

[130] Hutter E, Fendler JH. Exploitation of localized surface plasmon resonance. *Adv. Mater.* 2004;16:1685-706.

[131] Zhang H, Xu D, Huang Y, Duan X. Highly spectral dependent enhancement of upconversion emission with sputtered gold island films. *Chem. Comm.* 2011;47:979-81.

[132] Xu W, Xu S, Zhu Y, Liu T, Bai X, Dong B, Xu L, Song H. Ultra-broad plasma resonance enhanced multicolor emissions in an assembled Ag/$NaYF_4$:Yb,Er nano-film. *Nanoscale.* 2012;4:6971-3.

[133] Paudel HP, Zhong L, Bayat K, Baroughi MF, Smith S, Lin C, Jiang C, Berry M, May P. Enhancement of Near-Infrared-to-Visible Upconversion Luminescence Using Engineered Plasmonic Gold Surfaces. *J. Phys. Chem. C*. 2011;115:19028-36.

[134] Kannan P, Abdul Rahim F, Chen R, Teng X, Huang L, Sun H, Kim D. Au Nanorod Decoration on $NaYF_4$:Yb/Tm Nanoparticles for Enhanced Emission and Wavelength-Dependent Biomolecular Sensing. *ACS Appl. Mater. Interfaces.* 2013;5:3508-13.

[135] Schietinger S, Aichele T, Wang H-Q, Nann T, Benson O. Plasmon-Enhanced Upconversion in Single $NaYF_4$:Yb^{3+}/Er^{3+} Codoped Nanocrystals. *Nano Lett.* 2010;10:134-8.

[136] Zhang F, Braun GB, Shi Y, Zhang Y, Sun X, Reich NO,Zhao D, Stucky G. Fabrication of Ag@SiO_2@Y_2O_3:Er nanostructures for bioimaging: tuning of the upconversion fluorescence with silver nanoparticles. *J. Am. Chem. Soc.* 2010;132:2850-1.

[137] Sedlmeier A, Gorris HH. Surface modification and characterization of photon-upconverting nanoparticles for bioanalytical applications. *Chem. Soc. Rev.* 2015;44:1526-1560.

[138] Lemieux RU, Rudloff EV. Periodate-permanganate oxidation: I. oxidation of olefins. *Can. J. Chem.* 1955;33:1701-9.

[139] Zhou H-P, Xu C-H, Sun W, Yan C-H. Clean and flexible modification strategy for carboxyl/aldehyde-functionalized upconversion nanoparticles and their optical applications. *Adv. Funct. Mater.* 2009;19:3892-900.

[140] Chen Z, Chen H, Hu H, Yu M, Li F, Zhang Q, Zhou Z, Yi T, Huang C. Versatile synthesis strategy for carboxylic acid−functionalized upconverting nanophosphors as biological labels. *J. Am. Chem. Soc.* 2008;130:3023-9.

[141] Hu H, Yu M, Li F, Chen Z, Gao X, Xiong L, Huang C. Facile Epoxidation Strategy for Producing Amphiphilic Up-Converting Rare-Earth Nanophosphors as Biological Labels. *Chem. Mater.*2008;20:7003-9.

[142] Rantanen T, Jarvenpaa M-L, Vuojola J, Arppe R, Kuningas K, Soukka T. Upconverting phosphors in a dual-parameter LRET-based hybridization assay. *Analyst.* 2009;134:1713-6.

[143] Boyer J-C, Manseau M-P, Murray JI, van Veggel FCJM. Surface Modification of Upconverting $NaYF_4$ Nanoparticles with PEG−Phosphate Ligands for NIR (800 nm) Biolabeling within the Biological Window. *Langmuir*. 2010;26:1157-64.

[144] Zhan Q, Qian J, Liang H, Somesfalean G, Wang D, He S, Zhang Z, Andresson-Engels S. Using 915 nm Laser Excited Tm^{3+}/Er^{3+}/Ho^{3+}-Doped $NaYbF_4$ Upconversion Nanoparticles for in Vitro and Deeper in Vivo Bioimaging without Overheating Irradiation. *ACS Nano.* 2011;5:3744-57.

[145] Nyk M, Kumar R, Ohulchanskyy TY, Bergey EJ, Prasad PN. High Contrast in Vitro and in Vivo Photoluminescence Bioimaging Using Near Infrared to Near Infrared Up-Conversion in Tm^{3+} and Yb^{3+} Doped Fluoride Nanophosphors. *Nano Lett.* 2008;8:3834-8.

[146] Yi G, Peng Y, Gao Z. Strong Red-Emitting near-Infrared-to-Visible Upconversion Fluorescent Nanoparticles. *Chem. Mater.* 2011;23:2729-34.

[147] Yi GS, Chow GM. Synthesis of Hexagonal-Phase $NaYF_4$:Yb,Er and $NaYF_4$:Yb,Tm Nanocrystals with Efficient Up-Conversion Fluorescence. *Adv. Funct. Mater*. 2006;16:2324-9.

[148] Aldana J, Lavelle N, Wang Y, Peng X. Size-Dependent Dissociation pH of Thiolate Ligands from Cadmium Chalcogenide Nanocrystals. *J. Am. Chem. Soc*. 2005;127:2496-504.

[149] Li L-L, Wu P, Hwang K, Lu Y. An exceptionally simple strategy for DNA-functionalized up-conversion nanoparticles as biocompatible agents for nanoassembly, DNA delivery, and imaging. *J. Am. Chem. Soc*. 2013;135:2411-4.

[150] Cheng L, Yang K, Zhang S, Shao M, Lee S, Liu Z. Highly-sensitive multiplexed in vivo imaging using pegylated upconversion nanoparticles. *Nano Res.* 2010;3:722-32.

[151] Jiang G, Pichaandi J, Johnson NJJ, Burke RD, van Veggel FCJM. An Effective Polymer Cross-Linking Strategy To Obtain Stable Dispersions of Upconverting NaYF4 Nanoparticles in Buffers and Biological Growth Media for Biolabeling Applications. *Langmuir*. 2012;28:3239-47.

[152] Bian T, Wang C, Lu Z, Xie R, Yang Q-Z, Wu L-Z, Tung CH, Liu Z, Yin Y, Zhang T. A Versatile 'Click Chemistry' Route to Size-Restricted, Robust, and Functionalizable Hydrophilic Nanocrystals. *Small.* 2015;11:1644-8.

[153] Graf C, Vossen DLJ, Imhof A, van Blaaderen A. A General Method To Coat Colloidal Particles with Silica. *Langmuir.* 2003;19:6693-700.

[154] Yi DK, Selvan ST, Lee SS, Papaefthymiou GC, Kundaliya D, Ying JY. Silica-Coated Nanocomposites of Magnetic Nanoparticles and Quantum Dots. *J. Am. Chem. Soc*. 2005;127:4990-1.

[155] Selvan ST, Tan TT, Ying JY. Robust, Non-Cytotoxic, Silica-Coated CdSe Quantum Dots with Efficient Photoluminescence. *Adv. Mater*. 2005;17:1620-5.

[156] Stöber W, Fink A, Bohn E. Controlled growth of monodisperse silica spheres in the micron size range. *J Colloid Interface Sci.* 1968;26:62-9.

[157] Sivakumar S, Diamente PR, van Veggel FCJM. Silica-Coated Ln^{3+}-Doped LaF_3 Nanoparticles as Robust Down- and Upconverting Biolabels. *Chem. Euro. J.* 2006;12:5878-84.

[158] Ylihärsilä M, Valta T, Karp M, Hattara L, Harju E, Hölsä J, Saviranta P, Waris M, Soukka T. Oligonucleotide array-in-well platform for detection and genotyping human adenoviruses by utilizing upconverting phosphor label technology. *Anal. Chem.* 2011;83:1456-61.

[159] Hu H, Xiong L, Zhou J, Li F, Cao T, Huang C. Multimodal-luminescence core–shell nanocomposites for targeted imaging of tumor cells. *Chem. Eur. J*. 2009;15:3577-84.

[160] Li Z, Wang L, Wang Z, Liu X, Xiong Y. Modification of $NaYF_4$:Yb,Er@SiO_2 nanoparticles with gold nanocrystals for tunable green-to-red

upconversion emissions. *J. Phys. Chem. C*. 2011;115:3291-6.

[161] Faure A-C, Hoffmann C, Bazzi R, Goubard F, Pauthe E, Marquette CA, Blum LJ, Perriat P, Roux S, Tillement O. Functionalization of luminescent aminated particles for facile bioconjugation. *ACS Nano.* 2008;2:2273-82.

[162] Mialon G, Poggi M, Casanova D, Nguyen T-L, Türkcan S, Alexandrou A, Gacoin T, Boilot JP. Luminescent oxide nanoparticles with enhanced optical properties. *J. Lumin*. 2009;129:1706-10.

[163] Hermanson GT. The chemistry of reactive groups. *Bioconjugate techniques*. 2008;184.

[164] Rostovtsev VV, Green LG, Fokin VV, Sharpless KB. A stepwise huisgen cycloaddition process: copper(I)-catalyzed regioselective "Ligation" of azides and terminal alkynes. *Angew. Chem. Int. Ed.*2002;41:2596-9.

[165] Tornøe CW, Christensen C, Meldal M. Peptidotriazoles on Solid Phase: [1,2,3]-Triazoles by Regiospecific Copper(I)-Catalyzed 1,3-Dipolar Cycloadditions of Terminal Alkynes to Azides. *J. Org. Chem.* 2002;67:3057-64.

[166] Mader HS, Kele P, Saleh SM, Wolfbeis OS. Upconverting luminescent nanoparticles for use in bioconjugation and bioimaging. *Curr Opin Chem Biol.* 2010;14:582-96.

[167] Zhou J, Liu Z, Li F. Upconversion nanophosphors for small-animal imaging. *Chem. Soc. Rev.* 2012;41:1323-49.

[168] Lowry M, Fakayode SO, Geng ML, Baker GA, Wang L, McCarroll ME, Patonay G, Warner I. Molecular fluorescence, phosphorescence, and chemiluminescence spectrometry. *Anal Chem*. 2008;80:4551-74.

[169] Suyver JF, Aebischer A, Biner D, Gerner P, Grimm J, Heer S, Krämer KW, Reinhard C, Gudel H. Novel materials doped with trivalent lanthanides and transition metal ions showing near-infrared to visible photon upconversion. *Opt. Mater.* 2005;27:1111-30.

[170] Downing E, Hesselink L, Ralston J, Macfarlane R. A three-color, solid-state, three-dimensional display. *Science*. 1996;273:1185.

[171] Yuan C, Chen G, Prasad PN, Ohulchanskyy TY, Ning Z, Tian H, Sun L, Agren H. Use of colloidal upconversion nanocrystals for energy relay solar cell light harvesting in the near-infrared region. *J. Mater. Chem.* 2012;22:16709-13.

[172] Chen G, Seo J, Yang C, Prasad PN. Nanochemistry and nanomaterials for photovoltaics. *Chem. Soc. Rev*. 2013;42:8304-38.

[173] Qian Y, Wang R, Wang B, Zhang B, Gao S. Strong 1550 nm to visible luminescence in In/Er/Yb:LiNbO3 crystal considered as an upconverter for solar cells. *RSC Adv.* 2014;4:6652-6.

[174] Idris NM, Gnanasammandhan MK, Zhang J, Ho PC, Mahendran R, Zhang Y. In vivo photodynamic therapy using upconversion nanoparticles as remote-controlled nanotransducers. *Nat Med*. 2012;18:1580-5.

[175] Suzuki M, Tseeb V, Oyama K, Ishiwata Si. Microscopic detection of thermogenesis in a single HeLa cell. Biophys J. 2007;92:L46-L8.

[176] Zohar O, Ikeda M, Shinagawa H, Inoue H, Nakamura H, Elbaum D, Alkon D, Yoshoka T. Thermal imaging of receptor-activated heat production in single cells. *Biophys J.* 1998;74:82-9.

[177] Fischer LH, Harms GS, Wolfbeis OS. Upconverting nanoparticles for nanoscale thermometry. *Angew. Chem. Int. Ed.* 2011;50:4546-51.

[178] Vetrone F, Naccache R, Zamarron A, Juarranz de la Fuente A, Sanz-Rodríguez F, Martinez Maestro L,Rodriguez E, Jaque D, Sole J, Capobianco A. Temperature sensing using fluorescent nanothermometers. ACS nano. 2010;4:3254-8.

[179] Wang X, Kong X, Yu Y, Sun Y, Zhang H. Effect of annealing on upconversion luminescence of ZnO: Er^{3+} nanocrystals and high thermal sensitivity. *J. Phys. Chem. C*. 2007;111:15119-24.

[180] Singh SK, Kumar K, Rai S. Er^{3+}/Yb^{3+} codoped Gd_2O_3 nano-phosphor for optical thermometry. *Sens. Actuators A.* 2009;149:16-20.

[181] Sedlmeier A, Achatz DE, Fischer LH, Gorris HH, Wolfbeis OS. Photon upconverting nanoparticles for luminescent sensing of temperature. *Nanoscale.* 2012;4:7090-6.

[182] Zheng K, Song W, He G, Yuan Z, Qin W. Five-photon UV upconversion emissions of Er^{3+} for temperature sensing. *Opt. Express.* 2015;23:7653-8.

[183] Voraberger HS, Kreimaier H, Biebernik K, Kern W. Novel oxygen optrode withstanding autoclavation: technical solutions and performance. *Sens. Actuators B.* 2001;74:179-85.

[184] Huo C, Zhang H, Zhang H, Zhang H, Yang B, Zhang P, Wang Y. Synthesis and assembly with

mesoporous silica MCM-48 of platinum(II) porphyrin complexes bearing carbazyl groups: spectroscopic and oxygen sensing properties. *Inorg. Chem.* 2006;45:4735-42.

[185] Achatz DE, Meier RJ, Fischer LH, Wolfbeis OS. Luminescent sensing of oxygen using a quenchable probe and upconverting nanoparticles. *Angew. Chem. Int. Ed.* 2011;50:260-3.

[186] Liu L, Li B, Qin R, Zhao H, Ren X, Su Z. Synthesis and characterization of new bifunctional nanocomposites possessing upconversion and oxygen-sensing properties. *Nanotechnology.* 2010;21:285701.

[187] Ali R, Saleh SM, Meier RJ, Azab HA, Abdelgawad II, Wolfbeis OS. Upconverting nanoparticle based optical sensor for carbon dioxide. *Sens Actuators B.* 2010;150:126-31.

[188] Mader HS, Wolfbeis OS. Optical Ammonia sensor based on upconverting luminescent nanoparticles. *Anal. Chem.* 2010;82:5002-4.

[189] Liu J, Yang X, He X, Wang K, Wang Q, Guo Q, Shi H, Huang J, Huo X. Fluorescent nanoparticles for chemical and biological sensing. *Sci. China Chem.* 2011;54:1157-76.

[190] Sun L-N, Peng H, Stich MIJ, Achatz D, Wolfbeis OS. pH sensor based on upconverting luminescent lanthanide nanorods. *Chem Comm.* 2009:5000-2.

[191] Meier RJ, Simbürger JM, Soukka T, Schäferling M. Background-free referenced luminescence sensing and imaging of pH using upconverting phosphors and color camera read-out. *Anal. Chem*. 2014;86:5535-40.

[192] Liu J, Liu Y, Liu Q, Li C, Sun L, Li F. Iridium(III) complex-coated nanosystem for ratiometric upconversion luminescence bioimaging of cyanide anions. *J. Am. Chem. Soc*. 2011;133:15276-9.

[193] Liu Q, Peng J, Sun L, Li F. High-efficiency upconversion luminescent sensing and bioimaging of Hg(II) by chromophoric ruthenium complex-assembled nanophosphors. *ACS Nano.* 2011;5:8040-8.

[194] Wilhelm S, del Barrio M, Heiland J, Himmelstoß SF, Galbán J, Wolfbeis OS, Hirsch T. Spectrally matched upconverting luminescent nanoparticles for monitoring enzymatic reactions. *ACS Appl. Mater. interfaces*. 2014;6:15427-33.

[195] Siitari H, Hemmilä I, Soini E, Lövgren T, Koistinen V. Detection of hepatitis B surface antigen using time-resolved fluoroimmunoassay. *Nature*. 1983;301:258-260.

[196] Wang X-d, Stolwijk JA, Lang T, Sperber M, Meier RJ, Wegener J, Wolfbeis S. Ultra-small, highly stable, and sensitive dual nanosensors for imaging intracellular oxygen and pH in cytosol. *J. Am. Chem. Soc*. 2012;134:17011-4.

[197] Hong Y, Lam JW, Tang BZ. Aggregation-induced emission: phenomenon, mechanism and applications. *Chem. Comm.* 2009:4332-53.

[198] Zijlmans H, Bonnet J, Burton J, Kardos K, Vail T, Niedbala R, Tanke H. Detection of cell and tissue surface antigens using up-converting phosphors: a new reporter technology. *Anal. Biochem.* 1999;267:30-6.

[199] Zhang F, Shi Q, Zhang Y, Shi Y, Ding K, Zhao D, Stucky G. Fluorescence Upconversion Microbarcodes for Multiplexed Biological Detection: Nucleic Acid Encoding. *Adv. Mater.* 2011;23:3775-9.

[200] Achatz DE, Ali R, Wolfbeis OS. Luminescent chemical sensing, biosensing, and screening using upconverting nanoparticles. Luminescence applied in sensor science: *Springer;* 2011. p. 29-50.

[201] Zuiderwijk M, Tanke HJ, Niedbala RS, Corstjens PL. An amplification-free hybridization-based DNA assay to detect Streptococcus pneumoniae utilizing the up-converting phosphor technology. *Clin Biochem.* 2003;36:401-3.

[202] Hampl J, Hall M, Mufti NA, Yung-mae MY, MacQueen DB, Wright WH, Cooper DE. Upconverting phosphor reporters in immunochromatographic assays. *Anal Biochem.* 2001;288:176-87.

[203] Li L, Zhou L, Yu Y, Zhu Z, Lin C, Lu C, Yang R. Development of up-converting phosphor technology-based lateral-flow assay for rapidly quantitative detection of hepatitis B surface antibody. *Diagn Microbiol Infect Dis.* 2009;63:165-72.

[204] Zhao P, Wu Y, Zhu Y, Yang X, Jiang X, Xiao J, Zhang Y, Li C. Upconversion fluorescent strip sensor for rapid determination of Vibrio anguillarum. *Nanoscale.* 2014;6:3804-9.

[205] Yan Z, Zhou L, Zhao Y, Wang J, Huang L, Hu K, Liu H, Wang H, Guo Z,Song Y, Huang H,Yang R. Rapid quantitative detection of Yersinia pestis by lateral-flow immunoassay and up-converting phosphor technology-based biosensor. *Sens. Actuators B.* 2006;119:656-63.

[206] Corstjens PL, Zuiderwijk M, Nilsson M, Feindt H, Niedbala RS, Tanke HJ. Lateral-flow and up-converting phosphor reporters to detect single-stranded nucleic acids in a sandwich-hybridization assay. *Anal. Biochem.* 2003;312:191-200.

[207] Corstjens P, Zuiderwijk M, Brink A, Li S, Feindt H, Niedbala RS, Tanke H. Use of up-converting phosphor reporters in lateral-flow assays to detect specific nucleic acid sequences: a rapid, sensitive DNA test to identify human papillomavirus type 16 infection. *Clin. Chem.* 2001;47:1885-93.

[208] Corstjens PL, Chen Z, Zuiderwijk M, Bau HH, Abrams WR, Malamud D, Niedbala R, Tanke H. Rapid assay format for multiplex detection of humoral immune responses to infectious disease pathogens (HIV, HCV, and TB). *Ann N Y Acad Sci.* 2007;1098:437-45.

[209] Corstjens PL, van Lieshout L, Zuiderwijk M, Kornelis D, Tanke HJ, Deelder AM, Dam G. Up-converting phosphor technology-based lateral flow assay for detection of Schistosoma circulating anodic antigen in serum. *J Clin Microbiol.* 2008;46:171-6.

[210] Qu Q, Zhu Z, Wang Y, Zhong Z, Zhao J, Qiao F, Du X, Wang Z, Yang R, Huang L, Yu Y, Zhou L, Chen Z. Rapid and quantitative detection of Brucella by up-converting phosphor technology-based lateral-flow assay. *J Microbiol Methods.* 2009;79:121-3.

[211] Niedbala RS, Feindt H, Kardos K, Vail T, Burton J, Bielska B, Li S, Milunic D, Bourdelle P, Vallejo R. Detection of analytes by immunoassay using up-converting phosphor technology. *Anal. Biochem.* 2001;293:22-30.

[212] Tisone TC, O'Farrell B. Manufacturing the next generation of highly sensitive and reproducible lateral flow immunoassay *Lateral flow immunoassay; Springer*; 2009.

[213] Eliseeva SV, Bünzli J-CG. Lanthanide luminescence for functional materials and bio-sciences. *Chem. Soc. Rev.* 2010;39:189-227.

[214] Bünzli J-CG. Lanthanide luminescence for biomedical analyses and imaging. *Chem. Rev.* 2010;110:2729-55.

[215] Wang P, Ahmadov TO, Lee C, Zhang P. Ligase-assisted signal-amplifiable DNA detection using upconversion nanoparticles. *RSC Adv.* 2013;3:16326-9.

[216] Zhang C, Yuan Y, Zhang S, Wang Y, Liu Z. Biosensing platform based on fluorescence resonance energy transfer from upconverting nanocrystals to graphene oxide. *Angew. Chem. Int. Ed.* 2011;50:6851-4.

[217] Deng R, Xie X, Vendrell M, Chang Y-T, Liu X. Intracellular glutathione detection using MnO_2-nanosheet-modified upconversion nanoparticles. *J. Am. Chem. Soc.*2011;133:20168-71.

[218] Kuningas K, Rantanen T, Ukonaho T, Lövgren T, Soukka T. Homogeneous assay technology based on upconverting phosphors. *Anal. Chem.* 2005;77:7348-55.

[219] Wang Y, Wu Z, Liu Z. Upconversion fluorescence resonance energy transfer biosensor with aromatic polymer nanospheres as the lable-free energy acceptor. *Anal Chem*. 2013;85:258-64.

[220] Rabouw FT, den Hartog SA, Senden T, Meijerink A. Photonic effects on the Förster resonance energy transfer efficiency. *Nat. commun.* 2014;5.

[221] Zhang P, Rogelj S, Nguyen K, Wheeler D. Design of a highly sensitive and specific nucleotide sensor based on photon upconverting particles. *J. Am. Chem. Soc*. 2006;128:12410-1.

[222] Kumar M, Guo Y, Zhang P. Highly sensitive and selective oligonucleotide sensor for sickle cell disease gene using photon upconverting nanoparticles. *Biosens Bioelectron*. 2009;24:1522-6.

[223] Kumar M, Zhang P. Highly sensitive and selective label-free optical detection of DNA hybridization based on photon upconverting nanoparticles. *Langmuir*. 2009;25:6024-7.

[224] Wang M, Hou W, Mi C-C, Wang W-X, Xu Z-R, Teng H-H, Mao C, Xu S. Immunoassay of goat antihuman immunoglobulin G antibody based on luminescence resonance energy transfer between near-infrared responsive $NaYF_4$:Yb, Er upconversion fluorescent nanoparticles and gold nanoparticles. *Anal. Chem.* 2009;81:8783-9.

[225] Wang Y, Shen P, Li C, Wang Y, Liu Z. Upconversion fluorescence resonance energy transfer based biosensor for ultrasensitive detection of matrix metalloproteinase-2 in blood. *Anal. Chem.* 2012;84:1466-73.

[226] Grabolle M, Kapusta P, Nann T, Shu X, Ziegler J, Resch-Genger U. Fluorescence Lifetime Multiplexing with Nanocrystals and Organic Labels. *Anal. Chem.* 2009;81:7807-13.

[227] Templin MF, Stoll D, Bachmann J, Joos TO. Protein microarrays and multiplexed sandwich immunoassays: what beats the beads? *Comb chem high t scr*. 2004;7:223-9.

[228] de Jager W, Rijkers GT. Solid-phase and bead-based cytokine immunoassay: a comparison. *Methods*. 2006;38:294-303.

[229] Waterboer T, Sehr P, Pawlita M. Suppression of non-specific binding in serological Luminex assays. *J Immunol Methods.* 2006;309:200-4.

[230] Nichkova M, Dosev D, Gee SJ, Hammock BD, Kennedy IM. Multiplexed immunoassays for proteins using magnetic luminescent nanoparticles for internal calibration. *Anal Biochem.* 2007;369:34-40.

[231] Sefers SE, Li H, Tang Y-W. Simultaneous detection and differentiation of respiratory syncytial virus and other respiratory viral pathogens. *Diagnostic Virology Protocols.* 2011. p. 309-23.

[232] Liu Y, Xu Z-q, Zhang Q, Jin M, Yu J-m, Li J-s, Liu N,Cui S, Kong X, Wang H, Li H, Cheng W, Ma X, Duan Z. Simultaneous detection of seven enteric viruses associated with acute gastroenteritis by a multiplexed Luminex-based assay. *J. Clin. Microbiol.* 2012;50:2384-9.

[233] Yan X, Zhong W, Tang A, Schielke EG, Hang W, Nolan JP. Multiplexed flow cytometric immunoassay for influenza virus detection and differentiation. *Anal. Chem*. 2005;77:7673-8.

[234] Peng C, Li Z, Zhu Y, Chen W, Yuan Y, Liu L, Li Q, Xu D, Qiao R, Wang L, Zhu S, Jin Z. Simultaneous and sensitive determination of multiplex chemical residues based on multicolor quantum dot probes. *Biosens Bioelectron.* 2009;24:3657-62.

[235] Wu J, Yan F, Tang J, Zhai C, Ju H. A disposable multianalyte electrochemical immunosensor array for automated simultaneous determination of tumor markers. *Clin. Chem.* 2007;53:1495-502.

[236] Zong C, Wu J, Wang C, Ju H, Yan F. Chemiluminescence imaging immunoassay of multiple tumor markers for cancer screening. *Anal. Chem.* 2012;84:2410-5.

[237] Päkkilä H, Ylihärsilä M, Lahtinen S, Hattara L, Salminen N, Arppe R, Lastusaari M, Saviranta P, Soukka T. Quantitative multianalyte microarray immunoassay utilizing upconverting phosphor technology. *Anal. Chem.* 2012;84:8628-34.

[238] Ylihärsilä M, Harju E, Arppe R, Hattara L, Hölsä J, Saviranta P, Soukka T, Waris M. Genotyping of clinically relevant human adenoviruses by array-in-well hybridization assay. *Clin. Microbiol Infect.* 2013;19:551-7.

[239] Kraus W, Nolze G. *PowderCell for Windows*, V. 2.4. Federal Institute for Materials Research and Testing, Berlin, Germany. 2000.

[240] Harju E, Hyppänen I, Hölsä J, Kankare J, Lahtinen M, Lastusaari M, Pihlgren L, Soukka T. Polymorphism of $NaYF_4$:Yb^{3+},Er^{3+} up-conversion luminescence materials. *Zeitschrift für Kristallographie Proc.* 2011;2011:381-7.

[241] Klug HP, Alexander LE. X-Ray powder diffraction procedures. *Wiley,* New York, NY, USA; 1959.

[242] Knappe W-R, Wittmann F, Mosoiu D, Horn C, Hones J. Transparent support; quantitative analysis. *US Pat*; 2009.

[243] Bogdan N, Vetrone F, Ozin GA, Capobianco JA. Synthesis of ligand-free colloidally stable water dispersible brightly luminescent lanthanide-doped upconverting nanoparticles. *Nano Letters.* 2011;11:835-40.

[244] Wilhelm S, Kaiser M, Würth C, Heiland J, Carrillo-Carrion C, Muhr V, Wolfbeis O, Parak W, Genger U, Hirsch T. Water dispersible upconverting nanoparticles: effects of surface modification on their luminescence and colloidal stability. *Nanoscale.* 2015;7:1403-10.

[245] Grzechnik A, Khaidukov N, Friese K. Crystal structures and stability of trigonal $KLnF_4$ fluorides (Ln = Y, Ho, Er, Tm, Yb). *Dalt.Trans.* 2013;42:441-7.

[246] Shannon R. Revised effective ionic radii and systematic studies of interatomic distances in halides and chalcogenides. *Acta Crystallogr. Sec. A.* 1976;32:751-67.

[247] Thoma RE, Karraker RH. The sodium fluoride-scandium trifluoride system. *Inorg. Chem.* 1966;5:1933-7.

[248] Dyck NC, van Veggel FCJM, Demopoulos GP. Size-dependent maximization of upconversion efficiency of citrate-stabilized β-phase $NaYF_4$:Yb^{3+},Er^{3+} crystals via annealing. *Appl. Mater. Interfaces.* 2013;5:11661-7.

[249] Braud A, Girard S, Doualan JL, Thuau M, Moncorgé R, Tkachuk AM. Energy-transfer processes in Yb:Tm-doped KY_3F_{10}, $LiYF_4$, and BaY_2F_8 single crystals for laser operation at 1.5 and 2.3 μm. *Phys. Rev. B.* 2000;61:5280-92.

[250] Chroboczek J, Bieber F, Jacrot B. The sequence of the genome of adenovirus type 5 and its comparison with the genome of adenovirus type 2. *Virology.* 1992;186:280-5.